NUMERICAL STUDY OF OPTIMIZATION AND PERFORMANCE OF MONOPILE-SUPPORTED OFFSHORE WIND TURBINES WITH TLCD

MAURÍCIO VITALI MENDES

TESE DE DOUTORADO EM ESTRUTURAS E CONSTRUÇÃO CIVIL

DEPARTAMENTO DE ENGENHARIA CIVIL E AMBIENTAL

FACULDADE DE TECNOLOGIA

UNIVERSIDADE DE BRASÍLIA

UNIVERSIDADE DE BRASÍLIA

FACULDADE DE TECNOLOGIA

DEPARTAMENTO DE ENGENHARIA CIVIL E AMBIENTAL

NUMERICAL STUDY OF OPTIMIZATION AND PERFORMANCE OF MONOPILE-SUPPORTED OFFSHORE WIND TURBINES WITH TLCD

MAURÍCIO VITALI MENDES

ORIENTADOR: LINEU JOSÉ PEDROSO

CO-ORIENTADOR: MARCUS VINÍCIUS GIRÃO DE MORAIS

TESE DE DOUTORADO EM ESTRUTURAS E CONSTRUÇÃO CIVIL

PUBLICAÇÃO: E.TD –XXA/24

BRASÍLIA/DF: SETEMBRO – 2024

UNIVERSIDADE DE BRASÍLIA

FACULDADE DE TECNOLOGIA

DEPARTAMENTO DE ENGENHARIA CIVIL E AMBIENTAL

NUMERICAL STUDY OF OPTIMIZATION AND PERFORMANCE OF MONOPILE-SUPPORTED OFFSHORE WIND TURBINES WITH TLCD

MAURÍCIO VITALI MENDES

TESE DE DOUTORADO SUBMETIDA AO DEPARTAMENTO DE ENGENHARIA CIVIL E AMBIENTAL DA FACULDADE DE TECNOLOGIA DA UNIVERSIDADE DE BRASÍLIA COMO PARTE DOS REQUISITOS NECESSÁRIOS PARA A OBTENÇÃO DO GRAU DE DOUTOR EM ESTRUTURAS E CONSTRUÇÃO CIVIL.

COMISSÃO EXAMINADORA:

Prof. Dr. Ing. Lineu José Pedroso (UnB)
(Orientador)

Prof. Dr. Univ. Marcus Vinícius Girão de Morais, (UnB)
(Coorientador)

Prof. Dr. José Luís Vital de Brito (UnB)
(Examinador Interno)

Prof. Dr. Guilherme Rosa Franzini (USP)
(Examinador Externo)

Prof. Dr. Zenón José Guzmán Nuñez del Prado (UFG)
(Examinador Externo)

BRASÍLIA/DF, 16 DE SETEMBRO DE 2024

FICHA CATALOGRÁFICA

VITALI MENDES, MAURÍCIO

Numerical study of optimization and performance of monopile-supported offshore wind turbines with TLCD / Mauricio Vitali Mendes; orientador Lineu José Pedroso; co-orientador Marcus Vinícius Girão de Morais. [Distrito Federal] 2024.

xxiv, 138 p. (ENC/FT/UnB, Doutor, Estruturas e Construção Civil, 2024).

Tese de Doutorado – Universidade de Brasília.

Faculdade de Tecnologia.

Departamento de Engenharia Civil e Ambiental.

Palavras-chave:

1. Vibration control.
2. Tuned Liquid Column Damper.
3. Offshore Wind Turbines.
4. Random vibration.
5. Optimal design.
6. Performance-Based Wind Engineering.

I. José Pedroso, Lineu, orient.

II. Girão de Morais, Marcus Vinícius, co-orient.

III. Título.

REFERÊNCIA BIBLIOGRÁFICA

Mendes, Maurício V. (2024). Numerical study of optimization and performance of monopile-supported offshore wind turbines with TLCD. Tese de Doutorado em Estruturas e Construção Civil, Publicação E.TD-XXA/24, Departamento de Engenharia Civil e Ambiental, Universidade de Brasília, Brasília, Distrito Federal, xix, 128 p.

CESSAO DE DIREITOS

AUTOR: Maurício Vitali Mendes

TÍTULO DA TESE DE DOUTORADO:

GRAU / ANO: DOUTOR / 2024

Maurício Vitali Mendes

vitali.mendes@gmail.com

DEDICATION

I dedicate this work to my family.

Especially, to my parents.

ACKNOWLEDGMENTS

I would like to recognize and praise three great professors who were directly involved in the completion of this thesis.

Professor Lineu, my master's and doctoral advisor, I would like to thank him for his support and encouragement during all these years. A true professor in every aspect.

Second, my co-advisor Professor Marcus Girão. I am immensely grateful to him for sharing with me his enthusiasm and great knowledge for the development of the research and work involved in this thesis.

Also, I would like to thank Professor Petrini for the opportunity to work with him at Sapienza, Università Degli Studi di Roma. I strongly believe that his knowledge and guidance provided a great contribution to the work outcome. Furthermore, the months in Rome with him and the research group provided special moments that are worth a lifetime.

I acknowledge and thank CNPq for the scholarship provided throughout the doctoral period and CAPES for the scholarship provided which presented me with a unique opportunity to expand and deepen the studies carried out in the thesis.

Finally, I would like to thank my department colleagues and professors who indirectly encouraged the thesis development and acknowledge their value.

RESUMO

ESTUDO NUMÉRICO DE OTIMIZAÇÃO E DESEMPENHO DE TURBINAS EÓLICAS OFFSHORE SUPORTADAS POR MONOPILE COM TLCD

Autor: Maurício Vitali Mendes
Orientador: Lineu José Pedroso
Coorientador: Marcus Vinícius Girão de Morais
Programa de Pós-graduação em Estruturas e Construção Civil
Brasília, setembro 2024

Tecnologias de controle de vibração como o Tuned Liquid Column Damper (TLCD) podem auxiliar ou garantir o avanço do projeto, da fabricação e da construção de grandes turbinas eólicas offshore (OWTs). Esses dispositivos de controle aumentam a segurança e a durabilidade da OWT ao atenuar vibrações estruturais que surgem de cargas aleatórias de vento e ondas que podem comprometer a operação e a integridade da turbina eólica.

Para garantir um ganho máximo no desempenho estrutural da OWT com o uso do TLCD, um processo de otimização é empregado para buscar os parâmetros ótimos do TLCD que minimizem a resposta da OWT. O uso do TLCD ótimo apresentou uma redução nos deslocamentos longitudinais da OWT maior que 35% e atingiu uma redução máxima de 60%. O controle de vibração da OWT pelo TLCD ótimo provou ser eficiente e robusto sob diferentes fontes de incerteza, como parâmetros básicos de vento e onda e parâmetros estruturais. A resposta da OWT teve uma redução média de 45%.

Além do ganho de desempenho estrutural, o uso do TLCD em OWTs oferece a possibilidade de economia adicional em material e fabricação de estruturas de suporte da OWT (torre e fundação). O projeto ótimo simultâneo de OWT e TLCD é proposto e avaliado na tese. O procedimento adotado demonstra a viabilidade do uso de TLCD no projeto de OWTs com redução de custos de produção, mantendo o desempenho estrutural. Em conjunto com TLCD, a otimização do projeto de OWT reduz o volume da estrutura em até 17% e os custos de produção e fabricação em 20%. O processo de otimização é computado pelo método do Algoritmo Genético (GA) e a análise do desempenho estrutural é avaliada por uma abordagem simplificada do procedimento de Perfomance-Based Wind Engineering (PBWE).

Além disso, os dispositivos semiativos demonstram desempenho robusto no controle de vibrações causadas por cargas aleatórias, instilando confiança em sua confiabilidade. A tese investiga os TLCDs com amortecimento on-off regulado por um controlador geral. Uma válvula elétrica é empregada para controlar e alternar a razão de

bloqueio da válvula do TLCD, modulando assim o amortecimento do dispositivo. Entre as leis de controle semiativo convencionais, o controle Groundhook é adotado. A eficácia do TLCD semiativo é avaliada em OWTs de 5-MW, 10-MW e 15-MW. O desempenho das OWTs é analisado sob vários cenários de velocidade do vento e parâmetros de onda correspondentes. Os resultados indicam que os TLCDs semiativos reduzem significativamente os deslocamentos dos OWTs operacionais e estacionados.

Assim, a tese destaca a grande adaptabilidade e eficiência do TLCD em melhorar o desempenho estrutural dos OWTs sob cargas de vento e onda. Além disso, o trabalho contribui para a compreensão e o conhecimento relacionados às complexidades que envolvem a análise do controle de vibração de turbinas eólicas offshore

Palavras-chave: *Controle de vibrações; Amortecedor de coluna líquida sintonizado; Turbinas eólicas offshore; Vibração aleatória; Design ótimo; Perfomance-Based Wind Engineering.*

ABSTRACT

NUMERICAL STUDY OF OPTIMIZATION AND PERFORMANCE OF MONOPILE-SUPPORTED OFFSHORE WIND TURBINES WITH TLCD

Author: Maurício Vitali Mendes
Advisor: Lineu José Pedroso
Co-advisor: Marcus Vinícius Girão de Morais
Programa de Pós-graduação em Estruturas e Construção Civil
Brasilia, September 2024

Vibration control technologies like the Tuned Liquid Column Damper (TLCD) can aid or ensure the advance of large Offshore Wind Turbines (OWTs) design, manufacturing, and building. These control devices enhance the OWT safety and durability by mitigating structural vibrations that arise from random wind and wave loads that could compromise the wind turbine operation and integrity.

To ensure a maximum gain to the OWT structural performance with the TLCD use, an optimization process is employed to search for the TLCD optimal parameters that minimize the OWT response. The optimal TLCD use presented a decrease in the OWT longitudinal displacements, which was bigger than 35% and reached a 60% maximum decrease. The OWT vibration control by the optimal TLCD proved to be efficient and robust under different sources of uncertainty, such as basic wind and wave parameters and structural parameters. The OWT response had on average a 45% decrease.

In addition to the structural performance gain, the TLCD use in OWTs also offers the additional savings possibility in OWT support structures (tower and foundation) material and manufacturing. The OWT and TLCD simultaneous optimum design is proposed and evaluated in the thesis. The adopted procedure demonstrates the TLCD use feasibility in the OWTs design with production costs reduction while maintaining structural performance. In conjunction with TLCD, OWT design optimization reduces structure volume up to 17% and 20% costs in production and manufacturing. The optimization processes apply the Genetic Algorithm (GA) method, and the structural performance analysis is evaluated by simplified approach from the Performance-Based Wind Engineering (PBWE) procedure.

Also, semi-active devices demonstrate robust performance in controlling vibrations caused by random loads, instilling confidence in their reliability. The thesis investigates the TLCDs with on-off damping regulated by a general controller. An electro valve is employed to control and switch the TLCD valve blocking rate, thereby

modulating the device damping. Among conventional semi-active control laws, groundhook control is adopted. The semi-active TLCD effectiveness is evaluated on a 5-MW, a 10-MW, and a 15-MW OWT. The OWTs performance is analyzed under various wind speed scenarios and corresponding wave parameters. Results indicate that semi-active TLCDs significantly reduce operational and parked OWTs displacements.

Thus, the thesis highlights the great TLCD adaptability and efficiency in enhancing the OWTs structural performance under wind and wave loads. Also, the work contributes to comprehension and knowledge related to the complexities that involve offshore wind turbine vibration control analysis.

Keywords: *Vibration control; Tuned Liquid Column Damper; Offshore Wind Turbines; Random vibration; Optimal Design; Performance-Based Wind Engineering*

SUMMARY

1. INTRODUCTION 1

1.1 GENERALITIES 1

1.2 PROBLEMATIC 3

1.3 OBJECTIVES 5

1.4 METHODOLOGY 5

1.5 MOTIVATION AND CONTRIBUTION 7

1.6 SCOPE AND LIMITATIONS 8

1.7 TEXT ORGANIZATION 9

2. OWT & TLCD NUMERICAL MODELS 11

2.1 TUNED LIQUID COLUMN DAMPER (TLCD) 11

2.1.1 SEMI-ACTIVE TLCD 14

2.1.2 GROUNDHOOK CONTROL STRATEGIES FOR SEMI-ACTIVE TLCD 15

2.1.3 GROUNDHOOK STRATEGY BASED ON RESPONSE INCREMENTS . 17

2.2 OFFSHORE WIND TURBINE WITH TLCD 18

2.3 OWT MONOPILE 22

2.3.1 COUPLED SPRINGS 26

2.3.2 DISTRIBUTED SPRINGS 30

2.3.3 ADVANCED METHODS 34

3. RANDOM VIBRATION 37

3.1 FREQUENCY RESPONSE FUNCTION 39

3.2 WIND LOAD ON THE OWT SUPPORT STRUCTURE 41

3.3 WIND LOAD ON THE OWT BLADES 44

3.4 WAVE LOAD ON OWT MONOPILE 49

3.5 WIND AND WAVE RANDOM LOADS IN TIME DOMAIN 55

3.5.1 WIND LOAD ON STRUCTURE 55

3.5.2 WIND ROTOR THRUST 57

3.5.3 WAVE LOAD 59

4. OPTIMAL DESIGN 62

4.1 GENETIC ALGORITHM COMPUTATIONAL ROUTINE 63

4.1.1 OBJECTIVE FUNCTION 64

4.1.2 SELECTION 64

4.1.3 CROSSOVER 65

4.1.4 ELITISM AND DECIMATION 66

4.1.5 MUTATION 66

4.2 TLCD OPTIMIZATION 66

4.3 OWT AND TLCD SIMULTANEOUS OPTIMIZATION 67

5. OFFSHORE WIND TURBINE STRUCTURE PERFORMANCE 71

5.1 SOURCES OF UNCERTAINTY FOR AN OWT 72

5.2 SIMPLIFIED APPROACH TO STRUCTURAL PERFORMANCE 73

5.3 MONTE CARLO SIMULATION FOR PERFORMANCE ANALYSIS 75

6. ANALYSIS & RESULTS 79

6.1 TLCD OPTIMIZATION AND PARAMETRIC EVALUATION 79

6.2 SIMULTANEOUS OPTIMIZATION OF OWT CONTROLLED BY TLCD CONSIDERING STRUCTURAL AND DAMPER PERFORMANCE CONSTRAINTS 91

6.3 OWT RESPONSE WITH SEMIATIVE TLCD 98

6.3.1 TLCD PRELIMINAR DESING 100

6.3.2 SEMI-ACTIVE TLCD ANALYSIS FOR OPERATING OWT 102

6.3.3 TLCD ANALYSIS FOR PARKED OWT 106

7. CONCLUSION & SUGGESTIONS 108

BIBLIOGRAPHY 111

APPENDIX A. ELASTIC BUCKLING STRENGTH OF AN UNSTIFFENED CIRCULAR CYLINDRICAL SHELL 125

APPENDIX B. SOME CONTINUOUS PROBABILITY DISTRIBUTIONS 127

APPENDIX C. ANALYSIS OF MESH CONVERGENCE AND GEOMETRIC STIFFNESS INFLUENCE OF THE NREL 5-MW REFERENCE WIND TURBINE 129

APPENDIX D. LIST OF PUBLICATIONS 138

LIST OF FIGURES

Figure 1.1. Evolution of Wind Turbine dimensions (Source: Burton et al., 2021)..... 2
Figure 1.2. Offshore wind turbines and some natural actions in the offshore environment (Source: Ciampoli & Petrini, 2010). 3
Figure 1.3.. OWT designs related to frequencies limited by environmental and mechanical loads (Source: Bhattacharya, 2019). 4
Figure 2.1. A TLCD visual representation and its parameters..... 12
Figure 2.2. Frequency response of a single degree of freedom structure controlled by passive (PSV) or semi-active TLCD regulated by VBG, DBG, and Δ-DBG groundhook strategies. 18
Figure 2.3. Schematic representation of TLCD (a), the OWT system and environmental loads (b), and OWT numerical model scheme (c). 20
Figure 2.4. Types of offshore wind turbine foundations. 23
Figure 2.5. Grounded foundation configurations of wind turbine rated power (MW) as a function of water depth (m) (Source: Bhattacharya et al., 2021)). 24
Figure 2.6. Coupled spring model at the seabed level..... 26
Figure 2.7. Model of independent p-y springs distributed along the pile length..... 31
Figure 2.8. Coefficients provided as a function of the soil's shear angle. (a) and initial modulus of subgrade reaction kh (b) (Fonte: Bhattacharya, 2019). 32
Figure 2.9. Joint approach to the phenomenon of soil-structure interaction using numerical and p-y spring methods (Source: Kaynia, 2021)..... 35
Figure 3.1. Response spectrum of the discrete structure under random wind and wave actions. 41
Figure 3.2. Normalized Kaimal spectrum ($fSuuf/\sigma k$ 2). 43
Figure 3.3. Passing gust during blades rotation (Source: Hau, 2013). 45
Figure 3.4. Blade section (Source: Manwell, 2009). 46
Figure 3.5. NREL 5-MW Reference OWT rotor thrust spectrum. 47
Figure 3.6. Relevant parameters for the rotationally sampled spectrum $Su\ o$ (Source: Sarkar & Chakraborty, 2017). 48
Figure 3.7. Normalized rotationally auto-correlation function for alongwind wind fluctuations seen by points on a rotating blade at different radii. 49
Figure 3.8. Fluid domain (Source: Brebbia & Walker, 1979). 51
Figure 3.9. Wave force and its components in the monopile (Source: Brebbia & Walker, 1979). 52
Figure 3.10. Pierson-Moskowitz and JONSWAP spectrum for the given conditions. ... 55

Figure 3.11. OWT with monopile foundation under random wind and wave load in time. 55
Figure 3.12. Wind speed with the mean wind and turbulence speed superposition. 57
Figure 3.13 Random wind signal compared to Kaimal's expression..... 57
Figure 3.14. 10-MW OWT thrust as a function of wind speed. 58
Figure 3.15. 10-MW OWT approximate thrust force in time..... 58
Figure 3.16. Wave speed in time with amplitude related to the JONSWAP spectrum. .. 60
Figure 3.17. Wave acceleration in time with amplitude related to the JONSWAP spectrum. 60
Figure 3.18. Wave load in time domain..... 60
Figure 3.19. Random wave load signal compared to exact expressions. 61
Figure 4.1. Genetic Algorithm flowchart for optimizing the TLCD or OWT parameters. 64
Figure 5.1. OWT zones, sources, and types of uncertainties considered for the PBWE analysis (Source: Petrini, 2009). 72
Figure 5.2. Random samples of the structural parameter (SP) generated by the lognormal distribution function. 76
Figure 5.3. Random samples of the intensity measure parameter (IM) generated by the Weibull distribution function. 76
Figure 5.4. Occurrence frequency of the structural response in terms of the EDP parameter. 77
Figure 5.5. Probability of occurrence of the structural response in terms of EDP. 77
Figure 6.1. NREL 5-MW OWT configuration and discrete model adopted for the analysis. 80
Figure 6.2. Schematic representation of the NREL 5-MW OWT monopile foundation and the coupled springs SSI simplified model. 81
Figure 6.3. OWT under white noise load 3D response map: displacement at the tower top (a); and TLCD optimal damping ratio (b). 82
Figure 6.4. OWT under white noise load 2D response map: displacement at the tower top (a); and TLCD optimal damping ratio (b). 82
Figure 6.5. OWT under wind and wave load 3D response map: displacement at the tower top (a); and TLCD optimal damping ratio (b)..... 83
Figure 6.6. OWT under wind and wave load 2D response map: displacement at the tower top (a); and TLCD optimal damping ratio (b)..... 83

Figure 6.7. OWT under rotor thrust 3D response map: displacement at the tower top (a); and TLCD optimal damping ratio (b). 83
Figure 6.8 OWT under rotor thrust 2D response map: displacement at the tower top (a); and TLCD optimal damping ratio (b). 84
Figure 6.9. TLCD optimal parameters for OWT under white noise load: (a) tuning ratio γf; (b) damping ratio ζf. 85
Figure 6.10. TLCD optimal parameters for OWT structure under wind and wave load: (a) tuning ratio γf; (b) damping ratio ζf. 86
Figure 6.11. TLCD optimal parameters for OWT blades under wind load: (a) tuning ratio γf; (b) damping ratio ζf 86
Figure 6.12. OWT response for structure under white noise load. 88
Figure 6.13. OWT response for structure under wind and wave load. 88
Figure 6.14. OWT response for blades under wind load. 88
Figure 6.15. Mean wind velocity distribution at the hub height 89
Figure 6.16. Wave height (a) and peak period (b) distribution. 89
Figure 6.17. Offshore wind turbine material elasticity modulus (a) and damping ratio (b). 90
Figure 6.18. Risk curves related to the OWT longitudinal displacement (fore-aft) at the top due to wind and wave loads 90
Figure 6.19. OWT structure volume variation through generations in simultaneous optimization. 93
Figure 6.20. OWT support structure with TLCD optimal design values for the outer diameter (a) and thickness (b). 93
Figure 6.21. Optimum OWT outer diameter (a) and thickness (b) trough different generations. 94
Figure 6.22. Optimum OWT constrains: (a) tip displacement and (b) buckling ratio ($\sigma t, b/\sigma cr$) trough different generations. 95
Figure 6.23. Optimum TLCD liquid column maximum displacement trough different generations. 96
Figure 6.24. Mean wind velocity distribution at the hub height 97
Figure 6.25. Wave height (a) and peak period distribution (b). 97
Figure 6.26. Offshore wind turbine material elasticity modulus (a) and damping ratio (b). 97
Figure 6.27.Original reference 5-MW OWT and optimized 5-MW OWT with TLCD performance analysis. 98

Figure 6.28. 5-MW (a), 10-MW (b), and 15-MW (c) OWT with monopile foundation. 99
Figure 6.29 . Semi-active TLCD with electro valve positioned inside the OWT tower. 100
Figure 6.30. 5-MW OWT rms fore-aft top displacement decrease with passive and semiactive TLCD. 103
Figure 6.31. 5-MW OWT fore-aft displacement at the top for a mean wind speed of 11.40 m/s. 104
Figure 6.32. 10-MW OWT rms fore-aft top displacement decrease with passive and semiactive TLCD. 104
Figure 6.33. 10-MW OWT fore-aft displacement at the top for a mean wind speed of 10.75 m/s. 105
Figure 6.34. 15-MW OWT rms fore-aft top displacement decrease with passive and semiactive TLCD. 105
Figure 6.35. 15-MW OWT fore-aft displacement at the top for a mean wind speed of 10.59 m/s. 106
Figure 6.36. Parked 5-MW OWT rms fore-aft top displacement decrease with TLCD. 107
Figure 6.37. Parked 10-MW OWT rms fore-aft top displacement decrease with TLCD. 107
Figure 6.38. Parked 15-MW OWT rms fore-aft top displacement decrease TLCD..... 107
Figure B.1. Normal distribution. 127
Figure B.2. Lognormal distribution. 128
Figure B.3. Weibull distribution. 128
Figure C.1. OWT 1st Frequency according to number of elements of the discrete model. 131
Figure C.2. OWT 2nd Frequency according to number of elements of the discrete model. 131
Figure C.3. OWT 1st Frequency according to number of elements of the discrete model with a tower refined mesh. 133
Figure C.4. OWT 2nd Frequency according to number of elements of the discrete model with a tower refined mesh. 133
Figure C.5. Error of the numerical solution for the structure first and second vibration frequencies without the influence of geometric stiffness. 135
Figure C.6. Error of the numerical solution for the structure first and second vibration frequencies with the influence of geometric stiffness. 135

LIST OF TABLES

Table 2.1. Stiffness formulas for coupled springs in the case of piles considered flexible (Source: Bouzid, 2018). 27
Table 2.2. Stiffness formulas for coupled springs in the case of piles considered rigid (Source:Bouzid, 2018). 28
Table 6.1. NREL 5-MW OWT parameters and components values..... 80
Table 6.2. TLCD tuning ratio computed through GA and response map analyses. 84
Table 6.3. TLCD damping ratio obtained through GA and response map analyses..... 85
Table 6.4. OWT response mitigation for structure under white noise load. 87
Table 6.5. OWT response mitigation for structure under wind and wave load. 87
Table 6.6. OWT response mitigation for blades under wind load. 87
Table 6.7. Design variables of the standard OWT with lower and upper limits adopted for the DVs domain. 92
Table 6.8. Optimal design values for the best OWT solution with TLCD compared to the reference NREL OWT 5-MW. 93
Table 6.9. Reference OWTs and parameters considered for semiactive vibration control analysis. 99
Table 6.10. 5-MW OWT response mitigation obtained by the semi-active TLCD blocking ratio combination. 102
Table 6.11. 10-MW OWT response mitigation obtained by the semi-active TLCD blocking ratio combination. 102
Table 6.12. 15-MW OWT response mitigation obtained by the semi-active TLCD blocking ratio combination. 102
Table B.1. Continuous distribution functions employed for performance analysis. 127
Table C.1. Natural frequencies of the OWT without considering geometric stiffness. 130
Table C.2. Natural frequencies of the OWT considering geometric stiffness. 130
Table C.3. Natural frequencies of the OWT without considering geometric stiffness for tower refined mesh. 132
Table C.4. Natural frequencies of the OWT without considering geometric stiffness for tower refined mesh. 132
Table C.5. Estimation of the numerical solution for Natural frequencies of the OWT without considering geometric stiffness..... 134
Table C.6. Estimation of the numerical solution for Natural frequencies of the OWT considering geometric stiffness. 134

Table C.7. Error of the numerical solution for the structure first and second vibration frequencies without the influence of geometric stiffness..... 136
Table C.8. Error of the numerical solution for the structure first and second vibration frequencies with the influence of geometric stiffness..... 137

LIST OF SYMBOLS

A_i	wind area incidence on the structure	F_0	harmonic force amplitude
A_f	liquid column cross-sectional area	f	frequency
A_o	wave amplitude	$f(t)$	force in time domain
B_f	liquid column part in the tube horizontal section	$\bar{f}(t)$	mean wind force
C_1	soil dimensionless coefficient	f_{CS}	OWT fundamental frequency with coupled springs
C_2	soil dimensionless coefficient	f_{FB}	OWT fundamental frequency with fixed base
C_3	soil dimensionless coefficient	f_p	peak frequency
C_ϕ	foundation dimensionless flexibility coefficients	$f_t(t)$	wind turbulence force
C_S	foundation dimensionless flexibility coefficients	G	OWT self-weight
C_x	foundation dimensionless flexibility coefficients	g	gravity acceleration
C_d	drag coefficient	g_σ	wind peak factor
C_i	inertia coefficient	H	structure frequency response function
C_l	lift coefficient	H_s	wave height
C_m	added mass coefficient	$H_{u_i u_j}$	turbulence spectral amplitude
Coh	coherence function	H_{η_i}	wave spectral amplitude
$\boldsymbol{c}$	system damping matrix	h	seabed depth
$c(r)$	blade chord	h_f	liquid column part in the tube vertical section
c_f	liquid column linear damping	I_{ref}	turbulence intensity reference value
c_s	structure damping	I_p	monopile moment of inertia
D_b	tower base diameter	I_T	tower moment of inertia
D_p	pile diameter	J	soil load-deflection curve parameter
D_t	tower top diameter	K_{py}	spring stiffness for p-y curve
d_m	monopile diameter	K_{xx}	soil-pile assembly translational stiffness
$d_{t,b}$	tower base diameter	$K_{\phi\phi}$	soil-pile assembly rotational stiffness
$d_{t,t}$	tower top diameter	$K_{x\phi}$	soil-pile assembly coupled stiffness
E	Expectation	$\boldsymbol{k}$	system stiffness matrix
E_p	pile Young modulus	k_f	liquid column stiffness
E_{py}	p-y curve secant stiffness	k_h	substrate initial reaction modulus
E_{SD}	soil strength at one pile diameter depth	k_s	structure stiffness
E_T	tower Young modulus	L_c	coherence scale parameter
EI_η	tower equivalent bending stiffness	L_k	turbulence scale integral parameter

L_f	liquid column total length	s_u	soil submerged unit weight
L_i	lower limit	T	period
L_p	pile length	t	time
L_s	upper limit	t_i	time step
L_T	tower length	t_m	monopile thickness
l_i	pile tributary length	t_T	tower average thickness
M	moment	$t_{t,b}$	tower base thickness
$\boldsymbol{m}$	system mass matrix	$t_{t,t}$	tower top thickness
m_f	liquid column mass	$\overline{U}$	wind mean velocity
m_{RNA}	rotor-nacelle assembly mass	$\overline{U}_{ref}$	wind reference mean velocity
m_s	structure mass	$\overline{U}_{10}$	average wind speed at 10 meters height
m_T	tower mass	u	wind turbulence velocity
$\boldsymbol{m_{sf}}$	system mass coupling matrix	u_x	horizontal wave velocity
N_{ger}	number of generations	$\dot{u}_x$	horizontal wave acceleration
p	soil reaction per pile unit length	$\vec{v}$	Velocity vector
p_u	ultimate soil resistance	X_0	structure response amplitude
p_{ud}	ultimate soil resistance with deep mechanism	$\boldsymbol{x}$	system displacement vector
p_{us}	ultimate soil resistance with shallow mechanism	x_p	structure particular solution
R	autocorrelation function	x_s	structure horizontal displacement
r	Radius	$x_{t,max}$	max tower top horizontal displacement
$rand$	random value	$x_{t,lim}$	tower top horizontal displacement limited
r_f	tower and monopile bending stiffness ratio	$\dot{\boldsymbol{x}}$	system velocity vector
r_l	tower and monopile length ratio	$\dot{x}_s$	structure horizontal velocity
$r_{t,b}$	tower base radius	$\ddot{\boldsymbol{x}}$	system acceleration vector
r_{σ_x}	OWT response decrease	$\ddot{x}_s$	structure horizontal acceleration
Δr	distance between radii	y	pile horizontal deflection
P_i	Probability	y_c	soil parameter
q_i	cumulative probability	y_f	liquid column displacement
S	PSD	$\dot{y}_f$	liquid column velocity
S_{ff}	random force PSD	$\ddot{y}_f$	liquid column acceleration
$S_{f_t f_t}$	wind load PSD	$y_{f,max}$	liquid column maximum displacement allowed
$S_{u_i u_j}$	wind turbulence PSD	z_{ref}	reference height
S_u^o	rotationally sampled power spectrum	Δz	vertical distance between points
S_{xx}	OWT response PSD	z	vertical axis position
s	Distance between a fixed and moving point on the rotating blade	z_R	soil parameter

α	wind shear exponent
α_b	blade attack angle
α_f	TLCD aspect ratio
α_{js}	peak shape exponent
γ	peak shape parameter
γ'	clay undrained shear strength
γ_f	TLCD tuning ratio
$\gamma_{f_{GA}}$	optimum TLCD tuning ratio by GA
$\gamma_{f_{map}}$	optimum TLCD tuning ratio by map response
$\gamma_{f,opt}$	optimum TLCD tuning ratio
ε_c	soil load-deflection curve parameter
Δ	response increment
ζ_f	TLCD damping ratio
$\zeta_{f_{GA}}$	optimum TLCD damping ratio by GA
$\zeta_{f_{map}}$	optimum TLCD damping ratio by map response
$\zeta_{f,opt}$	optimum TLCD damping ratio
ζ_s	structure damping ratio
η	fluid surface slope
η_x	foundation dimensionless stiffness coefficients
$\eta_{x\phi}$	foundation dimensionless stiffness coefficients
η_ϕ	foundation dimensionless stiffness coefficients
θ_i	random phase angle
K	Bessel function
κ	Wavenumber
κ_u^o	rotationally correlation function
λ	monopile loading type
μ_f	TLCD mass ratio
μ_x	process mean
ξ_f	head loss coefficient
ρ_a	air density
ρ_f	liquid density
ρ_s	sea density
σ_b	bending stress
σ_{cr}	critical buckling stress
σ_M	blade root bending moment standard deviation
$\sigma_{t,b}$	tower base stress
σ_u	gust speed standard deviation on the rotor
σ_{u_x}	wave velocity standard deviation
$\sigma_x{}^2$	process variance
σ_y	liquid column displacement standard deviation
τ	time step
ϕ_i	structure rotation in the horizontal axis
Φ	fluid velocity potential.
ψ_o	valve area blocking ratio
ψ_{min}	minimum valve area blocking ratio
ψ_{max}	maximum valve area blocking ratio
Ω	force frequency
Ω_r	rotor rotation frequency,
ω	circular frequency
ω_f	TLCD natural frequency
ω_s	structure natural frequency

ABBREVIATIONS

ABBEolica	Associação Brasileira de Energia Eólica
API	American Petroleum Institute
DBG	Displacement-Based Groundhook
DFT	Discrete Fourier Transform
DM	Damage Measure Parameter
DNV	Det Norske Veritas
DOF	Degree of Freedom
DV	Design Variable
EDP	Engineering Demand Parameter
EPE	Empresa de Pesquisa de Energética
FFT	Fast Fourier Transform
GA	Genetic Algorithm
GBS	Gravity-Based Structures
IBAMA	Instituto Brasileiro do Meio Ambiente e dos Recursos Naturais Renováveis
IEA	International Energy Agency
IEC	International Electrotechnical Commission
IM	Intensity Measure
IP	Interaction Parameters
JONSWAP	Joint North Sea Wave Project
LRFD	Load and Resistance Factor Design
MDOF	Multiple Degrees of Freedom
MR-TLCD	Magneto-Rheological Tuned Liquid Column Damper
NBR	Normas Brasileiras Regulamentadoras
NREL	National Renewable Energy Laboratory
OWT	Offshore Wind Turbine
PBD	Performance-Based Design
PBWE	Performance-Based Wind Engineering
PM	Pierson-Moskowitz

PSD	Power Spectrum Density
PSV	Passive
RNA	Rotor Nacelle Assembly
SSI	Soil-Structure Interaction
SDOF	Single Degree of Freedom
SP	Structural Parameters
sTLCD	Semi-active Tuned Liquid Column Damper
SMAT	Semi-Active
TLCD	Tuned Liquid Column Damper
TLD	Tuned Liquid Damper
TMD	Tuned Mass Damper
VB	Vibration Control
VBG	Velocity-Based Groundhook

1. INTRODUCTION

1.1 GENERALITIES

Sustainable and renewable energy sources, such as wind energy, have been gaining traction and investment on global and national levels. Onshore wind energy in Brazil has an installed capacity of 25 GW, representing about 13% of the Brazilian electrical grid. According to the Brazilian Wind Energy Association (ABEEólica) the country holds the sixth position worldwide in installed capacity and is currently the third-largest investor in this sector.

In January 2022, a Brazilian decree was published, marking the beginning of a new phase for wind energy in the country: offshore wind energy generation. The decree regulates areas allocation and natural resources use in the coastal waters under the Federal domain for electricity generation.

Brazil has an extensive continental shelf with 7,367 km of coastline and 3.5 million km² of maritime space under its jurisdiction. As the Energy Research Company (EPE) pointed out, this space presents potential for offshore wind energy generation of almost 700 GW in waters with depths of up to 50 meters and 1000 GW in areas up to 100 meters deep. Aiming to resort part of this potential, 36 offshore wind farm projects (with a total 80 GW potential) are already in the bidding process, according to Instituto Brasileiro do Meio Ambiente e dos Recursos Naturais Renováveis (IBAMA). The Brazilian federal states involved are Piauí, Ceará, Rio Grande do Norte, Espírito Santo, Rio de Janeiro, and Rio Grande do Sul.

Alongside the available natural capacity, certain conditions surrounding offshore wind turbines offer significant advantages over onshore technology. Wind in the marine environment has higher average speeds and exhibits less turbulence (fluctuations in the average speed) due to the sea surface low roughness. Thus, benefiting from greater power and wind stability, Offshore Wind Farm projects in different regions have shown higher capacity than onshore projects.

Offshore wind technology has been identified as one of the leading solutions for producing green hydrogen, which employes electricity from renewable sources, replacing the current blue hydrogen produced with natural gas. In Brazil, green hydrogen production plants are built in ports. Naturally, offshore complexes emerge as an option for integrating the green hydrogen production system with wind farms.

Another factor pointing to the national potential for offshore wind energy generation is the natural possibility of integrating this sector with the oil and gas industry. Consequently, there is a scope economy resulting from the joint operation of the sector's existing infrastructure and all the technical and scientific knowledge acquired through the development of E&P projects (oil exploration and production). Offshore wind turbine technology resembles alternatives in the oil and gas sector. Offshore wind farms projects can accelerate their development while reducing technology costs.

Investment in research, innovation, and technology is crucial for the offshore industry growth, as high costs related are still a major obstacle to starting the offshore projects expansion. Over the years, the industry has been developing and designing larger turbines (Figure 1.1) aiming for higher productivity at a lower cost. Offshore wind turbines such as the IEA WIND 15-MW Offshore Reference Wind Turbine, as presented in the National Renewable Energy Laboratory (NREL) recent technical report (Gaertner et al., 2020), have a 240 meters rotor diameter and support structures (tower and foundation) sizing over 200 meters length.

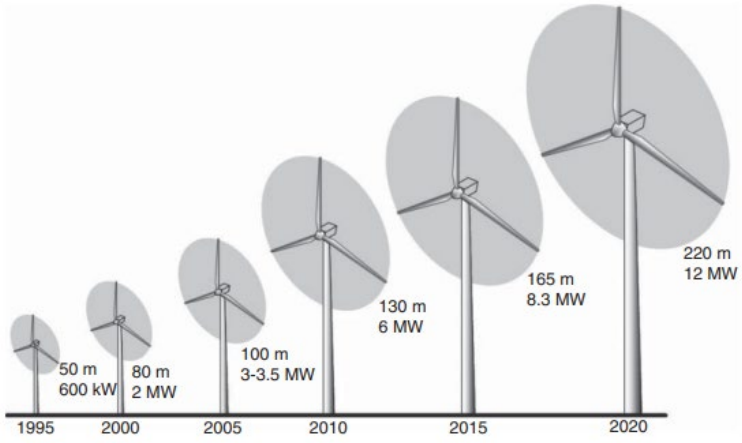

Figure 1.1. Evolution of Wind Turbine dimensions (Source: Burton et al., 2021).

The offshore wind turbines structural design, due to the offshore technology evolution, results in highly slender structures. Thus, these structures are known to be susceptible to vibration problems that can affect their efficiency, integrity, and lifespan. To preserve these turbines, which represent a significant investment, and extend their lifespan, this research investigates and analyzes the use of the Tuned Liquid Column Damper (TLCD).

Originating from naval engineering studies, this device has been adapted for numerous civil structures including buildings, bridges, towers, and, more recently, for wind turbines. Offering efficient random vibrations control from wind and sea forces, it presents low installation and maintenance costs compared to alternative damping devices, making it a standout choice for offshore wind turbine applications.

1.2 PROBLEMATIC

The offshore wind industry is moving towards larger wind turbines to generate more power per unit, rather than relying on numerous smaller units. This trend results in offshore wind turbines with larger, longer, and, consequently, more flexible towers and blades (Jahani et al., 2022).

These complex and dynamically active machines feature heavy rotating masses positioned atop slender and flexible structures, rendering them dynamically sensitive (Bhattacharya, 2019). Excessive vibrations in OWT various parts, including the foundation, tower, blades, hub, and drivetrain, may occur due to simultaneous loading from environmental forces (Figure 1.2).

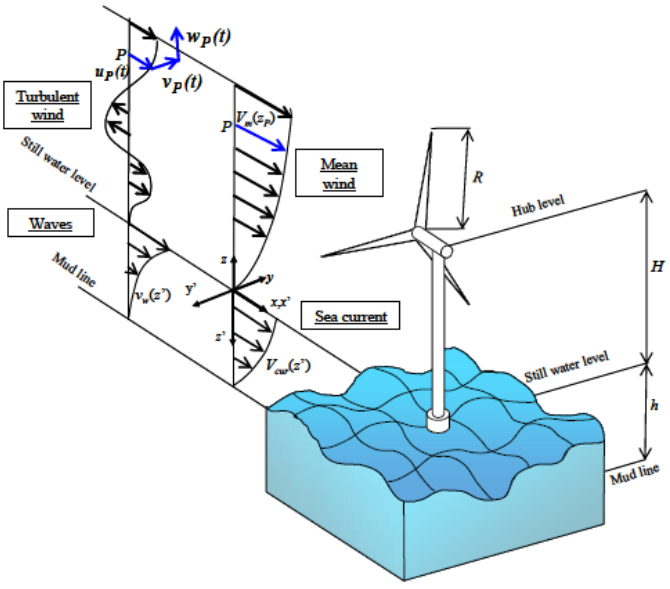

Figure 1.2. Offshore wind turbines and some natural actions in the offshore environment (Source: Ciampoli & Petrini, 2010).

Wind and wave load in the environment exhibit a random and irregular nature, characterized by fluctuations in intensity, frequency, and direction over time. These

characteristics pose challenges in defining the design solution and gathering data and information obtained through field observations.

Environmental loads (wind and waves) and mechanical loads (resulting from rotor vibration and blade passing, namely 1P and 3P, respectively) have frequencies that closely match the OWTs first frequencies (Figure 1.3)

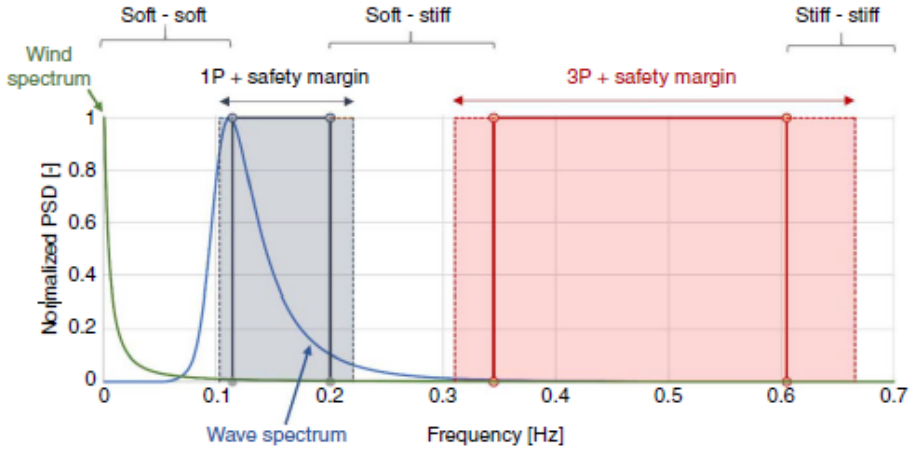

Figure 1.3.. OWT designs related to frequencies limited by environmental and mechanical loads (Source: Bhattacharya, 2019).

Under this aspect, three main regions are considered for offshore wind turbine design. The "soft-soft" region is associated with highly flexible structures and is hardly applicable for fixed-bottom foundations. Designing in the "stiff-stiff" region entails undesirable costs related to robust and massive structures. The "soft-stiff" region represents the current trend in OWT design concerning structural and sustainable performance.

Still, if the loading frequency approaches the structure natural frequency the displacements experienced will be dynamic amplified and excessive vibrations may compromise the OWT structural safety and integrity and could reduce its foreseen life span.

Random vibration suppression in offshore wind turbine components through passive, semi-active, or active control methods is a subject of great interest for many researchers, as highlighted by Machado & Dutkiewicz (2024). However, optimizing the control devices design and evaluating the wind turbines performance with and without damping devices in the offshore environment is a complex task. There are many sources of uncertainty related to the problem.

1.3 OBJECTIVES

The present study aims to contribute to numerical modeling, the optimum design, and the performance assessment of monopile-supported offshore wind turbines with vibration control under random wind and wave loads. Specific objectives are defined to achieve the thesis overall goal, such as:

(a) Evaluate the optimized Tuned Liquid Column Damper parameters to elucidate its behavior and to aid the control device preliminary design for monopile-supported OWTs.

(b) Assess OWTs performance with the optimal TLCD presence to observe its efficiency considering different wind and wave loads intensities.

(c) OWT structure and TLCD simultaneous design to reduce the tower and foundation mass and ensure the maintenance of the wind turbine structural performance.

(d) Address to the tuned liquid column damper an on-off damping regulated by a general controller to evaluate possible gains in the OWT vibration control with the use of the semi-active control approach and strategy.

1.4 METHODOLOGY

Slender structures, like monopile-supported offshore wind turbines, are susceptible to dynamic amplification issues due to the closely matched frequencies from the continuous dynamic loading from wind and waves in the offshore environment. Control devices installed in OWTs absorb and dissipate part of the energy contained in the oscillating structure (Lantz et al., 2019). Thus, as they reduce the structural vibration level the device control can enhance the wind turbine performance. Additionally, integrating the Tuned Liquid Column Damper (TLCD) into the OWT support structure design offers potential cost savings while maintaining the structural reliability regarding the natural hazards. This thesis investigates different TLCD applications in monopile-supported offshore wind turbines and evaluates its impact on the structure performance. This section outlines the methods and approaches presented and employed through the work to evaluate the research objectives mentioned.

To thoroughly explore the Tuned Liquid Column Dampers (TLCDs) potential applications in Offshore Wind Turbines (OWTs), reference models of OWTs are considered. These models include the NREL 5-MW Reference WT (Jonkman et al., 2009; Jonkman & Musial, 2010), the 10-MW OWT presented in by Bortolotti et al., 2019), and the IEA WIND 15-MW OWT (Gaertner et al., 2020). By employing these

reference models, the aim is to describe the influence and behavior of the parameters involved and elucidate their effects on the response of the support structure. The numerical model of the support structure for these offshore wind turbines were built using beam finite elements.

In the offshore environment, wind and wave conditions are characterized by randomness and irregularity. In this scenario, wind and wave actions on the structure are represented considering their respective power spectra. First, the OWT with TLCD structural response to random loads is evaluated by stochastic analysis in the frequency domain. Later, the wind and wave load are computed in the time domain trough their related PSD and a time history analysis for the OWT with TLCD is used to evaluate the semi-active vibration control.

To maximize the passive Tuned Liquid Column Dampers potential employed for controlling the OWTs random vibrations, a metaheuristic method such as the Genetic Algorithms (GA) is used for the optimization process, as described by Colherinhas et al. (2021) and Mendes et al. (2023). Initially, for comparison purposes and algorithm validation the damper optimization is obtained via response mapping. Subsequently, GA is explored to analyze variations in the TLCD optimal parameters. Based on this analysis, the OWT response decrease achieved by the optimal TLCD use is evaluated. A probabilistic performance analysis is computed to account the uncertainties related to the offshore environment and to predict and demonstrate the OWT performance with TLCD for different wind and wave intensities.

A rational and robust approach to evaluate the OWTs performance with a TLCD is computed through a probabilistic analysis by the Performance-Based Wind Engineering (PBWE) procedure (Augusti & Ciampoli, 2008; Petrini, 2009; Ciampoli et al., 2011). The OWTs structural performance with TLCD is defined by simplified probabilistic terms given the occurrence of uncertain parameters involved and considered in the analysis. Basic parameters definition in the offshore environment is typically limited and characterized by a high level of uncertainty. Similarly, some OWTs structural parameters are also uncertainties objects. These parameters characterization is achieved through probability distribution functions and the probabilistic analysis is computed through a Monte Carlo simulation.

After an initial case study evaluating the Genetic Algorithms (GA) routine employed in the thesis analysis and examining the behavior of optimal parameters of passive TLCDs and their influence on the structural response of the Offshore Wind Turbine (OWT), two additional applications of the damper in wind turbines are

explored. Firstly, simultaneous optimization of the wind turbine support structure with TLCD is proposed. Secondly, the response of the OWT with semi-active TLCD is evaluated by alternately controlling its damping using an electro valve.

The OWT and TLCD simultaneous optimization objective is to reduce the support structure volume, thereby leading to cost reduction, while maintaining similar performance compared to the reference and original OWT design. This structure volume decrease is achieved by modifying the tower and monopile diameter and thickness. The optimization process of the support structure design of the OWT with TLCD is computed using the GA routine. For the structure, local buckling at the tower base is assessed according to DNVGL (2017). Additionally, the displacement at the optimized tower top should not exceed that of the original tower and the tower top dimension is linked to the TLCD dimension. As a practical consideration, the TLCD is positioned within the tower top and the liquid column displacement is limited.

Finally, the semi-active TLCD is explored and the response decrease in different OWTs are evaluated under random wind and wave loads. The OWTs are considered in two conditions: operation or parked (for wind speeds exceeding the cut-out speed). Structural analysis is conducted in the time domain and calculated using the Newmark Method. For dynamic analysis in the time domain, methods presented in Borri & Pastò (2006), Augusti & Ciampoli, (2008), and Burton et al. (2021) are employed to account for the random action of wind over time, and Chakrabarti (2005) is used for the random action of waves over time. Through a parametric study, the combination of maximum and minimum damping of the semi-active TLCD is determined. The semi-active control method adopted is based on groundhook control. The response of the OWTs is observed at different mean wind speeds and, consequently, different wave heights and frequencies. The results obtained are compared with those computed for the passive TLCD.

The numerical studies conducted and presented in this thesis are computed using self-made codes or adapted from literature. Computational analysis of these routines are performed on the MATLAB© platform.

1.5 MOTIVATION AND CONTRIBUTION

Renewable and clean energies use, such as wind power, to produce electricity stands as a promising source for mitigating global warming and enhancing public health through the pollutant emissions decrease. Renewable energy sources offer increased

reliability and stability for electrical grids. Moreover, the resources available for energy production renders scarcity as a non-critical factor.

Offshore wind energy still faces challenges to become globally competitive compared to other renewable energy options. Offshore Wind Farms entail high production, operation, and maintenance costs. The control devices employed, such as TLCDs, aim to ensure greater safety and reliability for offshore wind turbines. They enable the reduction of structural risks and extend the structure's lifespan.

Compared to other control devices, the TLCD boasts low production costs, easy installation, and relatively straightforward adaptation to structures, along with simple maintenance procedures. Furthermore, it delivers competitive results in vibration control (accelerations, displacements, fatigue failure, etc.).

Thus, the content presented in this thesis contributes to scientific knowledge on vibration control in offshore wind turbines based on current bibliographic and theoretical references. It employs optimization processes, allowing for the mapping and understanding of parameters that can be directed in a more effective and efficient manner. The thesis introduces and applies recent concepts and procedures for the performance approach of OWTs, such as the simplified form of PBWE. Future research endeavors can benefit from the studies developed and presented in this research. This is a highly relevant topic in contemporary times, presenting promising prospects for the publication and dissemination of the research done by the Dynamics and Fluid-Structure Group (GDFE) and the Systems Dynamics Group (GDS).

1.6 SCOPE AND LIMITATIONS

It is worth highlighting both the scope and limitations of the theoretical formulation and numerical model employed in this research, which are focused on the OWTs vibration control numerical analysis.

The liquid inside the TLCD is considered incompressible. Its dynamic equilibrium equation is based on the liquid column rigid body behavior and modal forms related to sloshing are disregarded. Damping is solely attributed to local pressure loss due to the valve presence and computed according to the valve blocking ratio as per Wu et al. (2005). The coupling with the structure is inertial coupling and is limited to the longitudinal response of the structure.

The OWT support structure (tower and foundation) is modeled using 4-DOF (Degrees of Freedom) beam elements, considering the Euler-Bernoulli theory. The

rotor-nacelle assembly (RNA) is represented in the OWT model as a lumped mass at the tower top. The structural response is assumed to remain within the elastic regime.

The wind action is considered only in the longitudinal direction causing vibrations in the OWT out-of-plane direction. Wind velocities result in wind drag on the structure and thrust on the rotor. The wind structural loading is determined from the Kaimal spectrum, while the rotor thrust loading is computed using the rotationally sampled spectrum. The rotor loading in the time domain is approximately determined from the specified thrust curve for each rotor obtained from technical reports.

The wave force is determined by the Morison Equation, which comprises the inertial and drag components. To determine the wave velocity and acceleration the Linear Wave Theory based on the Linear Airy formulation is considered.

The structure does not account for any aeroelastic or hydro elastic phenomena. Therefore, conditional probabilities of interaction parameters given the occurrence of basic parameters of the environment and structure are disregarded.

1.7 TEXT ORGANIZATION

Initially, the Tuned Liquid Column Damper and the Offshore Wind Turbine theoretical formulation are presented in Chapter 2. Formulations for both passive and semi-active TLCDs are introduced. Next, the wind turbine with the coupled damper formulation is presented. Last, a brief literature review for offshore wind turbines foundations is provided, highlighting the main methods for soil-structure interaction in the monopile foundation, with a focus on the spring model (coupled and distributed).

The formulation used for random vibrations analysis is presented in the third chapter. The structure's response formulation in the frequency domain is defined. The expressions for the energy spectra and the random wind and wave forces considered in the analysis along the structure and rotor are discussed. Additionally, the formulation employed to compute the wind and wave actions in the time domain from their respective Power Spectral Densities (PSDs) is highlighted.

In Chapter 4, computational optimization processes are gathered and presented. The genetic algorithm stages used for optimizing the TLCD coupled to the offshore wind turbine are highlighted, as well as for the OWT with TLCD optimal design, considering the simultaneous structure and the damper optimization.

Chapter 5 addresses the OWT with TLCD analysis procedure the using the simplified Performance-Based Wind Engineering approach. The points of uncertainty

involved in the assessment are highlighted. The performance-based design simplified approach is presented and the solution method through a Monte Carlo simulation is detailed.

Chapter 6 presents the applications, analyses, and results obtained for the thesis study object. The first case studies and analyzes the optimal TLCD. Subsequently, the case of the OWT and TLCD simultaneous optimization is proposed and analyzed. The third and final case study evaluates the time history of different OWTs considering semi-active TLCD control.

In conclusion, Chapter 7 provides the findings of the study and outlines recommendations for further research on the random vibration control of OWTs using TLCDs.

2. OWT & TLCD NUMERICAL MODELS

In this chapter, the bibliography and the theoretical formulation used to build the OWT and TLCD numerical models are presented. Formulas for the passive and semi-active tuned liquid column damper, for the damper and offshore wind turbine coupling, and for the structure are detailed.

Initially, the passive TLCD standard formulation is highlighted, considering the U-shaped reservoir filled with water. Next, the governing equations of the semi-active TLCD are presented, designed by controlling the alternate blocking ratio of the electro valve. Finally, the system of equations for coupling the damper to the wind turbine is presented.

The offshore wind turbine support structure (tower and foundation) is numerically modeled using beam elements. Additionally, for a monopile foundation, the formulations of the soil-structure interaction phenomenon are presented, with a focus on three approaches adopted in the literature: coupled springs, distributed springs, and advanced models.

2.1 TUNED LIQUID COLUMN DAMPER (TLCD)

Usually, passive TLCDs are composed of a U-shaped tank partially filled with liquid, typically water. The liquid column motion inside the reservoir absorbs part of the energy from the vibrating structure (Yalla, 2001), in this case, the offshore wind turbine. Commonly, the liquid column oscillation is damped by an orifice positioned at the midpoint of the tube horizontal section (Balendra et al., 1995; Gao et al., 1997). By absorbing part of the energy from the oscillating structure and dissipating this energy by the liquid column passing through the orifice, it is possible to restore the structure equilibrium to which the TLCD is coupled.

The TLCD performance is comparable to the traditional Tuned Mass Dampers (TMD) and the Tuned Liquid Dampers (TLD) performances, offering advantages such as low cost, absence of moving mechanical parts, relatively easy installation or adaptation to existing structures, and simple maintenance (Hochrainer & Ziegler, 2006; Souza, 2003; Yalla, 2001).

To achieve significant structural vibration mitigation in the system where the TLCD is installed, careful consideration of the structure's characteristics is essential (Ashasi-Sorkhabi et al., 2017). TLCD offers versatile configuration options, including

variations in its geometric design (Altay & Klinkel, 2018; Ding et al., 2022; Konar & Ghosh, 2023; S. K. Lee et al., 2011; Rozas et al., 2016), adaptability for controlling vibrations induced by different types of dynamic forces (Chakraborty et al., 2012; Ghosh & Basu, 2004, 2005; Sonmez et al., 2016), and the capacity to incorporate complementary mechanisms for enhanced performance (Bhattacharyya et al., 2017; Gur et al., 2015; Hochrainer & Fotiu, 2018; Hochrainer & Ziegler, 2006; La & Adam, 2018; Park et al., 2018).

Indeed, the TLCD stands out as a prominent damper among many others, which justifies its study and development for application in structures subjected to significant dynamic actions, such as offshore wind turbines.

The damper's performance is strongly influenced by its parameters, such as its operating frequency, dimensions, and damping. Therefore, the optimization methods application is extremely pertinent for the TLCD design (Alkmim et al., 2018; Balendra et al., 1995; Gao et al., 1997; Mendes et al., 2023; Sarkar & Chakraborty, 2018; Wu et al., 2005).

Typically, the liquid column oscillation is damped by an orifice positioned halfway along the horizontal section of the tube. With the TLCD absorbing part of the structure's energy and dissipating it through the liquid's movement in the tube passing through the orifice, it is possible to restore the equilibrium of the structure to which the TLCD is attached (Figure 2.1).

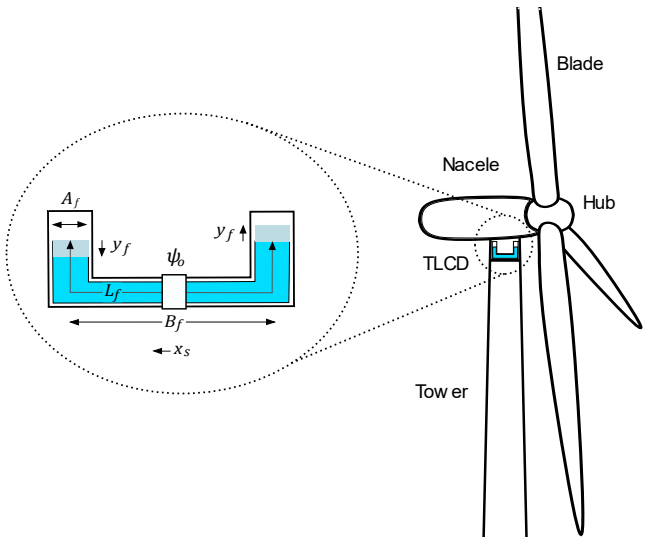

Figure 2.1. A TLCD visual representation and its parameters.

Considering the TLCD U-shaped tube with a constant liquid column cross-sectional area A_f, the tube mass is negligible compared to the liquid column mass, and

that the flow is incompressible, the equation of motion for the liquid inside the container, as presented by Yalla et al. (2000), is described by:

$$\rho_f A_f L_f \ddot{y}_f + \frac{1}{2}\rho_f A_f \xi_f |\dot{y}_f| \dot{y}_f + 2\rho_f A_f g y_f = -\rho_f A_f B_f \ddot{x}_s \tag{2.1}$$

where, ρ_f is the liquid density (water density), g is the gravity acceleration (9.8 m/s²), B_f is the liquid column part in the tube horizontal section, L_f is the liquid column total length ($L_f = B_f + 2h_f$), and h_f is the liquid column part in the tube vertical section. y_f, $\dot{y}_f$, and $\ddot{y}_f$ represent the liquid's response in the reservoir in terms of displacement, velocity, and acceleration, respectively. $\ddot{x}_s$ is the structure acceleration.

The head loss coefficient ξ_f is regulated by the valve area blocking ratio, ψ_o. For a random vibration analysis in the frequency domain, its equivalent linear form is employed. Among the available linearization methods in the literature, (Yalla, 2001) provides the equation of motion for the water in the TLCD, as presented below:

$$m_f \ddot{y}_f + c_f \dot{y}_f + k_f y_f = -\alpha_f m_f \ddot{x}_s \tag{2.2}$$

where, m_f is the liquid column mass within the tube, c_f is the liquid column linear damping, k_f is the liquid column stiffness and α_f is referred to as the TLCD aspect ratio (ratio between the liquid column horizontal and total length), expressed as:

$$m_f = \rho_f A_f L_f \tag{2.3}$$

$$c_f = 2 m_f \omega_f \zeta_f \tag{2.4}$$

$$k_f = 2\rho_f A_f g \tag{2.5}$$

$$\alpha_f = B_f / L_f \tag{2.6}$$

which ω_f and ζ_f indicates the TLCD natural frequency (rad/s) and damping ratio, respectively. The TLCD natural frequency is determined by:

$$\omega_f = \sqrt{k_f / m_f} = \sqrt{2g / L_f} \tag{2.7}$$

The structure response mitigation strongly depends on the device parameters. For a passive TLCD, parameters such as the aspect ratio α_f, tuning ratio γ_f (Equation (2.8)), mass ratio μ_f (Equation (2.9)), and damping ratio ζ_f are the set of relevant parameters to be observed in the damper design:

$$\gamma_f = \omega_f/\omega_s \tag{2.8}$$

$$\mu_f = m_f/m_s \tag{2.9}$$

where, ω_s and m_s represent, respectively, the OWT undamped fundamental frequency (rad/s) and the OWT mass.

2.1.1 SEMI-ACTIVE TLCD

Initially, a passive TLCD design includes defining its operating frequency, which is strongly related to the structure natural frequency and the liquid column damper dimensions. Also, the tuned liquid column damper design is influenced by the loading nature that acts on the structural system. Essentially, the design relates to the force amplitude and frequency characteristics. The device parameters are defined and fixed for its lifespan.

In the offshore wind turbines case, some of the loads acting on the structure, such as wind, wave, current, or even seismic forces, exhibit a random nature with varying amplitudes across a frequency range that changes over time. These forces are statistically represented through their respective power spectrum (British Standards Institution., 2006; 2009). In this scenario, the passive tuned liquid column damper may be required to operate outside its standard design (resonance with the structure).

Semi-active devices exhibit a robust performance in structural vibration control and yield good results for random loadings such as winds, waves (Sarkar & Chakraborty, 2018; Yalla et al., 2000, 2001), and earthquakes (La & Adam, 2018). Semi-active control devices mechanically operate like a passive control device. But certain device components are alternately or continuously switched according to a predetermined control strategy. The TLCD semi-active approach and design commonly alternates its damping and/or natural frequency over time.

The TLCD natural frequency can be regulated by changing the device stiffness. This adjustment can be achieved by closing the TLCD vertical section or by adding pressurized gas to this part (Bhattacharyya et al., 2017; Hochrainer & Fotiu, 2018; Hochrainer & Ziegler, 2006; Hokmabady et al., 2019; Mousavi et al., 2013; Shum et al., 2008). Another method for adjusting the TLCD frequency is proposed by Ghosh & Basu (2004) and Sonmez et al. (2016), where the TLCD is connected to the primary structure via a spring system. These two semi-active technologies involve increasing the stiffness of the TLCD, which raises the device's natural frequency. However, slender structures like OWTs typically oscillate at low frequencies. Therefore, these two semi-active methodologies applications may be outweighed by others for TLCD semi-active vibration control in wind turbines.

The effects of varying TLCD damping through alternate or continuous regulation have been studied. Anson et al. (2002), Ni et al. (2004), Sarkar & Chakraborty (2018), Wang et al. (2005), and Yang et al. (2002) employ a magnetorheological fluid and an electromagnet which through the magnetic field variation the device switches damping value. La & Adam (2018) and Yalla et al. (2000; 2001) used an electro valve to control the TLCD valve blocking ratio ψ_o and alter the device damping in an alternate or continuous manner.

The semi-active TLCD with an electro valve has its dynamic equilibrium equation equal to the passive damper (Equation (2.1), but the head loss coefficient ξ_f varies over time and is determined as a function of the valve blocking ratio ψ_o (Wu et al., 2005):

$$\xi_f(\psi_o) = (-0.6\,\psi_0 + 2.1\,\psi_0^{0.1})^{1.6}(1-\psi_o)^{-2} \tag{2.10}$$

2.1.2 GROUNDHOOK CONTROL STRATEGIES FOR SEMI-ACTIVE TLCD

As depicted, the semi-active TLCD absorbs a part of the energy from the primary system and dissipates this energy through its own damping mechanisms. Moreover, the semi-active device can be regarded as a passive damper with adjustable parameters that can be switched at any given moment.

The device functionality can be delineated through advanced technologies presented in the vibration control literature (Fitzgerald & Basu, 2020; Machado & Dutkiewicz, 2024; Saaed et al., 2015). Concepts originally applied to the automotive industry are employed into structural vibration control procedures (Altay, n.d.-a;

Casciati et al., n.d.; Koo et al. (2004) In Search of Suitable Control Methods for Semi-Active Tuned Vibration Absorbers, n.d.; La, 2012; Potter et al., 2010; Shen et al., 2013).

Among the methods analyzed for structural vibration control, the Groundhook control approach stands out. Its primary objective is to mitigate the vibrations within the primary system (OWT structure). Altay (2021), Casciati et al. (2006), and Koo et al (2004) present two Groundhook variants. One relies on the structure velocity $\dot{x}_s$ (Velocity Based Groundhook - VBG), and the other strategy centers on the structure displacement x_s (Displacement Based Groundhook - DBG). These laws were initially developed for a semi-active tuned mass damper.. Both control strategies focus on the semi-active control device velocity $\dot{y}_f$.

La & Adam (2018) and Yalla et al. (2000, 2001) apply these control laws to the semi-active Tuned Liquid Column Damper (sTLCD). Two scenarios are established: a maximum damping condition (associated with the maximum blocking ratio ψ_{max}) and a minimum damping condition (associated with the minimum blocking ratio ψ_{min}). The best choice for semi-active device damping is evaluated at each time step (t_i).

The sTLCD maximum damping condition is activated when the structure velocity $\dot{x}_s$ or displacement x_s is opposite (in signal) to the fluid column velocity $\dot{y}_f$. The objective is to maximize the sTLCD damping force when the structure and the damper motion have opposite directions. On the other hand, the minimum damping condition is activated to minimize the sTLCD damping force when the structure velocity $\dot{x}_s$ or displacement x_s has equal signal to the fluid column velocity $\dot{y}_f$. The goal is to minimize the sTLCD damping force so that the liquid column inertia does not "pull" the structure away from its equilibrium position.

In mathematical terms, we have the VBG control strategy expressed as

$$\dot{x}_s(t_i)\dot{y}_f(t_i) \leq 0\ , \quad \psi_o = \psi_{max} \tag{2.11}$$

$$\dot{x}_s(t_i)\dot{y}_f(t_i) > 0\ , \quad \psi_o = \psi_{min} \tag{2.12}$$

and the DBG control strategy as:

$$x_s(t_i)\dot{y}_f(t_i) \leq 0\ , \quad \psi_o = \psi_{max} \tag{2.13}$$

$$\dot{x}_s(t_i)\dot{y}_f(t_i) > 0\ , \quad \psi_o = \psi_{min} \tag{2.14}$$

2.1.3 GROUNDHOOK STRATEGY BASED ON RESPONSE INCREMENTS

In this study, for the semi-active control of structural vibrations in Offshore Wind Turbines, a control strategy is proposed with scenarios and evaluation parameters resembling the DBG control strategy (Equations (2.13) and (2.14)). A groundhook control law based on the response increments, referred to as Δ-DBG, evaluates the increments of the structure's displacement Δx_s and of the liquid column velocity $\Delta \dot{y}_f$ at each time step t_i instead of assessing the structure's displacement x_s and the fluid column velocity $\dot{y}_f$. This approach (Equations (2.15) and (2.16)) is used to determine the valve blocking ratio and consequently the sTLCD damping.

$$\Delta x_s(t_i)\Delta \dot{y}_f(t_i) \leq 0\ ,\ \ \psi_o = \psi_{max} \tag{2.15}$$

$$\Delta x_s(t_i)\Delta \dot{y}_f(t_i) > 0\ ,\ \ \psi_o = \psi_{min} \tag{2.16}$$

The dynamic equilibrium equation in time domain for a single-degree-of-freedom (SDOF) structure coupled with an sTLCD is defined as follows:

$$\begin{bmatrix} (m_s + m_f) & \alpha m_f \\ \alpha m_f & m_f \end{bmatrix} \begin{Bmatrix} \ddot{x}_s \\ \ddot{y}_f \end{Bmatrix} + \begin{bmatrix} c_s & 0 \\ 0 & c_f \end{bmatrix} \begin{Bmatrix} \dot{x}_s \\ \dot{y}_f \end{Bmatrix} + \begin{bmatrix} k_s & 0 \\ 0 & k_f \end{bmatrix} \begin{Bmatrix} x_s \\ y_f \end{Bmatrix} = \begin{Bmatrix} f(t) \\ 0 \end{Bmatrix} \tag{2.17}$$

The structure response considering the different groundhook control laws (VBG, DBG, and Δ-DBG) is compared next. For that purpose, a structure with a single degree of freedom modeled as a damped mass-spring system is employed. The SDOF structure has a unitary mass and stiffness and proportional damping ($c_s = 2\zeta_s m_s \omega_s$) with a damping ratio of 1%. Coupled to structure, a TLCD with 2% mass ratio (Equation (2.9)) and an 0.50 aspect ratio (Equation (2.6)) is adopted.

The system is subjected to a sinusoidal force $f(t)$ with frequency Ω and unit amplitude applied only to the structure (with a natural frequency ω_s). The structure response with TLCD is computed using the Constant Average Acceleration Method of Newmark (Clough & Penzien, 2003).

The passive TLCD tuning ratio and damping rate are determined from an analytical formulation presented in Hochrainer & Ziegler (2006), where the TLCD optimal parameters are based on the device mass ratio and aspect ratio:

$$\gamma_{f,opt} = \frac{\sqrt{1 + \mu_f\left(1 - \alpha_f^2\right)}}{1 + \mu_f} \tag{2.18}$$

$$\zeta_{f,opt} = \sqrt{\frac{3\alpha_f^2 \mu_f}{8\left(1 + \mu_f\right)}} \tag{2.19}$$

For the semi-active TLCD with alternately controlled damping, a maximum damping equal to twice the optimal passive damping ($c_f = 2\zeta_{f,opt}\mu_f m_s \gamma_{f,opt}\omega_s$) and a minimum damping equal to 60% of the optimal passive damping are considered.

Evaluating the structure displacements (normalized by the structure maximum displacement in steady state computed with the passive TLCD presence) for different frequencies and different groundhook control strategies (Figure 2.2), it is possible to observe that the proposed Δ-DBG control law, which defines the on-off damping at each time step based on the structure's displacement increment and liquid column velocity increment, shows greater response suppression over a frequency range relevant to the structure ($0{,}95 \leq \Omega/\omega_s \leq 1{,}05$). In this range, significant dynamic phenomena´s (resonance or beating) may occur and amplify the structure dynamic response.

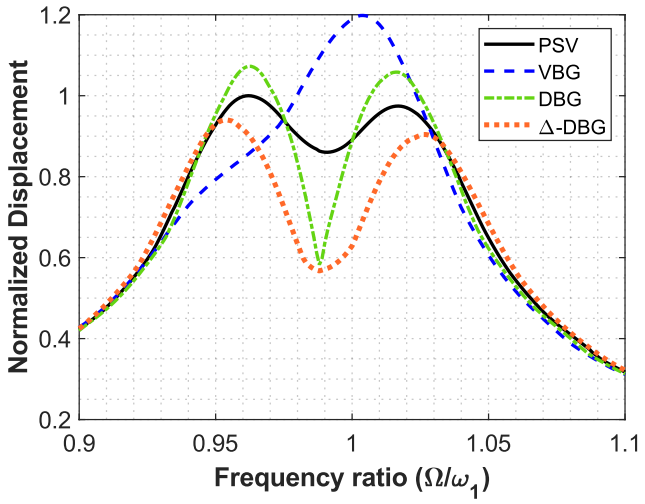

Figure 2.2. Frequency response of a single degree of freedom structure controlled by passive (PSV) or semi-active TLCD regulated by VBG, DBG, and Δ-DBG groundhook strategies.

2.2 OFFSHORE WIND TURBINE WITH TLCD

Studies and experiments for the application of TLCDs in wind turbines naturally arise from verifying the efficiency of this fluid dynamic device in mitigating vibrations. As offshore wind turbines increase in size, move further from the coast, and are

constantly subjected to greater wind and wave forces, it is essential to analyze their dynamic response and seek to minimize structural vibrations.

The control technologies use can assist or even enable the advancement of design and construction of OWTs with larger dimensions (Lantz et al., 2019). Control devices provide reliable OWT designs in the presence of wind and wave loads within a frequency range (close to the fundamental frequency of the structure) that could otherwise compromise structural safety and the OWT proper operation.

Moderate and frequent wind and wave loads can produce significant vibrations in the structure, reducing the OWT lifespan (Orlando et al., 2021). These vibrations can also cause malfunctions in turbine mechanical equipment that is sensitive to structural acceleration (Dueñas-Osorio & Basu, 2008). Colwell & Basu (2009) demonstrate that a monopile-type OWT equipped with a TLCD and subjected to wind and wave forces can achieve peak response reductions of up to 55%. It was also observed that implementing the damper in the turbine significantly extends its lifespan by analyzing the structure's fatigue. (Mensah & Dueñas-Osorio, 2014) show the vibration control effectiveness in towers and the consequent improvement in site-specific risk. Buckley et al. (2018) verify that the structure interaction with the soil plays a crucial role in the TLCD design for wind turbine towers vibration control. Optimal parameters, such as the TLCD mass ratio and tuning ratio to the tower's natural frequency, after considering soil-structure interaction, were key factors for the TLCD design to achieve better performance. Sarkar & Chakraborty (2017; 2019) evaluate the TLCD with magnetorheological fluid application effects in OWTs, considering different wind, sea, and ground motion conditions. The MR-TLCD demonstrates satisfactory performance, significantly reducing the tower's response.

The TLCD optimal parameters are linked to the considered random excitation and numerical results from (Gao et al., 1997; Yalla, 2001; Alkmim et al., 2018; Mendes et al., 2023) show that the device parameters are significantly affected by the load. To find the optimal TLCD parameters that minimize the OWT structural response optimization methods can aid the device control design.

For a monopile-supported OWT fragility study under wind, wave, and earthquake simultaneous load, Hemmati et al. (2019) numerically determines the optimal TLCD. The damper reduces the OWT fragility across all cases, resulting in a system reliability increase under multi-hazard conditions.

Implementing these devices can enhance the overall system reliability, thereby reducing downtime and maintenance needs, and leading to higher energy conversion

rates (Mensah & Dueñas-Osorio, 2014). The TLCDs use is effective for reducing vibrations in OWTs, whether they are in operation or parked position. This capability enables the manufacture and building of increasingly larger structures and with higher productive wind turbines.

Currently, offshore wind turbine structural analysis models have been significantly enhanced with new global implementation projects (Zuo et al., 2020). These turbines structural behavior is influenced by nonlinearities (Bisoi & Haldar, 2014, 2015; Damgaard et al., 2013), fragilities (Hemmati et al., 2019; Zhang et al., 2023), and many related environmental and structural interaction phenomena's (Barbato et al., 2010; Ciampoli & Petrini, 2010; Dai et al., 2021; Ishihara & Wang, 2019; Sørensen & Ibsen, 2013) which explain and contains complex factors related to the system structural analysis.

The finite element model (Figure 2.3) for the OWT structure is frequently used to analyze the macro effects of the OWTs structural response. This model is widely employed in numerical simulations in the field and represents an appropriate approach (Petrini et al., 2010) for both serviceability and ultimate OWTs analysis.

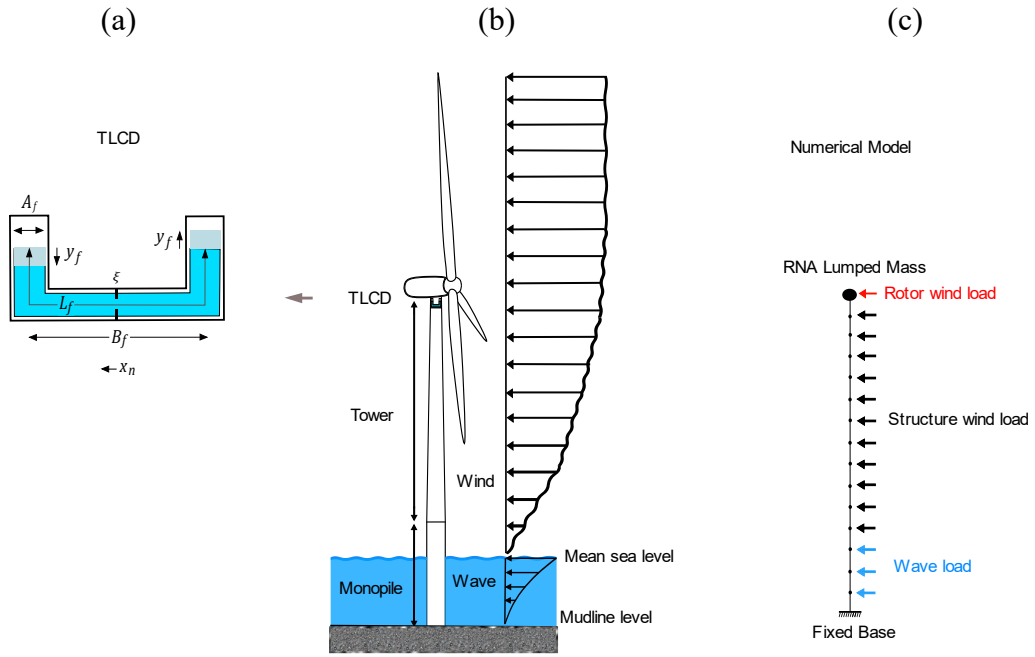

Figure 2.3. Schematic representation of TLCD (a), the OWT system and environmental loads (b), and OWT numerical model scheme (c).

Examining recent works in this scope, OWTs with TLCDs numerical models essentially consider the coupling between the damper and the structure in translation, as evidenced recent works (Colwell & Basu, 2009; Dueñas-Osorio & Basu, 2008;

Hemmati et al., 2019; Mensah & Dueñas-Osorio, 2014; Sarkar & Chakraborty, 2018). Some studies (Shum & Xu, 2004; Taflanidis et al., 2005) investigate the rotation influence in the TLCD performance for different vibration control scenarios. The damper demonstrates good efficiency in controlling both translational and rotational displacements. Shum & Xu, (2004) show that the TLCD rotation has an insignificant effect on its translational movement. Additionally, it is worth noting that OWTs should exhibit rotations of less than 0.5° (DNVGL-ST-0126, 2018; DNV-OS-J101, 2014). Thus, the coupling between the OWT and the TLCD is given as:

$$\boldsymbol{m} = \begin{bmatrix} \boldsymbol{m_s} & \boldsymbol{m_{sf}^T} \\ \boldsymbol{m_{sf}} & m_f \end{bmatrix} \tag{2.20}$$

$$\boldsymbol{m_{sf}} = \{\boldsymbol{0} \;\; \alpha_f m_f \;\; 0\} \tag{2.21}$$

$$\boldsymbol{c} = \begin{bmatrix} \boldsymbol{c_s} & \boldsymbol{0} \\ \boldsymbol{0} & c_f \end{bmatrix} \tag{2.22}$$

$$\boldsymbol{k} = \begin{bmatrix} \boldsymbol{k_s} & \boldsymbol{0} \\ \boldsymbol{0} & k_f \end{bmatrix} \tag{2.23}$$

where $\boldsymbol{m_s}$, $\boldsymbol{c_s}$, and $\boldsymbol{k_s}$ are the OWT mass, damping, and stiffness matrix, respectivelly. The mass and stiffness matrix for the OWT are computed from the Euler-Bernoulli beam theory. The rotor-nacelle assembly (RNA) mass is lumped at the structure last node. The damping matrix for the offshore wind turbine is determined considering the mass and stiffness proportional damping. The TLCD aspect ratio α_f is computed from Eq. (2.6). The TLCD mass m_f, damping c_f, and stiffness k_f parameters are defined in Equations (2.3)-(2.5). Thus, the dynamic response for the OWT and TLCD system is then expressed as

$$\boldsymbol{m}\ddot{\boldsymbol{x}}(t) + \boldsymbol{c}\dot{\boldsymbol{x}}(t) + \boldsymbol{k}\boldsymbol{x}(t) = \boldsymbol{f}(t) \tag{2.24}$$

which,

$$\begin{gathered} \boldsymbol{x}(t) = \{\boldsymbol{x_s}(t)\; y_f(t)\}^T \\ \boldsymbol{x}(t) = \{x_1(t)\; \phi_1(t) \ldots x_n(t)\; \phi_n(t)\; y_f(t)\}^T \end{gathered} \tag{2.25}$$

where the structure response in time $\boldsymbol{x_s}(t)$ in the fore-aft (out-of-plane) direction holds the monopile and tower nodal horizontal displacement $x_i(t)$ and rotation $\phi_i(t)$. The over dot expresses time differentiation. The force vector $\boldsymbol{f}(t)$ computes the wind and wave load on the OWT. These random loads are detailed later in the next chapter.

2.3 OWT MONOPILE

Wind turbines main components are the foundation, grid connection cables, tower, nacelle, power train gears, generator, and rotor blades. This section focuses on the monopile foundation, which is a crucial component that transfer the permanent (static) and dynamic loads from the structure to the soil throughout the wind turbine lifespan. Further discussion to other types of offshore foundations can be found in Morais et al. (2024).

In addition to the static actions, wind turbines are subjected to significant dynamic loads and cyclic loadings that act in ultimate and service-level forces combinations (Nardelli & Futai, 2022). The progressive increases in turbine sizes, tower heights, and rotor diameters result in significant increases in the foundations overturning moments, which increase the tower and foundation costs. Despite the foundation importance for the proper wind turbine functioning, wind turbine sites are rarely located in favorable terrain (Pham et al., 2018).

The wind turbine foundations costs can be defined by factors such as soil type, construction materials, power capacity, tower height, and surface roughness (Horgan, 2013). The choice of wind turbine foundation types and sizes is affected by the site geotechnical conditions, the wind turbine rated power, and the tower type (Hassanzadeh, 2012; Milititsky, 2019).

Figure 2.4 presents some OWTs foundations common configurations: (a) single large gravity-based, (b) monopile, (c) suction bucket, (d) tripod, (e) jacket foundation, (f) tension leg platforms, (g) semisubmersible platforms, (h) spar-buoy platforms, and barge-based. These OWT foundations can be divided into shallow water foundations (a-e) and floating structures (f-h).

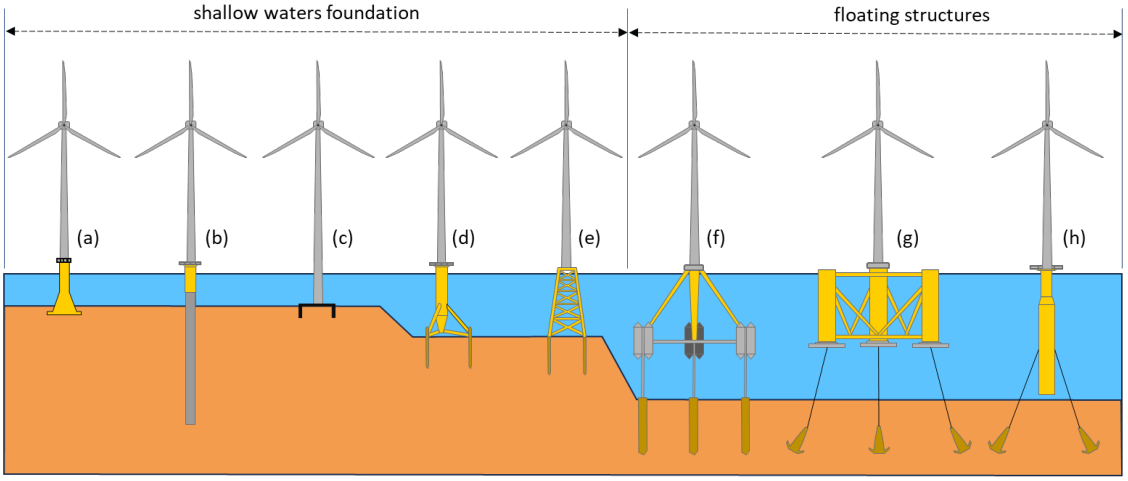

Figure 2.4. Types of offshore wind turbine foundations.

In water depths ranging as deep as 50 metres (Jahani et al., 2022; X. Wang et al., 2018; X. Wu et al., 2019) or 60 metres (Musial et al., 2022), several fixed bottom foundation types can be considered for OWTs based on the site-specific conditions and project requirements. Some of the commonly recommended foundation options for this depth range include the following:

(a) Gravity-Based Structures (GBS): GBS foundations, which utilize large concrete or steel structures placed on the seabed, can be considered for water depths up to 20-30 metres. These foundations rely on their weight to provide stability and resist dynamic loads.

(b) Monopile Foundations: Monopiles can still be a viable option in the 30-50 metre depth range, depending on soil conditions. However, as the water depths increase, the diameter and wall thickness of monopiles may need to be larger to ensure sufficient structural stability.

(c) Suction Bucket Foundations: Suction bucket foundations are another innovative option that are suitable for the 5–50 metre depth range. These foundations are installed by creating a vacuum in the bucket, which allows them to be embedded into the seabed (Byrne et al., 2002). They provide a stable and cost-effective solution for certain soil conditions.

(d) Tripod Foundations: Tripod foundations are another option that can be suitable for water depths in the 30-50 metre range. These structures have three main piles that are connected at the top and provide stability and load-bearing capacity.

(e) Jacket Structures: Jacket structures, consisting of a lattice-like framework of steel tubular members, are often used in water depths that are beyond the range

of traditional monopiles. They provide a stable and robust foundation solution for deeper waters, including the 20-50 metre range.

(Bhattacharya et al., 2021)classified the current OWT foundations as a function of rated power versus water depth (Figure 2.5). Grounded foundations (e.g., GBSs, monopiles, and jackets) are suitable for water depths from 50 to 60 metres up to rated powers of 10 MW. The most appropriate foundation type selection within the depth range of 30-50 meters depends on factors such as soil conditions, site-specific considerations, cost-effectiveness, installation methods, and project-specific requirements. A thorough analysis of these factors is necessary to determine the optimal foundation solution for a given offshore wind project.

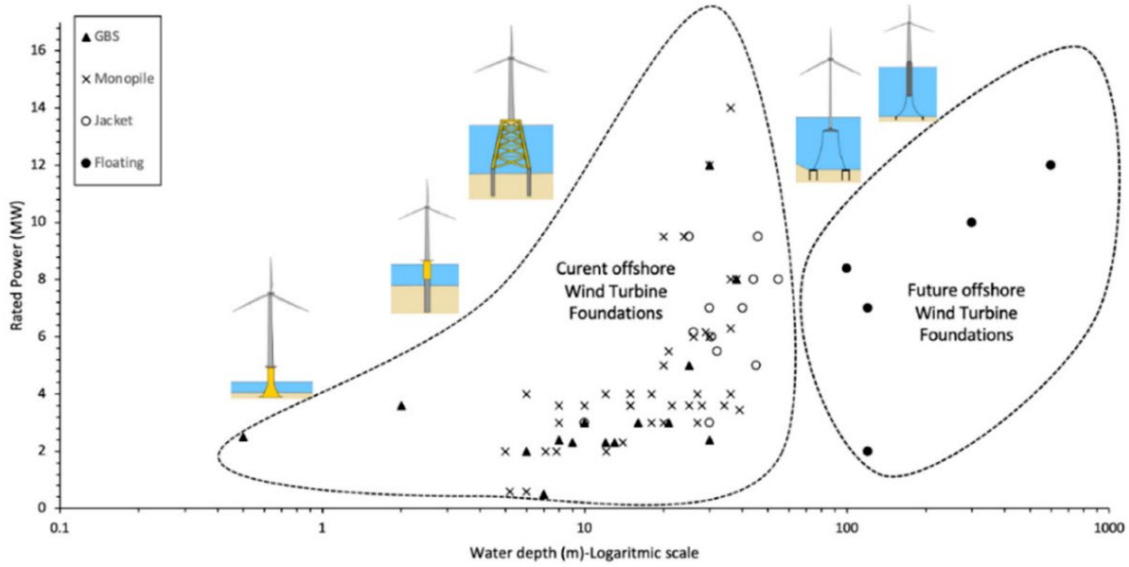

Figure 2.5. Grounded foundation configurations of wind turbine rated power (MW) as a function of water depth (m) (Source: Bhattacharya et al., 2021)).

Monopile foundations are a commonly used foundation type for offshore wind turbines (Passon, 2015). They are designed to provide stability and support for wind turbine structures in relatively shallow water depths, typically up to approximately 30-50 metres (Kallehave et al., 2015).

Monopile foundations consist of single large-diameter steel piles that are driven vertically into the seabed (Jenkins et al., 2021; Letcher, 2023). The piles are typically cylindrical in shape and have conical or tapered tips to facilitate easier penetration into the soil. The monopiles diameters and wall thicknesses depend on various factors, including the structural requirements, soil conditions, and expected loads from the wind turbine.

The monopile installation process involves using specialized equipment (Jiang, 2021), such as pile driving hammers or hydraulic jacking systems, to drive the pile into the seabed. The pile is driven until it reaches a predetermined depth, and factors such as the soil strength and the needed embedment depth for stability are typically considered. This operation causes high-level broadband noise with a notable impact on marine life (Jiang, 2021; Kikuchi, 2010).

Once a monopile is fully installed, a transition piece is attached to the pile top of (Chaves Júnior et al., 2020). The transition piece provides a connection point between the monopile and the wind turbine tower. It also provides support to an accessing platform. The transition piece is a monopile foundation design weakness to be optimized (Esteban et al., 2015; Hamilton & Abadie, 2023; Y. S. Lee et al., 2014).

Monopile foundations offer several advantages: (a) relatively cost-effective, (b) straightforward installation, especially in comparison to other foundation types, and (c) versatile application for a wide range of soil conditions, including sandy, clayey, or mixed soil profiles. However, the monopile foundations limitations are primarily evident in relatively shallow water depths. As the water depth increases, the monopile diameter and wall thickness may need to be larger to ensure sufficient structural stability with some soil-structure interactions considerations. There are some foundation concepts that use hybrid monopiles with footing plates to improve their performance in terms of the horizontal and overturning moments (Trojnar, 2019).

Additionally, in areas with challenging soil conditions, such as soft clays or loose sands, additional measures, such as predrilling or soil improvement techniques, may be needed to enhance the foundation's stability. Despite these limitations, monopile foundations remain a popular choice for OWTs due to their cost-effectiveness, simplicity, and proven performance in various offshore wind projects worldwide (Passon, 2015).

During the design process of OWTs, several design tasks and criteria analyses are necessary to ensure that the foundation do not exceed relevant limit states and allowable turbine-specific natural frequency ranges (DNV & Risø, 2002; DNVGL-ST-0126, 2018b; DNV-RP-C205, 2007; Jenkins et al., 2021; Letcher (Ed.), 2023).

In the offshore wind turbine design context, three prominent methods address the soil-structure interaction (SSI) phenomenon (Bhattacharya, 2019). These include simplified models with coupled springs, models with distributed springs, and numerical methods such as finite elements, discrete elements, finite differences, and boundary elements. Significant standards and technical reports (British Standards Institution.,

2006a; DNV-OS-J101, 2014; Jonkman et al., 2009) refer to SSI for offshore wind turbine design.

2.3.1 COUPLED SPRINGS

The simplified method with coupled springs represents the soil-monopile coupling stiffness by a set of springs in the translational and the rotational directions, along with a cross-term (Bhattacharya, 2019). This model can be expressed in a matrix form as:

$$\begin{bmatrix} K_{xx} & K_{x\phi} \\ K_{\phi x} & K_{\phi\phi} \end{bmatrix} \begin{Bmatrix} x \\ \phi \end{Bmatrix} = \begin{Bmatrix} F \\ M \end{Bmatrix} \tag{2.26}$$

where for the soil-pile assembly K_{xx} represents the translational stiffness, $K_{\phi\phi}$ represents the rotational stiffness, and $K_{x\phi}$ and $K_{\phi x}$ represents the coupled stiffness. This formulation assumes that a transverse force also induces the foundation-soil system rotation and, likewise, an applied moment causes translation.

At the seabed level, the springs set is superimposed onto the monopile element (Figure 2.6), while above this level, the monopile is modeled conventionally with its properties. In this method, no additional mass is added to the substructure (foundation) at the seabed level due to soil-structure interaction. Additionally, the SSI damping effects can be accounted (Damgaard et al., 2013; Ishihara & Wang, 2019; Medina et al., 2023; Padrón et al., 2022).

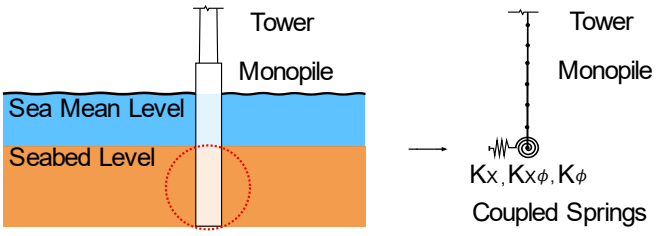

Figure 2.6. Coupled spring model at the seabed level.

In the simplified coupled-springs models the spring system stiffness is calculated using closed-form solutions. Initially, based on parameters related to the wind turbine foundation and the soil in which the monopile is driven, the pile behavior must be determined. This can be characterized as either a long flexible pile or a short rigid pile. The flexible pile fails due to the formation of plastic hinges within the pile, while the rigid short pile exhibits rigid-body rotation with failure occurring in the soil (Arany et al., 2016).

The simplified model's formulation (coupled springs) for piles is extensively developed and documented in the literature. For long and flexible piles (Table 2.1), notable formulations are presented (Gazetas, 1984, 1991; Pender, 1993; Randolph, 1981; Shadlou & Bhattacharya, 2016). For spring stiffness calculation, some parameters depend on the pile foundation, such as the pile Young modulus E_p, the pile diameter D_p, and the pile length L_p. Regarding the soil, it's necessary to know its strength at a depth equivalent to one pile diameter E_{SD} and how to characterize its resistance profile. In the formulas proposed in the literature, there's a distinction between soils with a constant, linear, or parabolic resistance profile, indicating typically overconsolidated clay, normally consolidated clay, or sandy soils, respectively.

Table 2.1. Stiffness formulas for coupled springs in the case of piles considered flexible (Source: Bouzid, 2018).

Formula per	Soil profile	$K_{xx}/E_{SD}D_p$	$K_{x\phi}/E_{SD}D_p^2$	$K_{\phi\phi}/E_{SD}D_p^3$
	Constant			
Randolph (1981)		$1.63(E_p/E_{SD})^{0.14}$	$-0.34(E_p/E_{SD})^{0.43}$	$0.20(E_p/E_{SD})^{0.71}$
Gazetas (1991)		$1.00(E_p/E_{SD})^{0.21}$	$-0.22(E_p/E_{SD})^{0.50}$	$0.18(E_p/E_{SD})^{0.73}$
Shadlou e Bhattacharya (2016)		$1.58(E_p/E_{SD})^{0.19}$	$-0.33(E_p/E_{SD})^{0.50}$	$0.20(E_p/E_{SD})^{0.73}$
	Linear			
Randolph (1981)		$0.85(E_p/E_{SD})^{0.33}$	$-0.31(E_p/E_{SD})$	$0.19(E_p/E_{SD})^{0.78}$
Gazetas (1991)		$0.60(E_p/E_{SD})^{0.35}$	$-0.59(E_p/E_{SD})$	$0.15(E_p/E_{SD})^{0.80}$
Shadlou e Bhattacharya (2016)		$0.86(E_p/E_{SD})^{0.34}$	$-0.29(E_p/E_{SD})$	$0.19(E_p/E_{SD})^{0.78}$
	Parabolic			
Gazetas (1991)		$0.80(E_p/E_{SD})^{0.28}$	$-0.24(E_p/E_{SD})$	$0.15(E_p/E_{SD})^{0.77}$
Shadlou e Bhattacharya (2016)		$1.11(E_p/E_{SD})^{0.27}$	$-0.32(E_p/E_{SD})$	$0.19(E_p/E_{SD})^{0.76}$

Meanwhile, formulations for short rigid piles (Table 2.2) can be found in the works of Abed et al., (2016), Aissa et al. (2017), Poulos & Davis (1980), and Shadlou & Bhattacharya (2016).These studies primarily focus on formulations applicable to wind turbines with monopile foundations. Additionally, the works of Varghese et al. (2022) also provide solutions for other types of offshore foundations, such as caisson, gravity, and jacket.

Table 2.2. Stiffness formulas for coupled springs in the case of piles considered rigid (Source: Bouzid, 2018).

Formula per	Soil profile	$K_{xx}/E_{SD}D_p$	$K_{x\phi}/E_{SD}D_p^2$	$K_{\phi\phi}/E_{SD}D_p^3$
	Constant			
Aissa et al. (2017)		$2.76(L_p/D_p)^{0.67}$	$-1.595(L_p/D_p)^{1.64}$	$1.73(L_p/D_p)^{2.49}$
Shadlou e Bhattacharya (2016)		$3.49(L_p/D_p)^{0.62}$	$-1.935(L_p/D_p)^{1.56}$	$1.80(L_p/D_p)^{2.5}$
	Linear			
Abed et al. (2016)		$1.71(L_p/D_p)^{1.67}$	$-1.23(L_p/D_p)^{2.66}$	$1.15(L_p/D_p)^{3.60}$
Shadlou e Bhattacharya (2016)		$2.56(L_p/D_p)^{1.53}$	$-1.93(L_p/D_p)^{2.50}$	$1.73(L_p/D_p)^{3.45}$
	Parabolic			
Abed et al. (2016)		$2.84(L_p/D_p)^{1.00}$	$-2.93(L_p/D_p)^{1.77}$	$3.89(L_p/D_p)^{2.56}$
Shadlou e Bhattacharya (2016)		$2.91(L_p/D_p)^{1.07}$	$-1.96(L_p/D_p)^{2.00}$	$1.77(L_p/D_p)^{3.00}$

2.3.1.1 OWT Frequency with Coupled Springs

The use of simplified models with coupled or lumped springs to determine the soil-foundation system stiffness allows the foundation displacements and rotations calculation at ground level (standards establish limits). Also, it can provide an estimate to the OWT natural frequency considering the soil presence.

The wind turbine natural frequencies and vibration modes modeled by beam elements with coupled springs can be computed numerically by solving the eigenvalue and eigenvector problem. As an alternative, Arany et al., (2016) present an analytical method ((2.27) to determine the monopile-supported OWT fundamental frequency with coupled springs (f_{CS}) based on the OWT fundamental frequency with fixed base (f_{FB}) considered as a cantilever beam and influenced by dimensionless flexibility coefficients.

$$f_{CS} = C_x\, C_\phi\, C_S\, f_{FB} \tag{2.27}$$

The tower fundamental frequency, simulated by a cantilever beam with a lumped mass at the tip, is computed by:

$$f_{FB} = \frac{1}{2\pi}\sqrt{\frac{3E_T I_T}{L_T^3\left(m_{RNA} + \frac{33}{140}\, m_T\right)}} \tag{2.28}$$

where m_{RNA} is the RNA mass, m_T is the tower mass, L_T is the tower length, and E_T is the Young modulus of the material composing the tower. The tower inertia I_T with variable section is given by:

$$I_T = \frac{1}{16} t_T \pi (D_b^3 + D_t^3) \tag{2.29}$$

with,

$$t_t = \frac{m_T}{\rho_T L_T D_T \pi} \tag{2.30}$$

$$D_T = (D_b + D_t)/2 \tag{2.31}$$

where, ρ_T, t_T, D_b, and D_t represents the tower specific mass, the average tower thickness, the tower diameter at the base, and the tower diameter at the top.

The OWT fundamental frequency shift due the substrate presence (soil) is accounted through the dimensionless flexibility coefficients (C_x and C_ϕ) using the following functions:

$$C_x = 1 - \frac{1}{1 + a\left(\eta_x - \eta_{x\phi}^2/\eta_\phi\right)} \quad \text{, with} \quad a = 0{,}5 \tag{2.32}$$

$$C_\phi = 1 - \frac{1}{1 + b\left(\eta_\phi - \eta_{x\phi}^2/\eta_x\right)} \quad \text{, with} \quad b = 0{,}6 \tag{2.33}$$

where,

$$\eta_x = \frac{K_x L_T^3}{EI_\eta} \tag{2.34}$$

$$\eta_{x\phi} = \frac{K_{x\phi} L_T^2}{EI_\eta} \tag{2.35}$$

$$\eta_\phi = \frac{K_\phi L_T}{EI_\eta} \tag{2.36}$$

where EI_η, the tower equivalent bending stiffness, is given by:

$$EI_\eta = E_T\, I_T\, f(q) \tag{2.37}$$

$$f(q) = \frac{1}{3}\,\frac{2q^2(q-1)^3}{2q^2\,\ln q - 3q^2 + 4q - 1} \quad \text{, with} \quad q = D_b/D_t \tag{2.38}$$

Finally, the foundation flexibility coefficient C_s is obtained by:

$$C_s = \sqrt{\frac{1}{1 + r_f\,(1 + r_l)^3 - r_f}} \tag{2.39}$$

with the bending stiffness ratio r_f (between tower and monopile) and the length ratio r_l (between tower and monopile) are given by:

$$r_f = E_T I_T / E_P I_P \tag{2.40}$$

$$r_l = L_S / L_T \tag{2.41}$$

where L_S is the length from the bottom of the tower to the seabed level, E_p is the foundation material Young modulus, and I_p is the monopile moment of inertia.

The calculations sequence presented above estimates the OWT fundamental frequency with lumped springs in an approximate manner. A more detailed OWT modal analysis considering SSI can be computed using analytical methods Ferreira et al. (2024) or numerical methods with distributed springs to achieve higher precision results.

2.3.2 DISTRIBUTED SPRINGS

In this methodology, the soil-structure interaction is modeled through independent springs distributed along the length of the pile. It is based on the theory presented in Winkler (1867) and Hetényi (1946) classical works where an analytical solution for the beam deflection on an elastic base is developed.

For laterally loaded piles the distributed spring model approach to soil-structure interaction phenomenon operates on the key assumption that the soil reaction is directly linked to the soil-pile system displacement. In this context, the pile deflection (y) at a specific depth (z) induces a corresponding soil reaction force (p) at the same location of the pile's displacement.

This soil-foundation system behavior is numerically modeled using distributed independent springs along the pile length (Figure 2.7). The springs are positioned at the

elements nodes that constitute the monopile. Typically, the monopile is represented by Euler-Bernoulli beam element or frame elements.

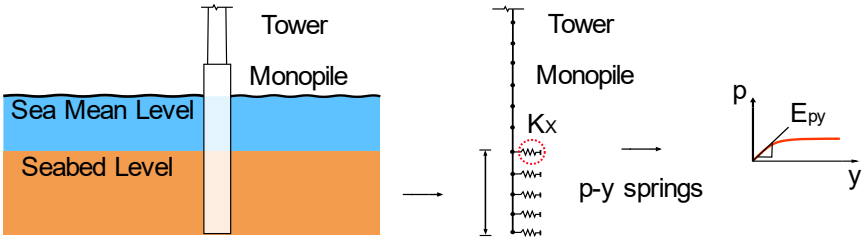

Figure 2.7. Model of independent p-y springs distributed along the pile length.

Initially, for specific piles geometry and soil types (Matlock, 1970; Reese et al., 1974; O'Neil and Murchinson, 1983) charts provided the relation for the pile deflection y (in meters) and the soil reaction per pile unit length p (in N/m). These charts are referred to as p-y curves. Therefore, through these curves, it is possible to represent the physical soil-structure system behavior. Numerically, the soil reaction p value is computed based on the loading characteristics, the soil resistance, and the substrate reaction modulus at the analyzed depth.

For typically sandy soils, the expression for the hyperbolic soil reaction to the monopile deflection y originates from Reese et al. (1974) and O'Neil and Murchinson (1983) relevant studies:

$$p = \lambda p_u \tanh\left(\frac{k_h\, z}{\lambda p_u} y\right) \tag{2.42}$$

where, the value of λ depends on the loading type (0.9 for cyclical loading), p_u is the ultimate soil resistance, and k_h is the initial substrate reaction modulus at depth z below the seabed level, in the case of the OWTs monopile. The ultimate soil resistance p_u for sandy soils is given by the minimum value between p_{us} (shallow mechanism) and p_{ud} (deep mechanism).

$$p_{us} = \left(C_1\, z + C_2\, D_p\right) \gamma' z \tag{2.43}$$

$$p_{ud} = C_3\, D_p\, \gamma'\, z \tag{2.44}$$

where C_1, C_2, and C_3 (Figure 2.8.a) and the initial soil subgrade reaction modulus k_h (Figure 2.8.b) are coefficients given as a function of the soil's shear angle φ'.

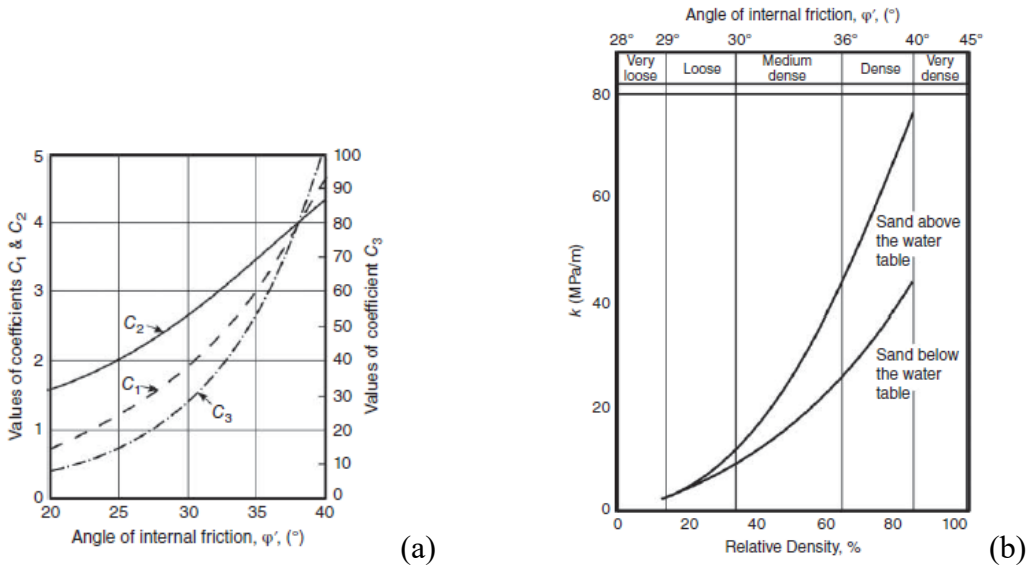

Figure 2.8. Coefficients provided as a function of the soil's shear angle. (a) and initial modulus of subgrade reaction k_h (b) (Fonte: Bhattacharya, 2019).

For typically clayey soils, Bhattacharya (2019), Bisoi & Haldar (2014; 2015), and Wang et al. (2018) with reference to design standards, which are based on the experimental works of Matlock (1970) and Reese et al. (1975), present the p-y curve formulation for this type of soil. Considering the parameters z_R and y_c defined by:

$$z_R = 6s_u D_p/(\gamma' + Js_u) \tag{2.45}$$

$$y_c = 2{,}5\ \varepsilon_c\ D_p \tag{2.46}$$

where s_u is the submerged unit weight of the soil and γ' is the undrained shear strength of the clay. ε_c and J are parameters that reflect the load-deflection curve. Bisoi & Haldar (2014) adopt 0.01 and 0.5 for ε_c and J values, respectively. Meanwhile, Wang et al. (2018) considering stiff clay, adopts a value of 0.25 for J.

From the z_R and y_c values, computed by equations above, the soil resistance per pile unit length p (N/m) can be determined for $z \leq z_R$

$$p = \begin{cases} 0{,}50\ p_u\ (y/y_c)^{1/3} & , \quad for\ y \leq 3y_c \\ 0{,}72\ p_u\{1-(1-z/z_R)(y-3y_c)/12y_c\} & , \quad for\ 3y_c < y \leq 15y_c \\ 0{,}72\ p_u & , \quad for\ y > 15y_c \end{cases} \tag{2.47}$$

and for $z > z_R$, considering

$$p = \begin{cases} 0{,}50\ p_u\ (y/y_c)^{1/3} & , \quad for\ y \leq 3y_c \\ 0{,}72\ p_u & , \quad for\ y > 3y_c \end{cases} \tag{2.48}$$

where, the ultimate soil resistance per pile unit length p_u (N/m) for typically clayey soils expressed by:

$$p_u = \begin{cases} 3s_u + \gamma' z + Js_u z/D_p & , \quad for\ z \leq z_R \\ 9s_u & , \quad for\ z > z_R \end{cases} \tag{2.49}$$

The p-y curves for sandy and clayey soils presented in this section are just some examples of p-y curves available in the literature. Several other authors have studied, developed, and proposed expressions for the constitutive behavior predicted for different soil types (Welch and Reese, 1972; Reese and Nyman, 1978; Johnson et al., 2006; Rollins et al., 2005; Simpson & Brown, 2003; Franke and Rollins, 2013; Wang and Reese, 1998; Liang et al., 2009).

As previously described, the approach to soil-structure interaction using the distributed spring model considers the pile supported laterally by independent springs, without interaction between adjacent springs. These springs represent the soil reaction to foundation deflection with the system (soil-structure) mechanical behavior described by p-y curves.

Meanwhile, the pile can be modeled using analytical formulations or through numerical methods, typically, employing beam elements or frame elements to discrete models. The spring elements' stiffness is determined from the p-y curve slope.

(Damgaard et al. (2013) uses numerical integration method to determine the p-y curve secant stiffness, thereby establishing the spring stiffness. Meanwhile, Carswell et al. (2015) and Bouzid (2018) compute the spring stiffness K_{py} (Equation (2.52) by taking the p-y curve derivative with respect to y and multiplying by the pile tributary length l_i (commonly one meter).

$$K_{py} = l_i \frac{dp}{dy} = l_i\ E_{py} \tag{2.50}$$

For typically sandy soils represented by the p-y curve in Eq. ((2.42.), we have:

$$K_{py} = l_i \, E_{py} = l_i \, \frac{dp}{dy} = l_i \, \left\{ k_h \, z \left(1 - \tanh^2 \frac{k_h \, z}{\lambda \, p_u} y \right) \right\} \tag{2.51}$$

For the monopile-supported OWT analysis with soil-structure interaction some authors (Amar Bouzid, 2018; Carswell et al., 2015; Damgaard et al., 2013) assume the springs linearization based on the initial secant stiffness, given by:

$$K_{py} = l_i \, \left. \frac{dp}{dy} \right|_{y=0} = l_i \, (k_h \, z) \tag{2.52}$$

For small vibrations, due to the general behavior of OWTs, modeling the springs as linear elements (inside an elastic regime) for modal analysis is commonly accepted in the literature. Also, some authors (Kallehave et al., 2012; Sørensen, 2012; Sørensen et al., 2010; Wiemann et al., 2004) propose an analytical formulation and alteration for the initial stiffness by considering the pile geometry and stiffness.

Moreover, the distributed springs methodology with a constitutive relationship demonstrated by p-y curves has been employed for OWT modal analysis (Ferreira et al., 2024), for dynamic analysis considering various scenarios such as rotor-stopping vibration (Damgaard et al., 2013), for wind and waves loads analysis in wind turbines (Bisoi & Haldar, 2014; P. Wang et al., 2018) and extreme events like earthquakes (Medina et al., 2023; Padrón et al., 2022). Additionally, different authors have assessed the structural effects on OWT (tower and monopile) due to dynamic actions using soil-structure interaction through p-y curves, for risk mitigation and performance incrementation using passive devices (Colherinhas et al., 2024), for a fragility analysis (Hemmati et al., 2019), for a confidence study developed (Carswell et al., 2015), or for scour effects evaluation on monopile foundations (Sørensen & Ibsen, 2013). Furthermore, significant standards refer to this methodology for OWTs design.

2.3.3 ADVANCED METHODS

The approach of soil-structure interaction using advanced methods aims for a robust and detailed analysis of foundations and soil. Numerical methods employed for such analysis include finite element methods, discrete element methods, finite difference methods, etc. Traditionally, the Finite Element Method (FEM) is the most widely used..

The model and structural analysis of foundation design using advanced numerical methods enable detailed sizing for the foundation and, consequently, for the turbine. It is possible to incorporate complex soil behavior into the numerical model, such as appropriate material properties, constitutive models (elastic, nonlinear elastic, plastic), and stratified and varied profiles according to different locations (Kaynia, 2021).

The approach with advanced methods allows addressing soil behavior under cyclic loading conditions. By accurately considering the constitutive model of the soil, it becomes possible to reproduce the more realistic behavior of soil under dynamic loading conditions (Andersen, 2015; Jostad et al., 2014).

The use of advanced numerical methods allows for estimating the deformation mobilized in the soil field near the foundation and determining changes in soil strength due to loading cycles. The discrete element model of soil facilitates incorporating results from advanced soil testing, such as in the PISA project for piles (Byrne et al., 2017, 2019). In this approach, the numerical model is structurally employed to obtain foundation stiffness, deflection, and moment in the pile in the presence of soil.

Results obtained from advanced analysis can be applied to calibrate the springs (Figure 2.9), either through simplified methods (Abed et al., 2016; Aissa et al., 2017) or through distributed springs (Amar Bouzid et al., 2013; B. W. Byrne et al., 2019; Kaynia, 2021). This methodology has been well developed and explored in literature, as spring methods (especially p-y springs) demonstrate good application characteristics, understanding, and computational efficiency (Byrne et al., 2019), enjoying widespread acceptance in the industry.

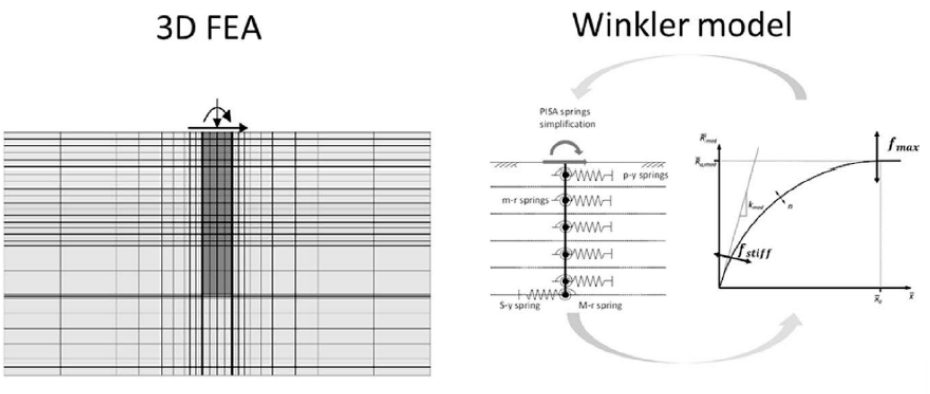

Figure 2.9. Joint approach to the phenomenon of soil-structure interaction using numerical and p-y spring methods (Source: Kaynia, 2021).

This combined approach to the soil-structure interaction phenomenon using advanced and simplified methods presents significant prospects for foundation design.

Initially, the complex behavior of the soil is simulated using finite element or discrete element methods. Subsequently, equivalent springs are derived based on the results obtained from numerical models. This results in greater computational efficiency for structural analysis and the sizing of both the foundation and the wind turbine.

3. RANDOM VIBRATION

The loads which Offshore Wind Turbines are subjected, such as wind and wave, are random in nature. The structure dynamic analysis can be taken and determined in stochastic terms (Clough & Penzien, 2003; Newland, 2003; Blessmann, 2005; Borri & Pastò, 2006; Li & Chen, 2009; Inman, 2014) since the load is understood as a random process. The forces are considered stationary, where the process statistical moments (mean, square mean, variance and standard deviation) are invariant for any instant in time.

We can consider the structure response $x(t)$ subjected to an arbitrary force $f(\tau)$ as:

$$x(t) = \int_{-\infty}^{+\infty} h(t-\tau) f(\tau) d\tau \tag{3.1}$$

where $f(\tau)$ is the force that represents the stationary random process and $h(t-\tau)$ is the structure response function. It is assumed that $x(t) = 0$ for $(t-\tau) < 0$, that is, the response is zero when it is evaluated an instant before the force application. Considering the variable change $\theta = t - \tau$, we have:

$$x(t) = \int_{-\infty}^{+\infty} h(\theta) f(t-\theta) d\theta \tag{3.2}$$

assuming $h(\theta) = 0$ for $\theta < 0$.

To analyze the OWT vibration under random loads $f(\theta)$, the autocorrelation function is employed. The autocorrelation function $R_{xx}(\tau)$ is determined as the expectation $E(\cdot)$ between the process sampled at time t and time $t + \tau$:

$$E[x(t)x(t+\tau)] = R_{xx}(\tau) \tag{3.3}$$

Introducing the value of $x(t)$ expressed in Equation (3.2), we have

$$\begin{aligned} E[x(t)x(t+\tau)] &= E\left[\int_{-\infty}^{+\infty} h(\theta_1) f(t-\theta_1) d\theta_1 \int_{-\infty}^{+\infty} h(\theta_2) f(t+\tau-\theta_2) d\theta_2\right] \\ &= \int_{-\infty}^{+\infty} h(\theta_1) d\theta_1 \int_{-\infty}^{+\infty} h(\theta_2) d\theta_2 \; E[f(t-\theta_1) f(t+\tau-\theta_2)] \\ &= \int_{-\infty}^{+\infty} h(\theta_1) d\theta_1 \int_{-\infty}^{+\infty} h(\theta_2) d\theta_2 \; R_{ff}(\tau) \end{aligned} \tag{3.4}$$

Using the Fourier Transform (Eq. (3.5) and the inverse Fourier Transform (Eq. (3.6) it is possible to express the relationship between the autocorrelation function $R(\tau)$ and the power spectral density $S(\omega)$ of the random process as:

$$S(\omega) = \frac{1}{2\pi}\int_{-\infty}^{+\infty} R(\tau)e^{-i\omega\tau}d\tau \tag{3.5}$$

$$R(\tau) = \int_{-\infty}^{+\infty} S(\omega)e^{i\omega\tau}d\omega \tag{3.6}$$

Applying the inverse Fourier Transform relation (3.6) to $R_{ff}(\tau)$, we obtain:

$$\begin{aligned} R_{xx}(\tau) = \int_{-\infty}^{+\infty} h(\theta_1)d\theta_1 \int_{-\infty}^{+\infty} h(\theta_2)d\theta_2 \; R_{ff}(\tau) = \\ = \int_{-\infty}^{+\infty} h(\theta_1)d\theta_1 \int_{-\infty}^{+\infty} h(\theta_2)d\theta_2 \int_{-\infty}^{+\infty} S_{ff}(\omega)e^{i\omega(\tau-\theta_2+\theta_1)}d\omega \\ = \int_{-\infty}^{+\infty} \left[\int_{-\infty}^{+\infty} h(\theta_1)d\theta_1 \int_{-\infty}^{+\infty} h(\theta_2)d\theta_2\right] S_{ff}(\omega)e^{i\omega(\tau-\theta_2+\theta_1)}d\omega \\ = \int_{-\infty}^{+\infty} \left[\int_{-\infty}^{+\infty} h(\theta_1)e^{i\omega\theta_1}d\theta_1 \int_{-\infty}^{+\infty} h(\theta_2)e^{-i\omega\theta_2}d\theta_2\right] S_{ff}(\omega)e^{i\omega\tau}d\omega \end{aligned} \tag{3.7}$$

In the expression above, the two integrals inside the bracket represent the structure frequency response function H and its conjugate H^*. Rewriting this expression, we have

$$R_{xx}(\tau) = \int_{-\infty}^{+\infty} H(\omega)\, H^*(\omega)\, S_{ff}(\omega)e^{i\omega\tau}d\omega \tag{3.8}$$

or, simply, by observing the inverse transform in Equation (3.6):

$$S_{xx}(\omega) = |H(\omega)|^2\, S_{ff}(\omega) \tag{3.9}$$

where S_{xx} is the OWT response power spectrum. It's relevant to elucidate that the equation above represents the random force input into the system and its response. The random force is characterized by its power spectrum S_{ff} and the system by the frequency response function H.

After defining the autocorrelation function for the random process and considering the loading stationary properties, we can characterize the OWT random

response from the first and second order statistic moments (mean μ_x and variance ${\sigma_x}^2$, respectively), by:

$$E[x(t)] = E[x] = \mu_x \tag{3.10}$$

$${\sigma_x}^2 = E\{[x(t) - \mu_x][x(t+\tau) - \mu_x]\} = R_{xx}(\tau) - \mu_x^2 \tag{3.11}$$

For the analysis of stationary random processes, the standard procedure separates the static component and the dynamic (fluctuating) component. Where, the first relates to the mean and the second to the variance. Considering $\tau = 0$, we have:

$${\sigma_x}^2 = E[x(t)^2] = R_{xx}(0) = \int_{-\infty}^{+\infty} |H(\omega)|^2 S_{ff}(\omega) d\omega \tag{3.12}$$

3.1 FREQUENCY RESPONSE FUNCTION

The SDOF frequency response function for any kind of loading is easily determined. The dynamic equilibrium equation for a damped structural system represented solely by a SDOF is given as:

$$m\,\ddot{x}(t) + c\,\dot{x}(t) + k\,x(t) = f(t) \tag{3.13}$$

where m, c, and k represent, respectively, the system mass, damping, and stiffness. $x(t)$ is the oscillating structure displacement, while the over dot represents differentiation in time.

Considering a harmonic force $f(t)$ expressed in the complex domain

$$f(t) = F_0 e^{i\omega t} \tag{3.14}$$

and the structure particular solution $x_p(t)$ given by

$$x_p(t) = X_0 e^{i\omega t} \tag{3.15}$$

Substituting these terms in Eq. (3.13) we have

$$X_0 = H(\omega) F_0 \tag{3.16}$$

where,

$$H(\omega) = \frac{1}{(k - \omega^2 m + i\omega c)} \tag{3.17}$$

The structure response amplitude X_0 in the frequency domain depends on the harmonic force amplitude F_0 and the function $H(\omega)$, so called the frequency response function.

A discrete structure represented numerically by multiple degrees of freedom (MDOF) has its dynamic equilibrium given by Equation (2.24). For the discrete structure the frequency response function is expressed by:

$$\boldsymbol{H}(\omega) = [\boldsymbol{k} - \omega^2\, \boldsymbol{m} + \imath\, \omega\, \boldsymbol{c}]^{-1} \tag{3.18}$$

where,

$$\boldsymbol{H}(\omega) = \begin{bmatrix} H_{11}(\omega) & \cdots & H_{1n}(\omega) \\ \vdots & \ddots & \vdots \\ H_{n1}(\omega) & \cdots & H_{nn}(\omega) \end{bmatrix} \tag{3.19}$$

The OWT is characterized by the frequency response function $\boldsymbol{H}(\omega)$ under random loading expressed in terms of its power spectrum $\boldsymbol{S_{ff}}(\omega)$ has its structural response computed through the power spectrum $\boldsymbol{S_{xx}}(\omega)$ (Figure 3.1). Expanding Equation (3.9) to a discrete structure with MDOF, we have

$$\boldsymbol{S_{xx}}(\omega) = |\boldsymbol{H}(\omega)|^2\, \boldsymbol{S_{ff}}(\omega) \tag{3.20}$$

with

$$\boldsymbol{S_{xx}}(\omega) = \begin{bmatrix} S_{x_1x_1}(\omega) & \cdots & S_{x_1x_n}(\omega) \\ \vdots & \ddots & \vdots \\ S_{x_nx_1}(\omega) & \cdots & S_{x_nx_n}(\omega) \end{bmatrix} \tag{3.21}$$

$$\boldsymbol{S_{ff}}(\omega) = \begin{bmatrix} S_{f_1f_1}(\omega) & \cdots & S_{f_1f_n}(\omega) \\ \vdots & \ddots & \vdots \\ S_{f_nf_1}(\omega) & \cdots & S_{f_nf_n}(\omega) \end{bmatrix} \tag{3.22}$$

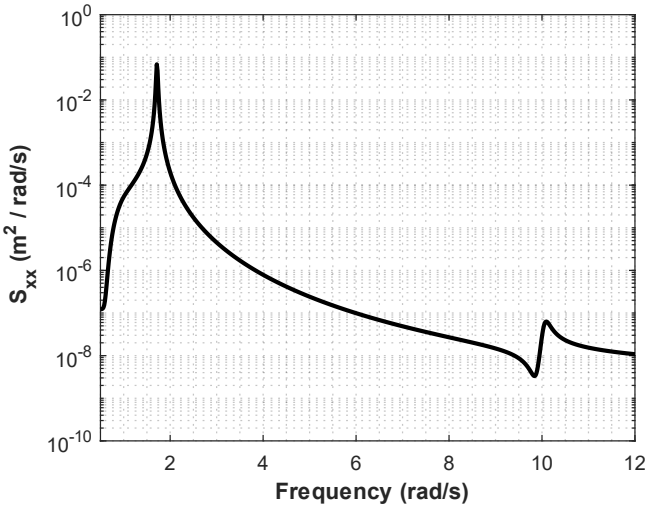

Figure 3.1. Response spectrum of the discrete structure under random wind and wave actions.

3.2 WIND LOAD ON THE OWT SUPPORT STRUCTURE

Atmospheric turbulence produces a fluctuating wind load (gust) that can cause considerable forces on the structure over time. Depending on the excitation frequency, the OWT can have its dynamic response amplified and present accelerations, displacements, deformations and stresses relevant to service and/or ultimate performance.

For the OWT random vibration analysis under wind loading along the tower and the monopile above mean sea level the force power spectral density matrix $\boldsymbol{S_{ff}}$ (Eq. (3.9)) is consequence of the wind turbulence (fluctuating portion). The wind load spectrum is obtained from the longitudinal wind speed.

The longitudinal wind loading (Blessmann, 2005; Borri & Pastò, 2006) is represented by the drag force generated in the structure. From its density ρ_a, the wind area incidence on the structure A_i, the pressure coefficient related to the drag coefficient C_d, the wind velocity given by the superposition of its average speed $\overline{U}(z)$, and from its floating component (turbulence) $u(z,t)$ we have the longitudinal wind load $f(z,t)$ as:

$$\begin{aligned} f(z,t) &= \frac{1}{2}\rho_a A_i C_d[\overline{U}(z) + u(z,t)]^2 \\ &= \frac{1}{2}\rho_a A_i C_d[\overline{U}(z)^2 + 2\overline{U}(z)u(z,t) + u(z,t)^2\ ] \end{aligned} \tag{3.23}$$

Considering $u(z,t)^2$ negligible when compared to the other terms, we have the wind load given by the sum between the average component $\bar{f}$ and the fluctuating component (turbulence) $f_t(z,t)$

$$f(z,t) = \frac{1}{2}\rho_a A_i C_d \bar{U}(z)^2 + \rho_a A_i C_d \bar{U}(z) u(z,t) = \bar{f}(z) + f_t(z,t) \tag{3.24}$$

where

$$\bar{f}(z) = \frac{1}{2}\rho_a A_i C_d \bar{U}(z)^2 \tag{3.25}$$

$$f_t(z,t) = \rho_a A_i C_d \bar{U}(z) u(z,t) \tag{3.26}$$

For the discrete offshore wind turbine model, we can assume the loading generated by turbulence on the structure at a height z above mean sea surface level, as:

$$f_t(z,t) = \rho_a C_d \bar{U}(z) \int_A u(z,t) dA \tag{3.27}$$

Turbulence can be represented in stochastic terms and considered as a random and stationary process (Blessmann, 2005; Borri & Pastò, 2006; Li & Chen, 2009; Burton et al., 2021). Considering the stationary stochastic process for $f_t(z,t)$ and applying the autocorrelation function (Eq. (3.3)) to statistically characterize the random process, we have:

$$\begin{aligned} R_{f_t f_t}(z,\tau) &= E[f_t(z,t)\, f_t(z,t+\tau)] \\ &= \left[\rho_f C_d \bar{U}(z)\right]^2 \int_A \int_A E[u(z,t)\, u(z,t+\tau)] dA dA \\ &= \left[\rho_f C_d \bar{U}(z)\right]^2 \int_A \int_A R_{uu}(z,\tau) dA dA \end{aligned} \tag{3.28}$$

Applying the Fourier transform (Eq. (3.5)), the turbulent wind loading spectrum can be defined as:

$$S_{f_t f_t}(z,f) = \left\{\rho_f C_d \bar{U}(z)\right\}^2 S_{u_i u_j}(z,f) \tag{3.29}$$

As elucidated in Blessmann (2005), Borri & Pastò (2006), Li & Chen (2009), and Burton et al. (2021), for the above equation, a unitary value was considered for the

aerodynamic admittance. Furthermore, considering the discretized structure in MDOF, the turbulent wind spectrum includes spatial correlation information, expressed by:

$$S_{u_i u_j}(z,f) = \sqrt{S_{u_i u_i}(z_1,f)\, S_{u_j u_j}(z_2,f)}\; Coh(z_1,z_2,f) \tag{3.30}$$

where S_{uiuj} is the wind cross spectral density between the vertical coordinates i and j and defined the wind auto spectrum $S_{u_i u_i}$ and $S_{u_j u_j}$ related to wind fluctuations at the vertical coordinates z_i and z_j. The coherence function $Coh(z_i, z_j, f)$ describes the turbulence spatial correlation between two points separated vertically. The coherence function is given by:

$$Coh\big(z_i, z_j, f\big) = \exp(-12\Delta z\ [\,(f/\,\overline{U})^2 + (0.12/L_c\,)^2\,]\,) \tag{3.31}$$

where L_c is the coherence scale parameter (assumed equal to L_k) and Δz is vertical distance between points z_i and z_j.

In the applications and analysis made throughout the thesis, the Kaimal spectrum (Figure 3.2) is considered to characterize the wind longitudinal turbulence load on the structure. The Kaimal spectrum formula (Burton et al., 2021) is expressed as:

$$S_{u_i u_i}(z,f) = \frac{4\,\sigma_k^2\, L_k/\overline{U}(z)}{\left(1 + 6f\ \dfrac{L_k}{\overline{U}(z)}\right)^{5/3}} \tag{3.32}$$

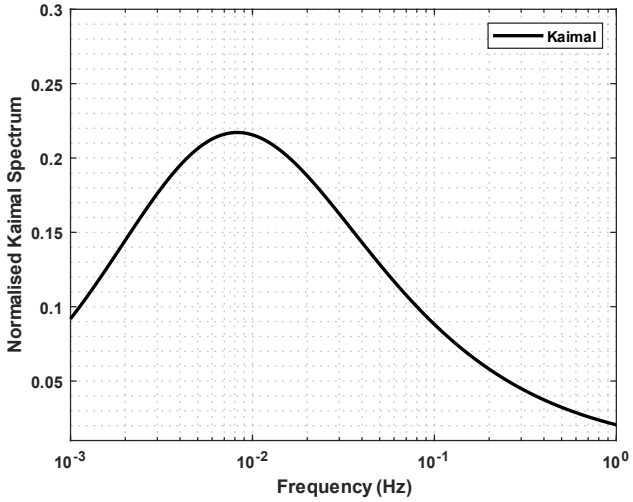

Figure 3.2. Normalized Kaimal spectrum ($fS_{uu}(f)/\sigma_k^2$).

The mean wind velocity $\overline{U}(z)$ for different heights z is calculated using the following potential law:

$$\overline{U}(z) = \overline{U}_{ref}\left(\frac{z}{z_{ref}}\right)^{\alpha} \tag{3.33}$$

where $\overline{U}_{ref}$ is the reference mean velocity at a given reference height z_{ref}, z is the analyzed height (vertical coordinate), and α is the wind shear exponent. For the longitudinal wind ($k = 1$), we have (Burton et al., 2021)

$$\sigma_1 = I_{ref}\ (0{,}75\ \overline{U}_{ref} + 5.6) \tag{3.34}$$

σ_1 represents the standard deviation of the wind speed variations about the mean wind and I_{ref} the reference value of the turbulence intensity. L_k is related to a scale integral parameter and for the longitudinal turbulence it is expressed by

$$L_1 = 8.1\ \Lambda_1 \tag{3.35}$$

where,

$$\Lambda_1 = 42\ m \text{ or } 0.7z \text{ , for } z < 60\ m \tag{3.36}$$

For the OWT analysis due to aerodynamic loading on the support structure (tower and monopile), the process begins with assembling the spectral matrix for longitudinal turbulence speed. A spectral matrix related to the longitudinal turbulence speed is created, according to the discrete structure. The turbulence spectrum matrix is then used to generate a spectral matrix of turbulence drag forces. These drag forces are applied to the tower and monopile above the mean sea level. This process simulates the aerodynamic loading due to turbulence in the vibration analysis of the OWT support structure.

3.3 WIND LOAD ON THE OWT BLADES

Wind loads in the OWT are of great importance. In addition to the wind turbulence that reaches the structure, the turbulence in the rotating blades (Figure 3.3) may produce excessive vibrations along the structure. The rotor experiences a thrust force in the OWT out-of-plane direction caused by passings gusts during the blade's

rotation. The wind fluctuation over the blades can be expressed in terms of the turbulence intensity and the correlation function for wind fluctuations (gusts) taken at different blade radii (Murtagh et al., 2005; Sarkar & Chakraborty, 2017; Colherinhas et al., 2020; Burton et al., 2021). Also, a power spectrum related to the phenomena describes how the energy content of a burst is distributed over different frequencies.

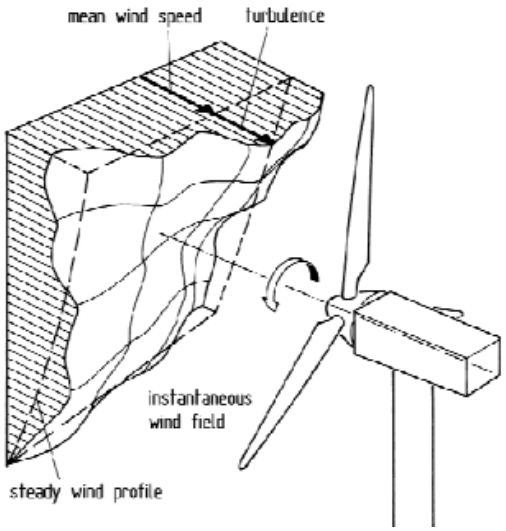

Figure 3.3. Passing gust during blades rotation (Source: Hau, 2013).

The representation and application of the turbulence load over the blades in the frequency domain takes basic assumptions, such as: the linear relationship between wind fluctuations and the resulting loads; the flexibility of the blade is not considered, being assumed completely rigid; the blades have constant local torsion, that is, they do not have a pitching movement; the blade remains unstalled, i.e., the variation of the lift coefficient with the angle of attack ($dC_l/d\alpha_b$) is constant (usually adopted as 2π); the drag term is ignored; the wake is 'frozen', that is, the induced speed remains constant despite fluctuations (Burton et al., 2021). Also, considering the turbulence scale much higher in relation to the blade radius, we have the blade root bending moment standard deviation in the OWT out-of-plane direction given by:

$$\sigma_M = \left(\frac{1}{2}\rho_a \Omega_\mathrm{r} \frac{dC_l}{d\alpha_b}\right) \sigma_u \int_0^R c(r)\, r^2\, dr \tag{3.37}$$

where σ_u is the standard deviation of gust speed that affects the rotor area, which, due to the frozen wave assumption, is equivalent to the standard deviation of wind turbulence

with undisturbed flow. Furthermore, ρ_a is the air density, Ω_r the rotor rotation frequency, and $c(r)$ is the blade section (Figure 3.4) length (chord) at radius r taken from the blade root.

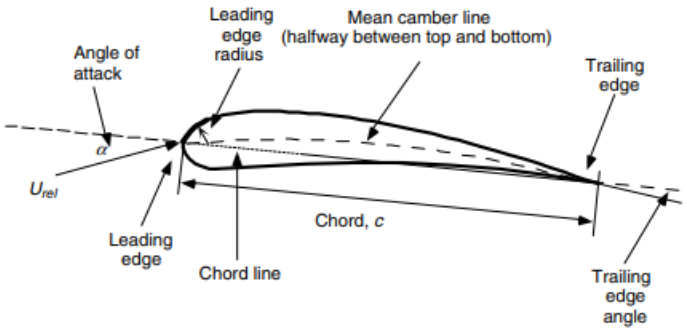

Figure 3.4. Blade section (Source: Manwell, 2009).

As described and presented in Burton et al. (2021), longitudinal wind fluctuations are not perfectly correlated, so the power spectrum generated by the blade's bending moment, due to wind fluctuations that affect the rotor disc, is defined using the correlation function:

$$S_M = \left(\frac{1}{2}\rho_a \Omega_r \frac{dC_l}{d\alpha_b}\right)^2 \int_0^R \int_0^R S_u^o(r_i, r_j, f_k) c(r_i) c(r_j) r_i^2 r_j^2 dr_i dr_j = \\ = \left(\frac{1}{2}\rho_f \Omega_r \frac{dC_l}{d\alpha_b}\right)^2 \sum_{i=1}^{m}\sum_{j=1}^{m} S_u^o(r_i, r_j, f_k) c(r_i)\, c(r_j)\, r_i^2 r_j^2 (\Delta r)^2 \quad (3.38)$$

where $c(r_i)$ and $c(r_j)$ are the lengths of the blade section at points (radii) r_i and r_j and Δr is the distance between radii r_i and r_j. Figure 3.5 presents the rotor thrust power spectrum for the NREL 5-MW Reference Offshore Wind Turbine (Jonkman et al., 2009; Jonkman & Musial, 2010) determined as presented in Equation (3.38).

The rotationally sampled power spectrum S_u^o for points r_i and r_j of the rotating blade is determined through the rotationally correlation function κ_u^o.

$$S_u^o(r_i, r_j, f_k) = 2\int_0^T \kappa_u^o(r_i, r_j, \tau)\cos(2\pi f_k \tau)\, d\tau \quad (3.39)$$

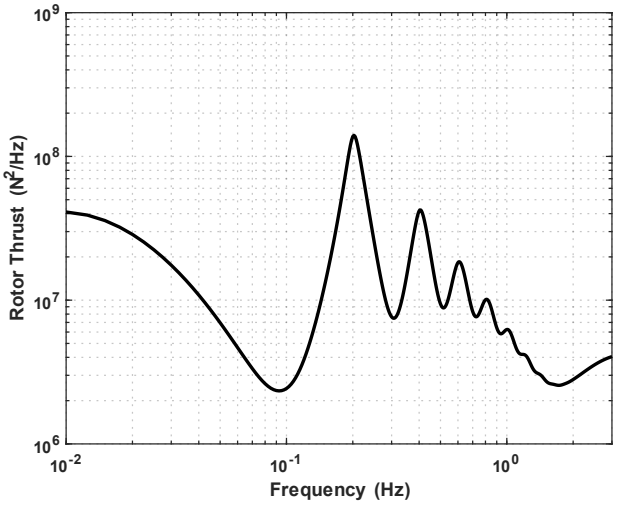

Figure 3.5. NREL 5-MW Reference OWT rotor thrust spectrum.

In practice, the rotationally sampled spectrum S_u^o is calculated using the Discrete Fourier Transform (DFT). To establish the correlation functions as periodic with respect to period T, the rotationally autocorrelation function and the cross-correlation function for $\tau > T/2$ are shifted from $\kappa_u^o(r_i, T-\tau)$ and $\kappa_u^o(r_i, r_j, T-\tau)$). Thus, with κ_u^{*o} (where the asterisk highlights the function shifted from $-\tau$ to $\tau > T/2$) the DFT of the rotational spectrum is expressed by:

$$S_u^o(r_i, r_j, f_k) = 2T\left[\frac{1}{N}\sum_{p=0}^{N-1}\kappa_u^{*o}(r_i, r_j, kT/N)\cos(2\pi f_k/N)\right] \tag{3.40}$$

where N instants are considered over the period T and for frequencies $\omega_k = k/T$ (with $k = 1, 2, \ldots, N-1$). The sum is calculated using the FFT algorithm with $N = 2^{12}$ and the wind turbulence duration as $T = 400\ s$. It is worth noting that the number of points analyzed directly affects the quality and precision of the results (Burton et al., 2021).

The rotationally sampled spectrum S_u^o for $r_i = r_j$ is computed from the rotationally autocorrelation function $\kappa_u^o(r_i, \tau)$ given by

$$\kappa_u^o(r,\tau) = \frac{2\sigma_k^2}{\Gamma(1/3)}\left(\frac{s/2}{1.34L_k}\right)^{\frac{1}{3}} \left[\mathrm{K}_{1/3}\left(\frac{s}{1.34L_k}\right) - \frac{s}{2\cdot 1.34L_k}K_{2/3}\left(\frac{s}{1.34L_k}\right)\left(\frac{2r\,\mathrm{sen}(\Omega_r\tau/2)}{s}\right)^2\right] \tag{3.41}$$

where K is a Bessel function, L_k is defined in Equation (3.35), Ω_r is the rotor frequency related to its rotations per minute (rpm), and s is the separation distance (Figure 3.6) between a fixed point and a position seen by a point at a radius r (or two radius) on the rotating blade is computed by:

$$s^2 = \overline{U}^2\tau^2 + 4{r_i}^2 \sin^2(\Omega_r\tau/2) \tag{3.42}$$

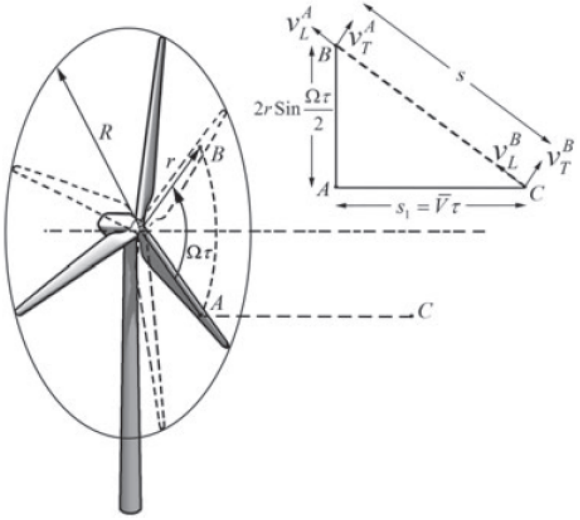

Figure 3.6. Relevant parameters for the rotationally sampled spectrum S_u^o (Source: Sarkar & Chakraborty, 2017).

For different points along the blade ($r_i \neq r_j$) the rotationally cross-correlation function κ_u^o is given by:

$$\kappa_u^o(r_i, r_j, \tau) = \frac{2{\sigma_k}^2}{\Gamma(1/3)}\left(\frac{s/2}{1.34L_k}\right)^{1/3} \left[\mathrm{K}_{1/3}\,\frac{s}{1.34L_k} - \frac{1}{2}\frac{s}{1.34L_k}K_{2/3}\left(\frac{s}{1.34L_k}\right)\left(\frac{r_i^2 + r_j^2 - 2r_i r_j\cos(\Omega_r\tau)}{s^2}\right)\right] \tag{3.43}$$

with s for $r_i \neq r_j$ obtained through:

$$s^2 = \overline{U}^2\tau^2 + r_i^2 + r_j^2 - 2r_i r_j\cos(\Omega_r\tau) \tag{3.44}$$

In short, the rotationally sampled spectrum quantifies the rotor thrust as a consequence of the turbulence load over the OWT rotating blades. The wind fluctuation energy content impinging on the turbine rotor is analyzed all over the blade length. It is worth noting that the OWT blades cut the gusts repeatedly, given that the gust period is

much greater than the blade revolution. When the blade may be thought of as encountering the initial gust after each full revolution, pronounced peaks of energy occur (Figure 3.7). This phenomenon is called gust slicing and explains the peaks shown in the rotationally sampled power spectrum (Figure 3.5).

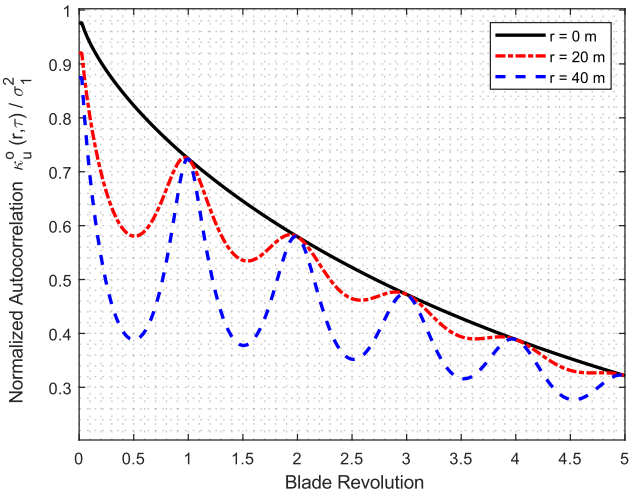

Figure 3.7. Normalized rotationally auto-correlation function for alongwind wind fluctuations seen by points on a rotating blade at different radii.

3.4 WAVE LOAD ON OWT MONOPILE

Besides wind load, wave loads may compromise the OWT performance. Wave load peak frequency approaches the structure natural frequency and the OWT can experience excessive vibrations Next, are presented the basic hypotheses, the boundary conditions and the formulation used to determine the wave load that occurs in the offshore wind turbine OWT monopile. The approach considers the stationary random process of wind waves, as they are commonly called. Thus, the sea behavior is defined based on its power spectrum, where the energy variation in its state is well represented.

Regarding the basic hypotheses to formulate the problem (Brebbia & Walker, 1979; Adams & Barltrop, 1991; Pedroso, 1992; Li & Chen, 2009; Sarpkaya, 2010), the sea is taken as an incompressible, an inviscid, and an irrotational fluid ($\nabla \times \vec{v} = 0$). Based on these hypotheses, we have

$$\vec{v} = \vec{\nabla}\Phi = \left(\frac{\partial \Phi}{\partial x}, \frac{\partial \Phi}{\partial y}, \frac{\partial \Phi}{\partial z}\right) \tag{3.45}$$

where $\Phi(x, y, z)$ is the fluid velocity potential and $\vec{\nabla}$ the gradient vector. A surface with constant Φ and constant potential energy is then defined.

From the hypothesis of incompressibility and considering the conservation of flow mass (Brebbia & Walker, 1979; Pedroso, 1992), we have

$$\frac{d\rho}{dt} + \rho\vec{\nabla} \cdot \vec{v} = 0 \tag{3.46}$$

$$d\rho/dt = 0 \tag{3.47}$$

Thus, by the incompressibility and mass conservation hypothesis:

$$\vec{\nabla} \cdot \vec{v} = 0 \tag{3.48}$$

By introducing Equation. (3.45) in (3.48) we have the condition to be met in the fluid domain, given by:

$$\nabla^2 \Phi = 0 \tag{3.49}$$

Regarding the boundary conditions for the fluid domain (Figure 3.8), the surface height η is considered small, and the surface tension is disregarded, while the bottom is considered horizontal, flat and impermeable (Brebbia & Walker, 1979; Adams & Barltrop, 1991; Pedroso, 1992; Li & Chen, 2009, Sarpkaya, 2010). Thus:

$$\frac{\partial \eta}{\partial t} = \frac{\partial \Phi}{\partial z} \qquad for \quad z = 0 \tag{3.50}$$

$$\frac{\partial \Phi}{\partial t} = -g\eta \quad for \quad z = 0 \tag{3.51}$$

$$\frac{\partial \Phi}{\partial z} = -\frac{1}{g}\frac{\partial^2 \Phi}{\partial t^2} \quad for \quad z = 0 \tag{3.52}$$

$$\frac{\partial \Phi}{\partial z} = 0 \quad for \quad z = -h \tag{3.53}$$

For the plane wave problem (two-dimensional), the following expression is assumed as a solution to the problem:

$$\Phi(x, z, t) = \varphi(x)\, H_\eta(z)\, g(t) \tag{3.54}$$

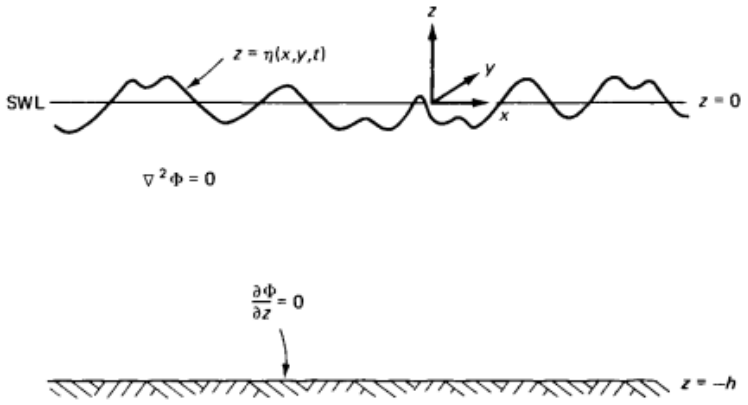

Figure 3.8. Fluid domain (Source: Brebbia & Walker, 1979).

Applying the variable separation method, considering the boundary conditions presented, and the Linear Wave Theory (Brebbia & Walker, 1979; Adams & Barltrop, 1991; Pedroso, 1992; Li & Chen, 2009; Sarpkaya, 2010), we have the following expression:

$$\Phi(x,z,\omega,t) = \frac{A_o g}{\omega}\frac{\cosh[\kappa(z+h)]}{\cosh(\kappa h)}\cos(\kappa x - \omega t) \tag{3.55}$$

where, A_o is the wave amplitude, g is the gravity acceleration (9.81 m/s²), ω the wave circular frequency (rad/s), h the seabed depth, and z the analyzed depth. The wavenumber κ is determined by the following expression:

$$\omega^2 = g\kappa \tanh(\kappa h) \tag{3.56}$$

The horizontal wave velocity u_x and acceleration $\dot{u}_x$, which will later be used to determine the wave force over the OWT monopile, are obtained by

$$\frac{\partial \Phi}{\partial x} = u_x(x,z,\omega,t) = -A_o\omega\frac{\cosh[\kappa(z+h)]}{\sinh(\kappa h)}\text{sen}(\kappa x - \omega t) \tag{3.57}$$

$$\frac{\partial^2 \Phi}{\partial x \partial t} = \dot{u}_x(x,z,\omega,t) = A_o\omega^2\frac{\cosh[\kappa(z+h)]}{\sinh(\kappa h)}\cos(\kappa x - \omega t) \tag{3.58}$$

To compute the force applied to the OWT monopile (slender and vertical cylinder) due to the action of the wind wave, the well-known Morison formula can be adopted (Brebbia & Walker, 1979; Adams & Barltrop, 1991; Pedroso, 1992; Li & Chen, 2009, Sarpkaya, 2010), which consists of the drag and inertia components superposition (Figure 3.9). Where, the drag force is related to the flow speed passing through the pile, while the inertia force is generated by the fluid acceleration. Thus, from the Morison Equation:

$$f(x,z,\omega,t) = \frac{1}{2}\rho_s C_d D_p |u_x| u_x + \rho_s C_i \frac{\pi D_p^2}{4} \dot{u}_x \tag{3.59}$$

where ρ_s is the density considered for the sea, C_d is the drag coefficient, C_i is the inertia coefficient, and D_p is the pile diameter.

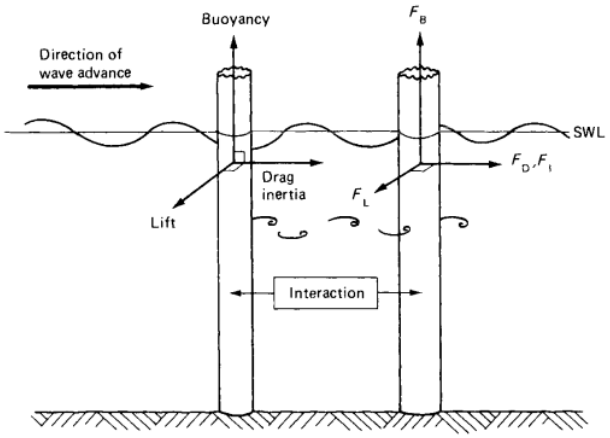

Figure 3.9. Wave force and its components in the monopile (Source: Brebbia & Walker, 1979).

Generally, the use of random vibration analysis assumes a linear analysis. However, drag force presents the nonlinear term for velocity. Through equivalent statistical linearization (Brebbia & Walker, 1979; Adams & Barltrop, 1991; Li & Chen, 2009; Sarpkaya, 2010), we have the linearized Morison Equation given by:

$$f(x,z,\omega,t) = \frac{1}{2}\rho_s C_d D_p \sqrt{8/\pi}\, \sigma_{u_x} u_x + \rho_s C_i \frac{\pi D_p^2}{4} \dot{u}_x \tag{3.60}$$

where σ_{u_x} is wave velocity u_x standard deviation.

If the waves at different points (x, z) are perfectly correlated along the x direction, the random field can be simplified to a random process (Brebbia & Walker, 1979; Adams & Barltrop, 1991; Li & Chen, 2009; Sarpkaya, 2010), given as

$$u_x(x, z, \omega, t) = H_\eta(\omega, z)\, \eta(x, t) \tag{3.61}$$

$$\dot{u}_x(x, z, \omega, t) = H_\eta(\omega, z)\, \dot{\eta}(x, t) \tag{3.62}$$

and due to the perfectly correlated points along x:

$$u_x(z, \omega, t) = H_\eta(\omega, z)\, \eta(t) \tag{3.63}$$

$$\dot{u}_x(z, \omega, t) = H_\eta(\omega, z)\, \dot{\eta}(t) \tag{3.64}$$

Thus, Equation (3.60) can be rewritten as:

$$f(z, \omega, t) = \frac{1}{2}\rho_s C_d D_p \sqrt{8/\pi}\, \sigma_{u_x} H_\eta(\omega, z)\, \eta(t) + \rho_s C_i \frac{\pi D_p^2}{4} H_\eta(\omega, z)\, \dot{\eta}(t) \tag{3.65}$$

As presented previously, a stationary random process $\eta(t)$ can be characterized by the correlation function $R_{\eta\eta}(0)$. From this relationship, the wave random process may be quantified employing the wave power spectrum $S_{\eta\eta}(\omega)$. Thus, the wave force spectrum is given by

$$S_{ff}(\omega, z) = \left[\frac{1}{2}\rho_s C_d D_p \sqrt{8/\pi}\, \sigma_{v_x} + \left(\rho_s C_i \frac{\pi {D_p}^2}{4}\omega\right)^2\right] H_\eta^2(\omega, z)\, S_{\eta\eta}(\omega) \tag{3.66}$$

where

$$H_\eta(\omega, z) = \omega\, \frac{\cosh[\kappa(z + h)]}{\sinh(\kappa h)} \tag{3.67}$$

Many variables and natural conditions control the formation of wind waves. Widely used, the Pierson-Moskowitz (PM) and Joint North Sea Wave Project (JONSWAP) spectrum are applicable for a zero-mean stationary stochastic process $S_{\eta\eta}$. For a given wave frequency f (s^{-1} or Hz) JONSWAP spectrum (IEC, 2009) is defined by:

$$S_{JS}(f) = C(\gamma)\, S_{PM}(f)\, \gamma^{\alpha_{js}} \tag{3.68}$$

The peak shape parameter γ and exponent α_{js} of the peak enhancement factor $\gamma^{\alpha_{js}}$ are determined by:

$$\gamma = \begin{cases} 5 & \text{for} \quad T_p/\sqrt{H_s} \leq 3.6 \\ \exp\left(5.75 - 1.15\, T_p/\sqrt{H_s}\right) & \text{for} \quad 3.6 < T_p/\sqrt{H_s} \leq 5 \\ 1 & \text{for} \quad T_p/\sqrt{H_s} > 5.0 \end{cases} \tag{3.69}$$

$$\alpha_{js} = exp\left[-\frac{\left(f - f_p\right)^2}{2c^2 f_p^2}\right], \qquad \text{for} \qquad c = \begin{cases} 0.07, f \leq f_p \\ 0.09\,, f > f_p \end{cases} \tag{3.70}$$

The peak frequency f_p $(= 1/T_p)$ (Holthuijsen, 2007) is computed from the average wind speed $\overline{U}_{10}$ at a height of 10 meters:

$$T_p = 7.14(1.075 \cdot\ \overline{U}_{10})/g \tag{3.71}$$

Finally, the Pierson-Moskowitz S_{PM} spectrum (British Standards Institution., 2009) is given by the following expression

$$S_{PM}(f) = 0{,}3125\, H_s^2\, f_p^4\, f^{-5} \exp\left[-1{,}25\left(f_p/f\right)\right] \tag{3.72}$$

where the wave height H_s (Holthuijsen, 2007) can be determined by:

$$H_s = 0.21(1.075 \cdot\ \overline{U}_{10})^2/g \tag{3.73}$$

Figure 3.10 presents an example, taken from (British Standards Institution., 2009), where the Pierson-Moskowitz spectrum and the JONSWAP spectrum are presented. For the sea state the significant wave height H_s is taken as 14.4 m, the peak frequency f_p as 0.065 Hz, and the peak shape parameter γ as 3.3.

Adopting the JONSWAP spectrum for the random process of wind waves $S_{\eta\eta}$, we have the wave load for a given frequency, as (Li & Chen, 2009):

$$S_{ff}(f, z) = \left[\frac{1}{2}\rho_s C_d D_p \sqrt{8/\pi}\, \sigma_{u_x} + \left(\rho_s C_i \frac{\pi {D_p}^2}{4}\omega\right)^2\right] H_\eta^2(\omega, z)\, S_{JS}(f) \tag{3.74}$$

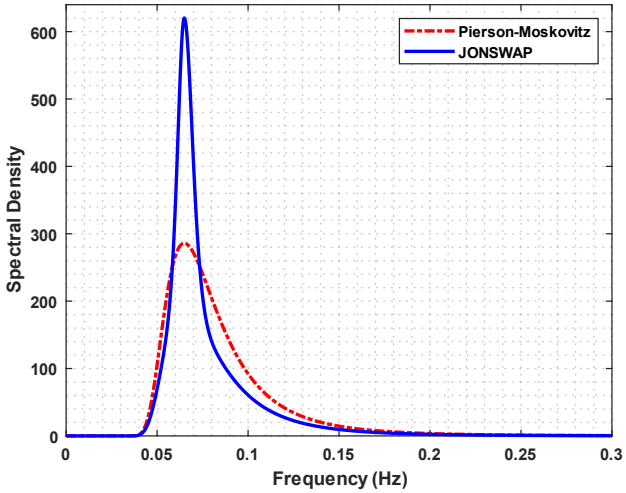

Figure 3.10. Pierson-Moskowitz and JONSWAP spectrum for the given conditions.

3.5 WIND AND WAVE RANDOM LOADS IN TIME DOMAIN

Wind and wave load on the OWT (Figure 3.11) are presented with a fairly approximation when expressed through their PSD (British Standards Institution., 2006, 2009). Based on the related PSD these random loads may be computed in time domain using harmonics. These are detailed in the following section for wind and wave loads.

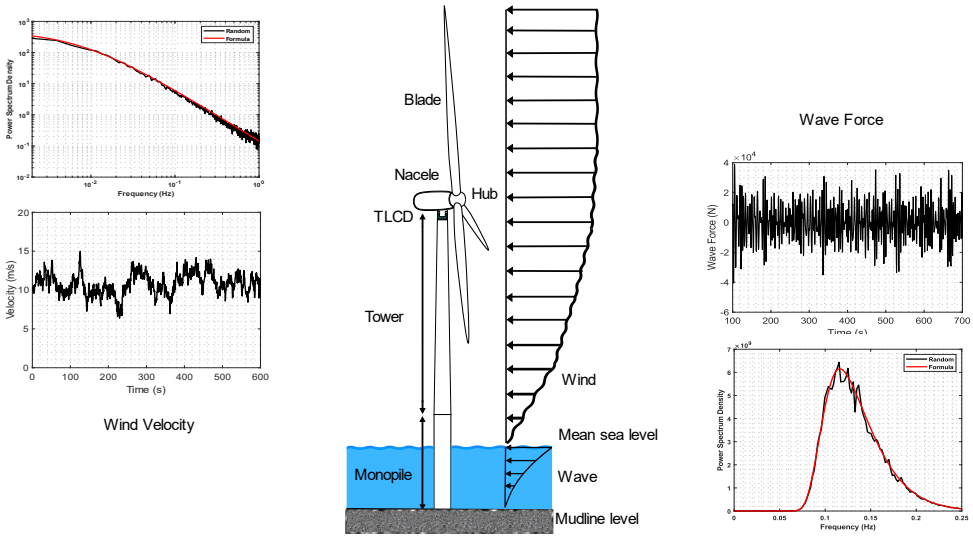

Figure 3.11. OWT with monopile foundation under random wind and wave load in time.

3.5.1 WIND LOAD ON STRUCTURE

The wind force $f(t)$ in the OWT structure is computed by the superposition of a mean component $\bar{f}$ and a turbulent component $f_t(t)$, considered as a stationary

Gaussian stochastic process (Borri & Pasto, 2006; Li & Chen, 2009). The mean component, related to the mean wind speed $\overline{U}(z)$, is given by:

$$\bar{f}(z_i) = \frac{1}{2}\rho_a C_d A_i \overline{U}_i{}^2(z_i) \tag{3.75}$$

The wind turbulent component, considered as a stationary Gaussian stochastic process with zero mean, over time can be understood as the superposition of harmonic functions. The wind gust speed $u_i(t)$ at height z_i can be expressed as follows (Borri & Pasto, 2006):

$$\begin{bmatrix} u_1(t) \\ u_2(t) \\ u_3(t) \\ \dots \\ u_n(t) \end{bmatrix} = \sum_{k=1}^{N} \begin{bmatrix} H_{u_1u_1}(\omega_k) & & & & \\ H_{u_2u_1}(\omega_k) & H_{u_2u_2}(\omega_k) & & & \\ H_{u_3u_1}(\omega_k) & H_{u_3u_2}(\omega_k) & H_{u_3u_3}(\omega_k) & & \\ & & & \dots & \\ H_{u_nu_1}(\omega_k) & H_{u_nu_2}(\omega_k) & H_{u_nu_3}(\omega_k) & \dots & H_{u_nu_n}(\omega_k) \end{bmatrix} \begin{bmatrix} cos(2\pi\omega_k t + \theta_1) \\ cos(2\pi\omega_k t + \theta_2) \\ cos(2\pi\omega_k t + \theta_3) \\ \dots \\ cos(2\pi\omega_k t + \theta_n) \end{bmatrix} \tag{3.76}$$

where $H_{u_iu_j}$ is the harmonic amplitude related to the height z_i, ω_k is the harmonic frequency in rad/s and θ_i the random phase angle from 0 to π. The harmonic amplitude $H_{u_iu_j}$ is determined by (Burton et al., 2021)

$$\begin{aligned} \boldsymbol{S_{u_iu_j}}(\omega_k) &= \boldsymbol{H}_{u_iu_j}(\omega_k) \cdot \boldsymbol{H}_{u_iu_j}(\omega_k)^{-1} \\ &= \begin{bmatrix} H_{u_1u_1}(\omega_k) & & & & \\ H_{u_2u_1}(\omega_k) & H_{u_2u_2}(\omega_k) & & & \\ H_{u_3u_1}(\omega_k) & H_{u_3u_2}(\omega_k) & H_{u_3u_3}(\omega_k) & & \\ & & & \dots & \\ H_{u_nu_1}(\omega_k) & H_{u_nu_2}(\omega_k) & H_{u_nu_3}(\omega_k) & \dots & H_{u_nu_n}(\omega_k) \end{bmatrix} \cdot \\ &\quad \begin{bmatrix} H_{u_1u_1}(\omega_k) & H_{u_2u_1}(\omega_k) & H_{u_3u_1}(\omega_k) & \dots & H_{u_nu_1}(\omega_k) \\ & H_{u_2u_2}(\omega_k) & H_{u_3u_2}(\omega_k) & \dots & H_{u_nu_2}(\omega_k) \\ & & H_{u_3u_3}(\omega_k) & \dots & H_{u_nu_3}(\omega_k) \\ & & & \dots & \\ & & & & H_{u_nu_n}(\omega_k) \end{bmatrix} \end{aligned} \tag{3.77}$$

with $S_{u_iu_j}$ can be found and defined in Eq. (3.30).

The wind drag force on the OWT support structure is computed by superimposing the two components:

$$f_i(t) = \frac{1}{2}\rho_a C_d A_i \{\overline{U}_i + u_i(t)\}^2 \tag{3.78}$$

Figure 3.12 presents the wind speed (mean plus fluctuation) computed at a height z of 80 m for $\overline{U}_{10}$ equal to 11.4 m/s at the reference height z_{ref} of 10 m with wind shear exponent α of 0.14 and the turbulence intensity I_{ref} of 0.14.

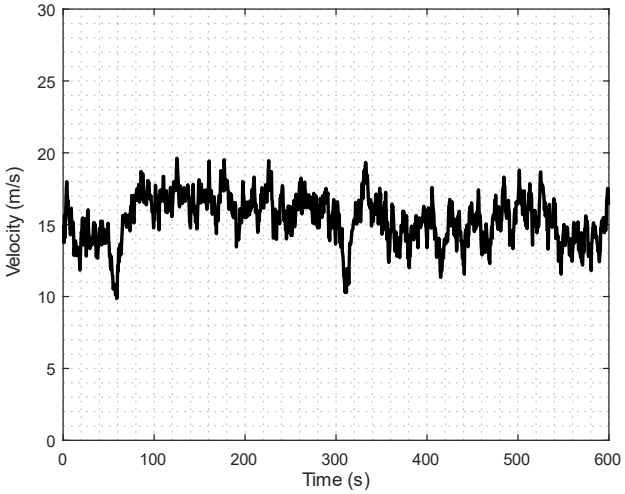

Figure 3.12. Wind speed with the mean wind and turbulence speed superposition.

The wind speed signal in time domain by Equation (3.76) transformed to the frequency domain and compared to the Kaimal spectrum generated by the exact expression (Eq. (3.32)) demonstrates that the random wind signal over time maintains the original spectrum characteristics (Figure 3.13).

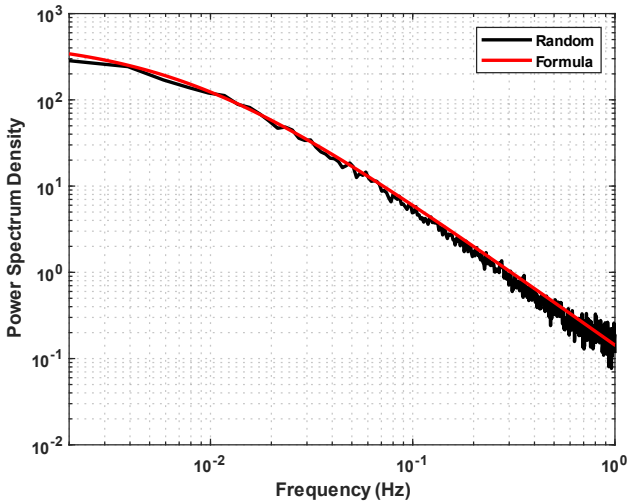

Figure 3.13 Random wind signal compared to Kaimal's expression.

3.5.2 WIND ROTOR THRUST

The thrust force on the rotor due to the wind load on the OWT rotating blades is approximately reproduced (Kjourlag, 2013). The technical reports of NREL 5-MW

Reference WT for Offshore (Jonkman et al., 2009), 10-MW OWT (Bortolotti et al., 2019), and IEA Wind 15-MW Offshore Reference WT (Gaertner et al., 2020) present in their respective documents' curves that define the thrust force on the rotor as a function of the wind speed, as discussed in (Lin et al., 2023). Figure 3.14 presents Thrust curve for the 10-MW OWT (Bortolotti et al., 2019).

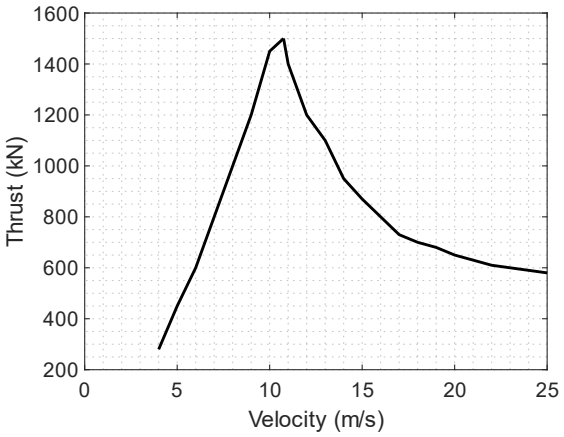

Figure 3.14. 10-MW OWT thrust as a function of wind speed.

In the analysis conducted in this work, the wind speed at the height of the OWT hub is first determined, obtained by the sum of the mean speed $\overline{U}(z)$ and the turbulence speed $u_i(t)$. Subsequently, using fit functions in MATLAB®, which express the thrust force as a function of speed, based on values defined for the NREL 5-MW (Jonkman et al., 2009), the 10-MW OWT (Bortolotti et al., 2019), and the IEA Wind 15-MW (Gaertner et al., 2020), the force on the OWT rotor in time domain is computed (Figure 3.15). The thrust force on the rotor is considered lumped and applied to the last node of the tower.

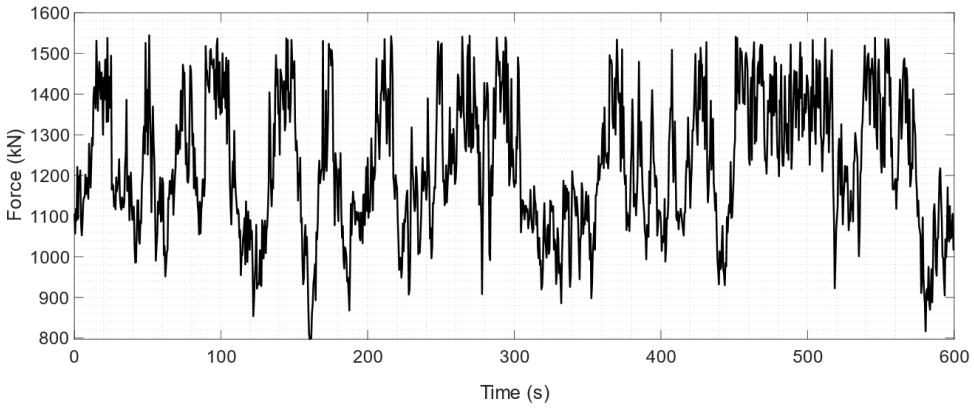

Figure 3.15. 10-MW OWT approximate thrust force in time.

3.5.3 WAVE LOAD

The wave force that impinges on the OWT monopile can be expressed by the Morison formula (Equation (3.59). Considering linear wave theory, the wave speed u and acceleration $\dot{u}$ at a given depth z at time t are given by (Chakrabarti, 2005):

$$u(z,t) = \sum_{i=1}^{N} \frac{H_{\eta_i}\,\omega_i}{\sinh \kappa_i h} \cosh[\kappa_i(h+z)] \cos(2\pi\omega_i t + \theta_i) \tag{3.79}$$

$$\dot{u}(z,t) = \sum_{i=1}^{N} \frac{H_{\eta_i}\,\omega_i^{\,2}}{\sinh \kappa_i h} \cosh[\kappa_i(h+z)] \sin(2\pi\omega_i t + \theta_i) \tag{3.80}$$

where, h is the seabed depth and θ_i a phase angle randomly computed from 0 to π. The wavenumber κ_i is determined iteratively by the expression:

$$\omega_i^{\,2} = g\kappa_i \tanh(\kappa_i h) \tag{3.81}$$

The wave spectral amplitude H_{η_i} is obtained from the JONSWAP spectrum (Eq. (3.68):

$$H_{\eta_i} = \sqrt{2 \int_{\omega_{i-1}}^{\omega_{i+1}} S_{js}(\omega) d\omega} \tag{3.82}$$

Figure 3.16. and Figure 3.17. presents the wave speed and acceleration at the 10 m depth for seabed level of 20 m. The peak frequency and wave height are defined by Equations (3.71) and (3.73) for the average wind speed at 10 m above sea level equal to 11.4 m/s.

The pile considered within his example has a diameter of 6 m. The drag coefficient is assumed to be 1.0 and the inertia coefficient equal to 2.0 for the pile. The sea water density is adopted equal to 1,025.0 g/m³. Considering these parameters and the wave speed and acceleration presented above, the wave force overtime defined by Morison's Equation is presented in Figure 3.18.

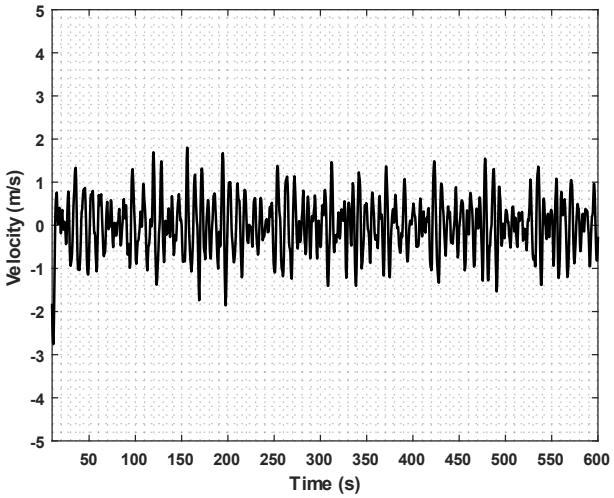

Figure 3.16. Wave speed in time with amplitude related to the JONSWAP spectrum.

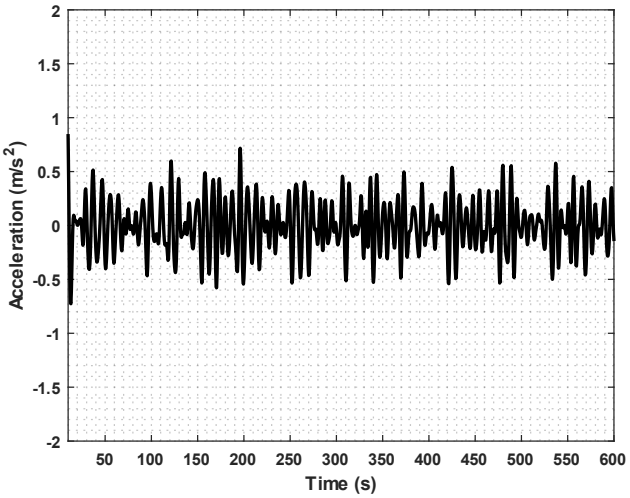

Figure 3.17. Wave acceleration in time with amplitude related to the JONSWAP spectrum.

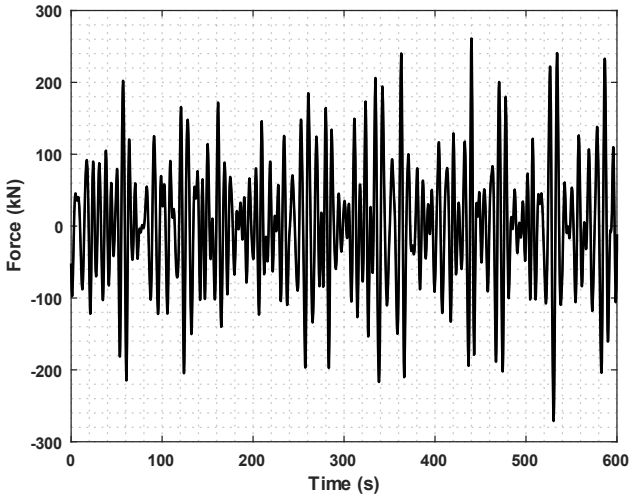

Figure 3.18. Wave load in time domain.

The definition of the wave velocity and acceleration with amplitude related to the JONSWAP spectrum by Equations (3.79) and (3.80) presents a random pattern given the phase angle θ_i random computation. The wave load transform from the signal in time domain to the frequency domain demonstrates that the random signal in time preserves the spectral characteristics of the exact expression (Eq. (3.68)) as shown in Figure 3.19.

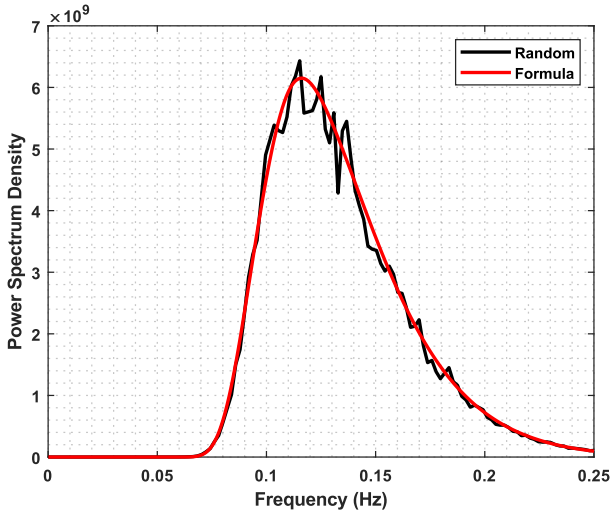

Figure 3.19. Random wave load signal compared to exact expressions.

4. OPTIMAL DESIGN

In recent years, a significant amount of capital has been invested in OWT farm design and construction. Despite a slowdown, 2022 represented the third-best year for the wind energy industry. Furthermore, by 2027 it is estimated that 680 GW of wind capacity will be installed globally, totaling 2 TW in operation by 2030 (Global Wind Energy Council, 2023).

The energy industry seeks optimal solutions that are economical and suitable for offshore wind turbine operation. The OWT support structure (tower, transition piece, and foundation) represents a significant amount of the cost (Stehly et al., 2023). Enhancing the reliability while reducing the material and manufacturing expenditure of the structure is feasible with the use of the Tuned Liquid Column Damper.

The optimal design of the TLCD for controlling vibrations in an OWT requires great effort. OWT are relatively complex structural and mechanical systems located in a highly demanding environment (Petrini et al., 2010). OWTs are subject to random and irregular environmental wind and wave conditions. Thus, the optimal design involving an offshore wind turbine is not a trivial task (Muskulus and Schafhirt, 2014).

Gradient methods (based on calculus) application for the optimal design of the TLCD such as Gao & Kwok (1997), Yalla (2001), Hochrainer & Ziegler (2006) present some limitations for the design accounting the OWT structure and the offshore environment. The use of meta-heuristic algorithms is preferred (Karpat, 2013; Gentils et al., 2017; Martinez-Luengo et al., 2017; Furlanetto et al., 2020; Colherinhas et al., 2021; Colherinhas et al., 2022; Al-Sanaad et al., 2021; Mendes et al., 2023; Yu et al., 2023).

To ensure a gain in structural performance, optimization seeks the optimal TLCD parameters that minimize the response of the OWT. Also, the tuned liquid column damper offers the possibility of additional savings in material and manufacturing of offshore wind turbine support structures. Thus, the simultaneous optimal design of the OWT and TLCD is also studied and proposed. For the optimization process in these cases, the Genetic Algorithms (GA) method is used.

Genetic Algorithms (GAs) were created and developed by John Henry Holland, his students, and colleagues at the University of Michigan during the 1960s and 1970s (Mitchell, 1998). The original objective was to formally study the adaptation phenomena occurring in nature. Goldberg (1989) introduced GAs as an optimization

technique in his book "Genetic Algorithms in Search, Optimization, and Machine Learning," through simulations of genetic systems.

Genetic Algorithms (GAs) have expanded across the academic community with applications in a variety of unconventional problem domains. GAs finds applications in various scientific fields, including optimization problems, machine learning, development of strategies and mathematical formulas, economic model analysis, engineering problems, and diverse applications in Biology. Examples include simulating bacteria, immune systems, ecosystems, and discovering the structure and properties of organic molecules (Mitchell, 1998; Luque & Alba, 2013).

Computational resources for numerical modeling have been increasingly in demand. Evolutionary computation has enabled the solution of multi-objective optimization problems, allowing for the simultaneous analysis of various design parameters. Below are presented parts of the workflow that comprise the Genetic Algorithm routine (Colherinhas, 2016; Colherinhas et al., 2020) adopted in this thesis.

4.1 GENETIC ALGORITHM COMPUTATIONAL ROUTINE

Figure 4.1 presents the algorithm flow. Initially, the first population is created with chromosomes (individuals' cases of OWT with TLCD) that have genes (OWT or TLCD parameters) determined from a random distribution within pre-established limits (minimum values L_i and maximum values L_s associated with the individuals' genes). These chromosomes or individuals have their value defined by the objective function through the analysis of one or more variables. The chromosomes undergo a selection process where the fittest (defined by the value associated with the objective function) have a greater ability to transfer their characteristics to the next generation of individuals through crossover. A small portion of the population may have their genetic information altered through a mutation process. Deterministic methods such as elitism can ensure that a percentage of the best individuals are present in the next generation, while decimation eliminates a percentage of the worst individuals. The algorithm terminates at the end of the specified number of generations N_{ger}.

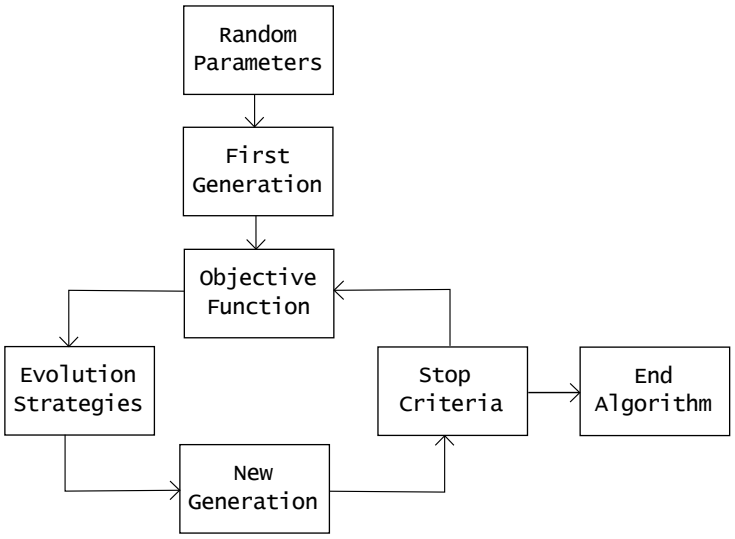

Figure 4.1. Genetic Algorithm flowchart for optimizing the TLCD or OWT parameters.

4.1.1 OBJECTIVE FUNCTION

The designation of the objective function $f_{obj}(i)$ is self-explanatory. It denotes the analysis of the optimization objective through a function, where the variable or parameter analyzed expresses the target of the optimization process. The goal is to maximize or minimize the defined variable or parameter for the analyzed problem.

Commonly, the objective function for a vibration control optimization assesses the structural response (displacements, accelerations, inter-story displacements, etc.) based on the parameters of the control device (Farshidianfar & Soheili, 2014; Colherinhas et al., 2020; Mendes et al., 2023). Meanwhile, for the OWT structures optimal design the focus relies on the structure's volume determined by tower and foundation parameters (Uys et al., 2006; Karpat, 2013; Gentils et al., 2017; Martinez-Luengo et al., 2017; Furlanetto et al., 2020; Al-Sanaad et al., 2021).

4.1.2 SELECTION

After evaluating the objective function for the N individuals in the population, a dedicated algorithm separates individuals (cases of OWT with TLCD) with the best parameters (evaluated according to the objective function) through random choices. Selection depends on the score assigned to each case. Among various selection approaches, the Roulette Wheel Selection method is employed (Katoch et al., 2021).

This is a classic method of proportional selection, where the probability P_i to one case i among a generation of N cases to be selected depends on the value associated

with the established objective function. This probability, also referred to as "slice," is expressed as:

$$P_i = \frac{f_{obj}(i)}{\sum_{i=1}^{N} f_{obj}(i)} \tag{4.1}$$

A case with a higher objective function value $f_{obj}(i)$ and a higher probability P_i has a greater chance of being selected. Subsequently, the cumulative probability q_i, defined as the sum of probabilities P_k, is given by

$$q_i = \sum_{k=1}^{i} P_k \tag{4.2}$$

The selection of case i for the subsequent stages of the algorithm depends on the following condition $rand < q_i$. Where $rand$ is a random value between zero and one.

4.1.3 CROSSOVER

Crossover, unlike elitism and culling, operates with the probability of individuals crossing over within the population. Descendants (new individuals) for the next generation are generated from this crossover, ensuring gene exchange. Thus, a new population is created, ensuring that genes are passed on. This step is crucial for subsequent generations, so it is advisable to adopt a crossover probability above 60% to ensure that more than half of the individuals produce offspring and pass on their genes.

For optimization studies in this research, employing the genetic algorithm developed by Colherinhas (2016), the crossover stage adopts the Blend Crossover (BLX-α) method, where a new case z is generated by the following expression from individuals x and y

$$z = x + \beta(y - x) \tag{4.3}$$

with

$$\beta \sim U(-\alpha, 1 + \alpha) \tag{4.4}$$

where U represents a uniform distribution and α is adopted as 0.25. There's a possibility that the descendant z may extrapolate beyond the genes of individuals x and y, precisely due to the use of the coefficient α. Therefore, through this coefficient,

individuals with genes beyond the limits established in the initial parameters can emerge, leading to new solutions and expanding the analysis range within the population. Consequently, there is greater genetic variability among the chromosomes (individuals) of the next generation.

4.1.4 ELITISM AND DECIMATION

Elitism and decimation are based on deterministic selection of individuals from the population based on the objective function. In elitism, a portion of the best cases, or those objectively most fit within the population, are guaranteed to be included in the next generation. Meanwhile, decimation eliminates some cases, specifically those with low fitness, ensuring they are not present in the next generation population. Thus, both deterministic methods aim to improve the next generation's population by selecting and eliminating the most and least fit individuals, respectively.

4.1.5 MUTATION

Mutation introduces randomly generated new information into the next generation. A probability of occurrence is defined for altering the parameter(s) of some cases in the next generation. It is important to note that the probability of mutation should not be high (suggested around 5%) to avoid a new population with individuals having lower objective function values, which could affect the analysis convergence.

In the genetic algorithm, uniform mutation is considered. For individuals undergoing genetic mutation, the altered gene of the individual is randomly selected within the interval $U(L_i, L_s)$, constrained by the lower limit L_i and upper limit L_s.

4.2 TLCD OPTIMIZATION

The optimization process of vibration absorbers dates to classical works such as Den Hartog (1956) and Warburton (1981; 1982). They developed and presented exact formulas to define the tuned vibration absorbers optimal parameters with the aim of minimizing structural vibrations.

Considering the previous approach, Kwok and Gao (1997), Yalla (2001), and Hochrainer and Ziegler (2006) elucidate and present optimal formulas to determine some of the TLCD parameters. The mass ratio μ_f and the aspect ratio α_f (Equations(2.9) and (2.6)) show predictable behavior for reducing the structural response. The work focuses on the formulation to define the optimal TLCD tuning ratio

γ_f and the damping ratio ζ_f. The analytical formulation presented is considered the spring-mass model for the primary system (structure) under different forces.

Proposing formulas for damper optimal parameters is an arduous task and it is not always possible to reach analytical solutions due to the complexity of the systems involved. Thus, robust optimization methods are applied to numerically define the damper parameters that present the best structure performance (Farshidianfar & Soheili, 2014; Colherinhas et al., 2020; Mendes et al., 2023; Colherinhas et al., 2024).

The TLCD optimization process focuses on the optimal tuning ratio γ_f and optimal damping ratio ζ_f search. In the process of finding the parameters that minimize the structural response, the objective function is defined as

$$f_{obj} = \frac{1}{{\sigma_x}^2} \tag{4.5}$$

with

$${\sigma_x}^2 = \int_{-\infty}^{+\infty} |\boldsymbol{H}(\omega)|^2 \boldsymbol{S_{ff}}(\omega) d\omega$$

The discrete OWT with TLCD frequency response matrix $\boldsymbol{H}(\omega)$ is composed according to Equations (2.20)-(2.24), while $\boldsymbol{S_{ff}}(\omega)$ contains the PSDs related to wind and wave action on the turbine. The remaining steps of the process follow the previous description summarized by the flowchart in Figure 4.1.

4.3 OWT AND TLCD SIMULTANEOUS OPTIMIZATION

Equipping the OWT with a TLCD also offers the possibility of additional savings in material and manufacturing of offshore wind turbine support structures (tower and foundation) besides enhancing structural performance. The simultaneous OWT support structure with TLCD optimizing process is based on searching DV values for the wind turbine structure and damper, which present the structure with its minimum volume. The solution presented must comply with the structural requirements defined for the tower and liquid column operating requirements.

For the optimization process, the set of DVs chosen to solve the analyzed problem is pre-defined. Each variable has minimum and maximum values established that form the domain of each variable Ω_{DV} in the search for the optimal design of the structure and

damper. The union of the domains of each DV makes up the optimization process domain Ω_{OPT}.

The objective of optimization is established by the objective function (OF) which must be minimized. In this work, the objective is to reduce the volume of the offshore wind turbine support structure with TLCD. For the structure optimization process, the analysis seeks optimal values for the monopile diameter d_m and the thickness t_m, for the tower diameter at the base $d_{t,b}$ and at the top $d_{t,t}$ and values for the tower thickness, also at the base $t_{t,b}$ and at the top $t_{t,t}$. The conical geometry of the original tower is maintained for optimized tower.

The search for the optimal structure with the help of TLCD requires also defining optimal damper parameters. The tuning ratio γ_f and the proportional damping ratio ζ_f are DVs for the TLCD. Other damper parameters, such as the mass ratio μ_f and the aspect ratio α_f, have their values previously defined and constant throughout the analysis.

During optimization, the DVs must present an optimal solution that complies with design constraints established for the structure and the liquid column damper. For the offshore wind turbine, it is established that the maximum horizontal dynamic displacement at the tower top $x_{t,max}$ must be less than or equal to an established limited displacement $x_{t,lim}$. The horizontal displacement at the tower top $x_{t,max}$ is computed by:

$$x_{t,max} = g_\sigma \sigma_x \tag{4.6}$$

where σ_x is the structure rms horizontal displacement at the top and g_σ is the peak factor for the stationary stochastic process. The peak factor is given by (Borri and Pastò, 2006):

$$g_\sigma = \sqrt{2\ln(\eta T)} + 0.5772/\sqrt{2\ln(\eta T)} \tag{4.7}$$

where η is taken as the fundamental frequency of the OWT and T (one hour) is the time interval over which the value is evaluated.

For OWT support structures with shell geometry special attention must be given to local buckling (Dimopoulos & Gantes, 2013; Dimopoulos et al., 2015): $\sigma_{t,b}$ stress at the tower base must be lower than the critical buckling stress σ_{cr} in the section. This assessment follows the conditions and formulation presented in DNVGL, (2017) and

explored by Uys et al. (2006) and Karpat (2013). The tower stress at the base $\sigma_{t,b}$ is considered as the sum of the axial stress σ_a generated by the OWT's self-weight G and the bending stress σ_b generated mainly by the moment M caused by the rotor thrust due to wind flow.

$$\sigma_{t,b} = \sigma_a + \sigma_b \leq \sigma_{cr} \tag{4.8}$$

with

$$\sigma_a = G/\left(2\pi r_{t,b} t_{t,b}\right) \quad \text{and} \quad \sigma_b = M/\left(\pi r_{t,b}^2 t_{t,b}\right) \tag{4.9}$$

where $r_{t,b}$ is the radius of the evaluated section, in this case, the base of the tower. The critical buckling stress σ_{cr} in the session is computed according to DNVGL, (2017) considering a shell segment of 18 meters with a stiffening ring for each segment, steel with elastic modulus of 210 GPa, yield stress of 355 MPa and shear modulus equal to 0.3.

The restriction established for the TLCD effectiveness in controlling the wind turbine vibrations follows the theoretical formulation where the liquid column maximum displacement allowed $y_{f,max}$ must not be greater than h_f. So that part of the liquid column that descends in one of the two vertical sections of the U-tube during the fluid oscillation remains in the vertical section (see Figure 1.1).

$$y_{f,max} < h_f \tag{4.10}$$

for

$$h_f = \left(L_f - B_f\right)/2 \tag{4.11}$$

The liquid column maximum vertical displacement $y_{f,max}$ is computed as

$$y_{f,max} = g_\sigma \sigma_y \tag{4.12}$$

with the liquid column displacement standard deviation σ_y inside the reservoir, given by:

$$\sigma_y^2 = \int_0^\infty S_{yy}(\omega) d\omega \tag{4.13}$$

After presenting the optimization objective, variables and design constraints, the optimization problem can be summarized as

$$\text{Find } \boldsymbol{D} \in \boldsymbol{\Omega_{OPT}}$$

$$\text{that minimizes OF}$$

$$\text{with } x_{t,max} \leq x_{t,lim},\ \sigma_{t,b} \leq \sigma_{cr}, \text{ and } y_{f,max} < h_f$$

with vector $\boldsymbol{D}$ containing the DVs and defined as

$$\boldsymbol{D} = \left\{d_m\ t_m\ d_{t,b}\ d_{t,t}\ t_{t,b}\ t_{t,t}\ \alpha_f\ \zeta_f\right\}^T$$

and the design variables domain $\boldsymbol{\Omega_{OPT}}$ containing each individual DV domain $\boldsymbol{\Omega_{DV}}$ from the structure and the tuned liquid damper:

$$\boldsymbol{\Omega_{OPT}} \in (\boldsymbol{\Omega_{d_m}} \cup \boldsymbol{\Omega_{t_m}} \cup \boldsymbol{\Omega_{d_{t,b}}} \cup \boldsymbol{\Omega_{d_{t,t}}} \cup \boldsymbol{\Omega_{t_{t,b}}} \cup \boldsymbol{\Omega_{t_{t,t}}} \cup \boldsymbol{\Omega_{r_\gamma}} \cup \boldsymbol{\Omega_{\zeta_f}})$$

5. OFFSHORE WIND TURBINE STRUCTURE PERFORMANCE

The design of complex structures like Offshore Wind Turbines (OWTs) are commonly based on results obtained from prescriptive structural analyses that employ the evaluation of limit states characterized in standards (DNV, DNV-GL, IEC, and NBR). The structural response is significantly affected by uncertainties due to the variability of both the environmental actions and the geometric and mechanical properties of the structure.

During its service lifespan, an OWT is subject to varying random actions over time, such as wind, waves, and ocean currents. The knowledge of the environment in which the OWT is located is generally limited and characterized by a high level of uncertainty. Moreover, the structure numerical model is a theoretical representation of the OWT, which does not account for potential discrepancies between the designed structure and the manufactured and constructed one.

Traditionally, the inherent uncertainties in structural design are characterized by load factors that increase actions and reduction factors that decrease the resistance of the structure. The prescriptive approach must meet the serviceability limit states and ultimate limit states. The semi-probabilistic design method, or Load and Resistance Factor Design (LRFD), is widely used.

Designing an OWT based on performance terms is also outlined in standards (DNV-GL, 2016) and constitutes a rational and efficient methodology. A performance-based approach states explicitly which are the performance requested and eventually the levels to be guaranteed with prefixed and acceptable margins of safety during the design (Petrini, 2009). The predicted performance in design represents a qualitative and quantitative measure of the system's efficiency when subjected to actions and loads throughout its service lifespan.

The approach highlighted in this chapter for the performance analysis of the OWT is based on the Performance-Based Wind Engineering framework and developed in Augusti and Ciampoli (2008), Petrini (2009), Ciampoli and Petrini (2010), and Ciampoli et al. (2011). Initially, the main sources of uncertainty considered for the OWT are highlighted. Next, the formulation used to evaluate the performance of OWT with TLCD using the PBWE method is presented. Finally, the Monte Carlo method used to solve the simplified formulation adopted for the PBWE is discussed.

5.1 SOURCES OF UNCERTAINTY FOR AN OWT

The main sources of uncertainty for an OWT (Figure 5.1), with its structure under wind and wave loads, can be separated into two zones for design in probabilistic terms (Ciampoli and Petrini, 2010). A zone (environment) comprising the random actions (wind and wave field) basic parameters and another zone characterizing the structural parameters and the interaction effects between the wind and wave field and the structure (exchange zone).

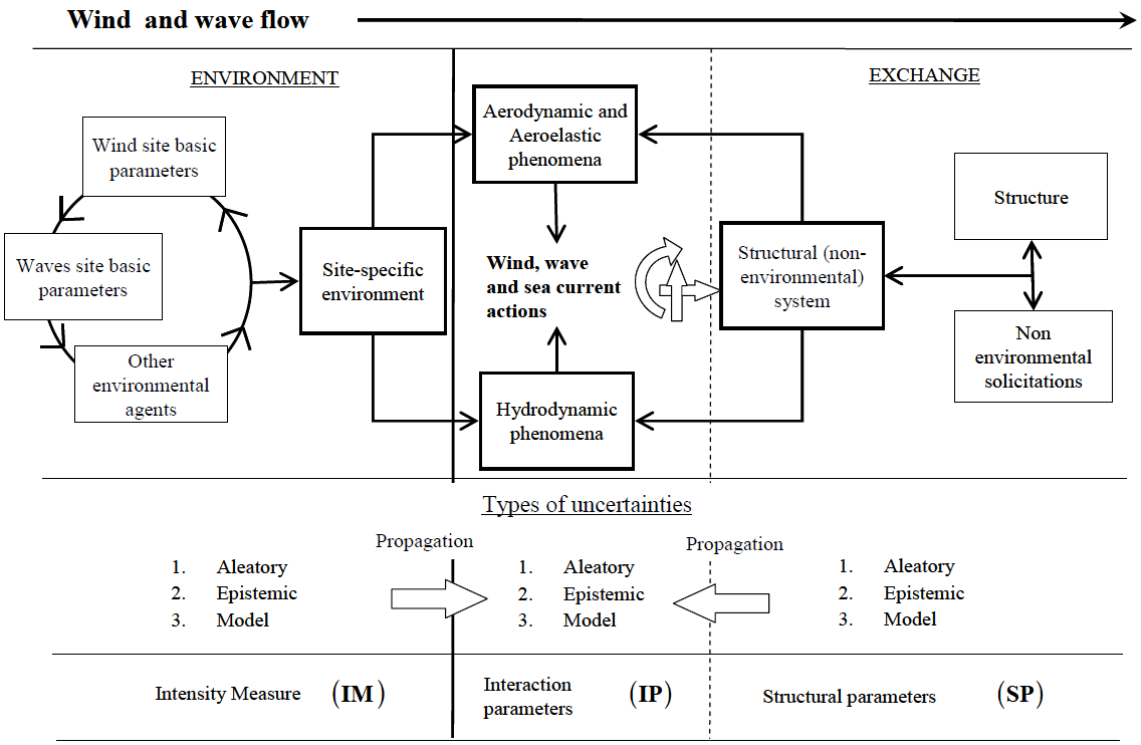

Figure 5.1. OWT zones, sources, and types of uncertainties considered for the PBWE analysis (Source: Petrini, 2009).

The uncertainties in the environment are related to their random and complex nature of wind, waves, and current actions with fluctuations in intensity, frequency, and direction over time. Also, uncertainty is related to the phenomenon modeling, possible lack of data and information, and errors made in field measurements (epistemic uncertainty).

In the exchange zone part of the uncertainty is linked to the OWT structural parameters which are mainly related to mechanical and material properties. Also, the exchange zone comprises interaction parameters. The interaction parameters are related to the uncertainties on the aerodynamic and aeroelastic parameters of the structure.

These parameters could be computed as structural parameters. Nevertheless, as previously stated, the aerodynamic and aeroelastic parameters are certainly subjected to the aleatoric uncertainties propagation from the environment zone (Petrini, 2009). Aeroelastic derivates and dimensionless wind and wave numbers are a few examples of interaction parameters.

For the wind turbine with TLCD probabilistic analysis in the offshore environment, the model uncertain parameters are separated into arrays considering the sources and zones of uncertainty. The $\boldsymbol{IM}$ intensity measurement vector is composed of the uncertain parameters of the offshore environment. The uncertain parameters in the exchange zone are grouped into two vectors, $\boldsymbol{IP}$ interaction parameters vector and the $\boldsymbol{SP}$ structural parameters vector.

The environment parameters $\boldsymbol{IM}$ and the structural parameters $\boldsymbol{SP}$ are uncorrelated and independent with respect to the interaction parameters $\boldsymbol{IP}$ (Ciampoli et al., 2009; Petrini, 2009; Ciampoli and Petrini, 2010). In other words, the occurrence of $\boldsymbol{IP}$ and $\boldsymbol{SP}$ has no impact on the occurrence of $\boldsymbol{IM}$. Also, the occurrence of $\boldsymbol{IP}$ and $\boldsymbol{IM}$ has no impact on the occurrence of $\boldsymbol{SP}$. Thus, the conditional probability $P(\cdot \mid \cdot)$ for $\boldsymbol{IM}$ and $\boldsymbol{SP}$ are given by:

$$P(\boldsymbol{IM}|\boldsymbol{IP}) = P(\boldsymbol{IM}|\boldsymbol{SP}) = P(\boldsymbol{IM}) \tag{5.1}$$

$$P(\boldsymbol{SP}|\boldsymbol{IP}) = P(\boldsymbol{SP}|\boldsymbol{IM}) = P(\boldsymbol{SP}) \tag{5.2}$$

However, the probability analysis of the problem can involve dependent parameters from other sources of uncertainty. The interaction parameters $\boldsymbol{IP}$ depend on the environment basic parameters $\boldsymbol{IM}$ and the structural parameters $\boldsymbol{SP}$. Therefore, the $\boldsymbol{IP}$ probability of occurrence given the occurrence of $\boldsymbol{IM}$ and $\boldsymbol{SP}$ is expressed as (Petrini, 2009; Ciampoli et al, 2011):

$$\begin{aligned} P(\boldsymbol{IM},\boldsymbol{IP},\boldsymbol{SP}) &= P(\boldsymbol{IP}|\boldsymbol{IM},\boldsymbol{SP}) \cdot P(\boldsymbol{IM}|\boldsymbol{SP}) \cdot P(\boldsymbol{SP}) \\ &= P(\boldsymbol{IP}|\boldsymbol{IM},\boldsymbol{SP}) \cdot P(\boldsymbol{IM}) \cdot P(\boldsymbol{SP}) \end{aligned} \tag{5.3}$$

5.2 SIMPLIFIED APPROACH TO STRUCTURAL PERFORMANCE

The theoretical and ideal objective of a Performance-Based Design procedure is to aid stakeholders (interested parties) decisions in defining design parameters based on a set of decision variables derived from specific performance criteria for the structure.

These criteria may consider many performance levels as ensuring no collapse, ensuring occupant safety, maintaining accessibility, achieving full functionality, and users discomfort.

Selecting decision variables based on performance criteria (whether they are low or high, linked respectively to ultimate and service states) required for the structure poses ethical and practical challenges. These criteria include consequences such as personal injury, restoration costs, expenses due to service loss or degradation, and changes in user comfort (Ciampoli et al., 2011). Therefore, the PBD procedure often focuses simply on assessing structural damage parameters (DM) (deemed unacceptable performance) and comparing various design alternatives.

The definition and characterization of one or more damage measures parameter for assessing building damage (considered as an unacceptable performance) must be aligned with the structural type and its relevant engineering demand parameters (EDP) (e.g., structural accelerations, rotations, displacements, inter-story drifts, stresses, etc.). The EDP are computed through structural analysis. Establishing appropriate relationships between relevant DMs and $EDPs$ enables the evaluation of damage states corresponding to specific values of a response parameter.

Considering the limit states related to the structure, the Performance-Based Design (PBD) procedure can be simplified by considering that structural damage occurs based on the probability of exceeding a limit state, which is quantified in terms of the Engineering Demand Parameter. Thus, as elucidated by Petrini (2009), Barbato and Petrini (2010), Ciampoli et al. (2011) and Colherinhas et al. (2024) the probabilistic response can be synthesized by the probability of occurrence $\lambda(\cdot)$ of the EDP by

$$\begin{aligned}\lambda(EDP) &= \int\int\int P(EDP|\boldsymbol{IM},\boldsymbol{IP},\boldsymbol{SP}) \cdot g(\boldsymbol{IM},\boldsymbol{IP},\boldsymbol{SP})\, dIM\, dIP\, dSP \\ &= \int\int\int P(EDP|\boldsymbol{IM},\boldsymbol{IP},\boldsymbol{SP}) \cdot g(\boldsymbol{IP}|\boldsymbol{IM},\boldsymbol{SP}) \cdot g(\boldsymbol{IM}) \cdot g(\boldsymbol{SP})\, dIM\, dIP\, dSP\end{aligned} \tag{5.4}$$

where, $g(\cdot)$ denotes a probability density function and $g(\cdot\,|\,\cdot)$ denotes a conditional probability density function. In this context the Engineering Demand Parameter (EDP) represents a structural response parameter. The basic parameters describing the offshore environment, such as mean wind speed, wave height, and wave peak frequency, are encapsulated in a vector of intensity measurements $\boldsymbol{IM}$. The vector comprises interaction parameters $\boldsymbol{IP}$ that may include aerodynamic and aeroelastic parameters of the structure to account for the interaction between the environment and the structure.

$\boldsymbol{SP}$ refers to the array that embraces the structural system parameters, such as Young modulus and structural damping rate, as well as non-environmental actions.

In this thesis, the focus is on the structural performance of the OWT due to the influence of the TLCD. The uncertainty parameters considered are related to the wind and wave field and to structural parameters. No structural parameters derived from phenomena's such as aeroelastic, aerodynamic, or hydrodynamic parameters are considered. For each of these, its own study would be appropriate. Thus, Equation Figure 5.4(5.4) may be simplified to:

$$\lambda(EDP) = \int\int P(EDP|\boldsymbol{IM},\boldsymbol{SP}) \cdot g(\boldsymbol{IM}) \cdot g(\boldsymbol{SP})\, dIM\, dSP \tag{5.5}$$

Among available methods (Song and Kawai, 2023) to solve Equation (5.5), a Monte Carlo simulation is employed.

5.3 MONTE CARLO SIMULATION FOR PERFORMANCE ANALYSIS

In the Monte Carlo method (Schneider e Vrouwenvelder, 2017; Melchers e Beck, 2018), a large number of experiments are simulated artificially and analyzed to compute the probability of occurrence of the evaluated engineering demand parameter (e.g., displacement of the tower at the top).

The first step in the simulation involves generating arrays with random values for each intensity measure $\boldsymbol{IM}$ and structural parameter $\boldsymbol{SP}$ considered in the analysis (e.g., mean wind velocity, wave peak period, wave height, structure Young Modulus, and structure damping ratio). Each array is generated based on their established statistical parameters such as the distribution mean value and the distribution standard deviation value. The occurrence of the random values related to a specific parameter is created using MATLAB's native function such as a lognormal random distribution function (Figure 5.2) and Weibull random distribution function (Figure 5.3). Detailed descriptions of the continuous distribution functions are written in Appendix B.

A sample of each $\boldsymbol{IM}$ and $\boldsymbol{SP}$ parameter array is selected for each dynamic analysis. The analysis with the selected parameters evaluates the structure response in terms of the Engineering Demand Parameter (EDP). In this thesis, solely the OWT dynamic displacement is observed.

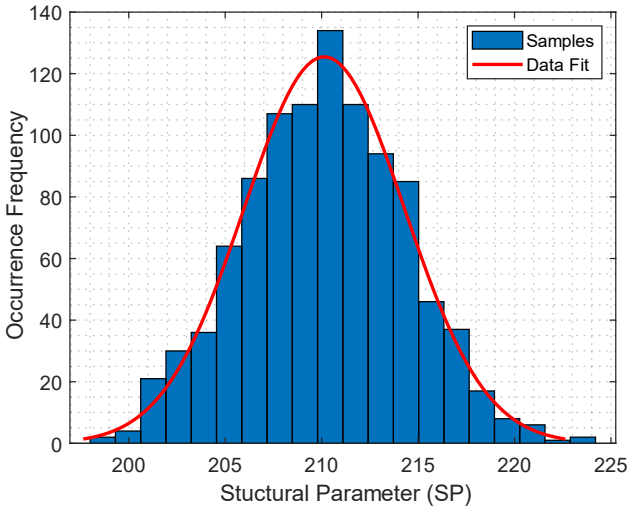

Figure 5.2. Random samples of the structural parameter (SP) generated by the lognormal distribution function.

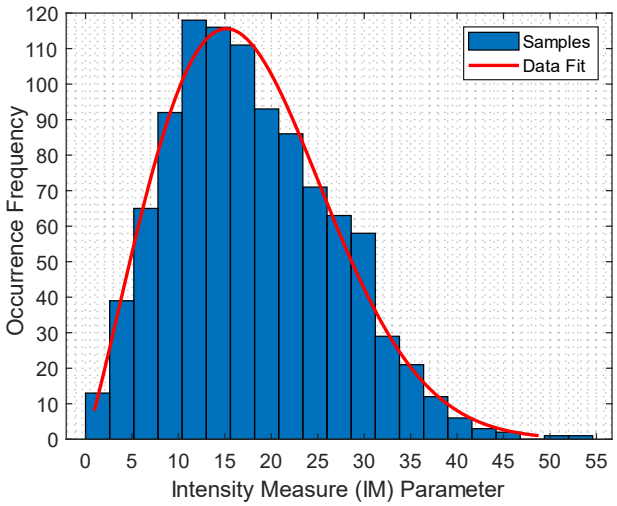

Figure 5.3. Random samples of the intensity measure parameter (IM) generated by the Weibull distribution function.

The process is repeated N times, where N is the size of the random parameter's arrays. The distribution of the EDP parameter can be visualized using a histogram, as depicted in Figure 5.4.

The values gathered on the $\boldsymbol{EDP}$ $(= \{EDP_1, EDP_2, \dots EDP_i \dots EDP_n\})$ array after N structural analysis of the OWT contains different response levels given the occurrence of the uncertain basic parameters IM (in a certain reference period) and the uncertain structural parameters SP. The $\boldsymbol{EDP}$ probability of occurrence may be characterized and computed by:

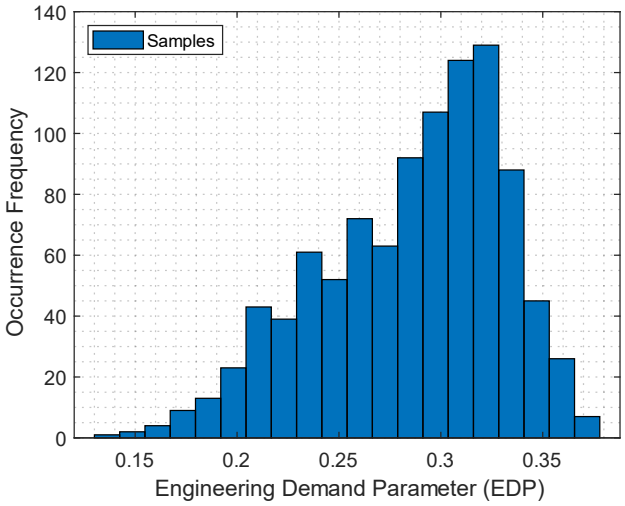

Figure 5.4. Occurrence frequency of the structural response in terms of the EDP parameter.

$$\lambda(EDP) = \sum_{i=1}^{n}\sum_{j=1}^{n}\frac{1}{N}I\left(EDP_i \leq EDP_j\right) \tag{5.6}$$

where $I(\cdot)$ is an 'indicator function' that is equal to 1, if $EDP_i \leq EDP_j$ is 'true', or 0, if $EDP_i \leq EDP_j$ is 'false'. Figure 5.5 shows the distribution and occurrence of the EDP parameter given the occurrence of IM and SP.

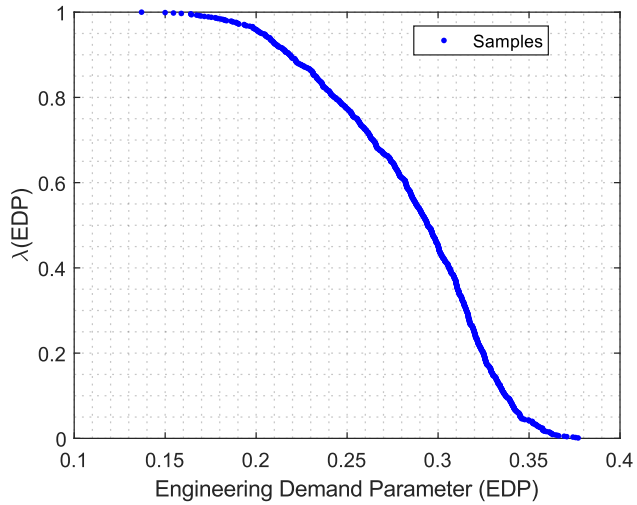

Figure 5.5. Probability of the occurrence of the structural response in terms of EDP.

Thus, instead of seeking the cumbersome solution of Eq. (5.6), the use of Monte Carlo simulation allows individual analysis and the response characterization for the

Offshore Wind Turbine with Tuned Liquid Column Damper considering random and uncertain parameters related to the offshore environment and the structure.

6. ANALYSIS & RESULTS

Within the thesis scope, which involves random vibration control, optimization processes, and performance assessment, this chapter explores and investigates various applications of tuned liquid column dampers in offshore wind turbines. The first study seeks to optimize the TLCD parameters and verify the OWT performance with the optimized TLCD. Next, the OWT's support structure (tower and foundation) and the TLCD simultaneous optimization is proposed and evaluated with the objective to reduce volume and save on material and manufacturing costs without compromising structural performance. Finally, different OWTs structural performance are analyzed. The reduction in structural response with the introduction of semi-active control in an alternating manner is studied.

The OWT numerical model is discretized into beam finite elements. The wind and waves random loads are taken in the frequency and time domain. The vibration analysis, the optimization processes (computed by the GA routine) and the Monte Carlo simulations involved in the studies were all written and computed through scripts produced or adapted for the MATLAB© computational code.

6.1 TLCD OPTIMIZATION AND PARAMETRIC EVALUATION

This first study aims to clarify and emphasize the TLCD parameters behavior and influence on the OWT response. A OWT reference model is employed to analyze the TLCD vibration control for the wind turbine under random wind and wave load. The reference offshore wind turbine is the 5-MW Wind Turbine with a monopile foundation from the National Renewable Energy Laboratory (Jonkman et al., 2009; Jonkman and Musial, 2010).

The NREL Reference 5-MW WT with monopile foundation (Figure 6.1) is widely known and adopted as the reference OWT for other vibration control studies (Bertollucci Colherinhas et al., 2021; Sun et al., 2019; Xie and Aly, 2020)**.** Relevant data for use in assembling the OWT numerical model is highlighted in Table 6.1. These are obtained from Jonkman et al (2009) and Jonkman and Musial (2010).

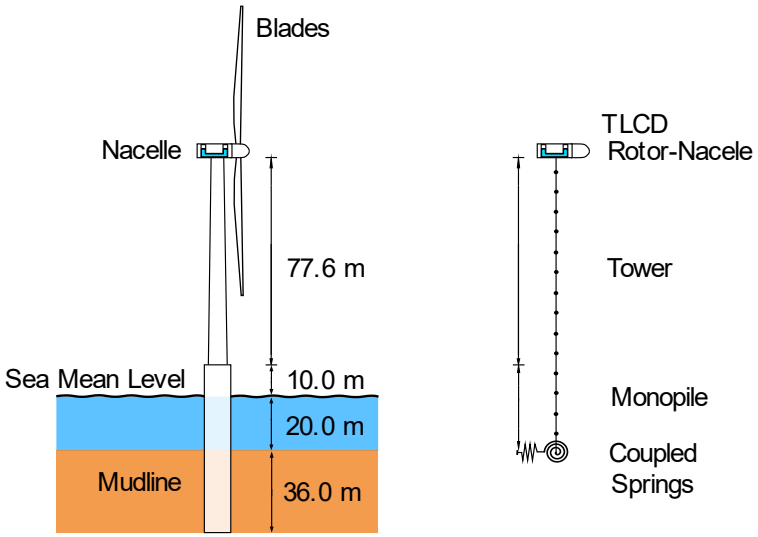

Figure 6.1. NREL 5-MW OWT configuration and discrete model adopted for the analysis.

Table 6.1. NREL 5-MW OWT parameters and components values.

RNA	Mass	350 t
	Inertia	4.505 10^7 kg.m²
Tower	Length	77.6 m
	Base diameter, base thickness	6 m, 0.027 m
	Top diameter, top thickness	3.87 m, 0.019 m
	Density, Young Modulus	8,500 kg/m³, 210 GPa
Monopile	Length	66 m
	Diameter, thickness	6 m, 0.06 m
	Density, Young Modulus	7,800 kg/m³, 210 GPa

The tower base has a diameter and thickness of 6 m and 0.027 m, respectively, and at the top a diameter and thickness of 3.87 m and 0.019 m. The cross-section reduction along the tower length is linear. The density of steel in the tower is considered higher than the regularly adopted density for steel, because it includes the presence of other items throughout the tower that are not directly modeled. Its monopile foundation is designed with 10 m above sea level, 20 m submerged, and 36 m buried below ground level (mudline). The monopile has a constant geometry along its length, with a diameter of 6 m and a thickness of 0.06 m

The wind turbine support structure (tower and pile) numerical model employes a discrete model with beam finite elements following the Euler-Bernoulli theory. The tower is discretized into 16 elements and the pile into 6 elements, providing both

elements with approximate lengths of 5 meters. The RNA is considered in a simplified form in the structure model as a lumped mass at the top of the tower.

The fluid-structure interaction is considered by the additional mass in the monopile (Pedroso, 1982) and the soil-structure interaction (SSI) is computed from the simplified model of coupled springs. Taken from the work of Passon (2006), the values adopted for the translational and rotational stiffness of the springs coupled to NREL 5-MW monopile are $K_{xx} = 2.58 \cdot 10^{9} N/m$, $K_{\phi\phi} = 2.64 \cdot 10^{11} N/rad$ and $K_{x\phi} = -2.26 \cdot 10^{10} Nm/rad$. The springs are superimposed to the monopile node at the ground line level (Figure 6.2). No additional mass or damping is considered due to soil-structure interaction.

For the wind load, L_c and L_k are adopted equal to $8.1\Lambda_1$. The values of 1.2 and 1.200 kg/m³ are assumed, respectively, for the tower's drag coefficient and air density. The wind profile and the wind speed are computed by a power law with α equal to 0.20, the mean reference speed of 12 m/s at the 90 m reference height (Hub). The 5-MW OWT rotor rotation frequency at this velocity is equal to 12.1 rpm. The blades parameters are taken from Jonkman et al (2009).

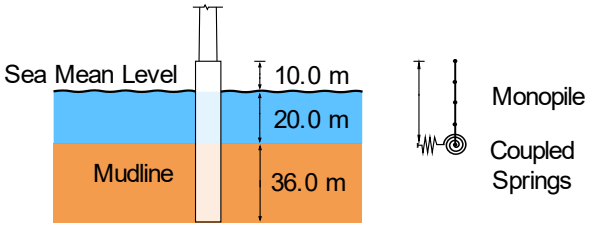

Figure 6.2. Schematic representation of the NREL 5-MW OWT monopile foundation and the coupled springs SSI simplified model.

To determine the wave load on the monopile through the JONSWAP spectrum, the drag and inertia coefficients are considered equal to 1.2 and 2.0, respectively, and the seawater density is adopted as 1025.0 kg/m³. The peak shape parameter γ is adopted as 3.3, the wave peak frequency as 0.1 Hz, and the wave height equal to 6.0 meters.

Initially, the TLCD parameters defined by genetic algorithm optimization are compared with the results obtained through a response map analysis. The search for the optimal TLCD parameters employing a mapping analysis has a high computational cost. Thus, is a process used only to assess the genetic algorithm results. Through an iterative process the script seeks the lowest OWT response (σ_x) associated with the TLCD mass ratio, tuning ratio, and damping ratio. The TLCD aspect ratio is constant and considered

equal to 0.90. The OWT response at the top is evaluated in terms of the longitudinal displacement by Equation (3.12).

The NREL 5-MW reference OWT with a passive TLCD is considered under different random forces. The analysis includes an unitary white noise load at the structure top (Figure 6.3 and Figure 6.4), the combined action of wind and waves (Kaimal and JONSWAP) along the tower and monopile (Figure 6.5 and Figure 6.6), and the wind load on the blades (Figure 6.7 and Figure 6.8). These figures respectively present the turbine response map and the ideal damping rate of the passive TLCD.

For the rotor wind load case the response map where its power spectral density (PSD) shows different peaks near the turbine's natural frequency, there is a marked variation in the TLCD tuning ratio (γ_f). The optimal values for the TLCD are obtained by mitigating these two peaks (related to both the strength and structure) rather than just the peak response of the OWT.

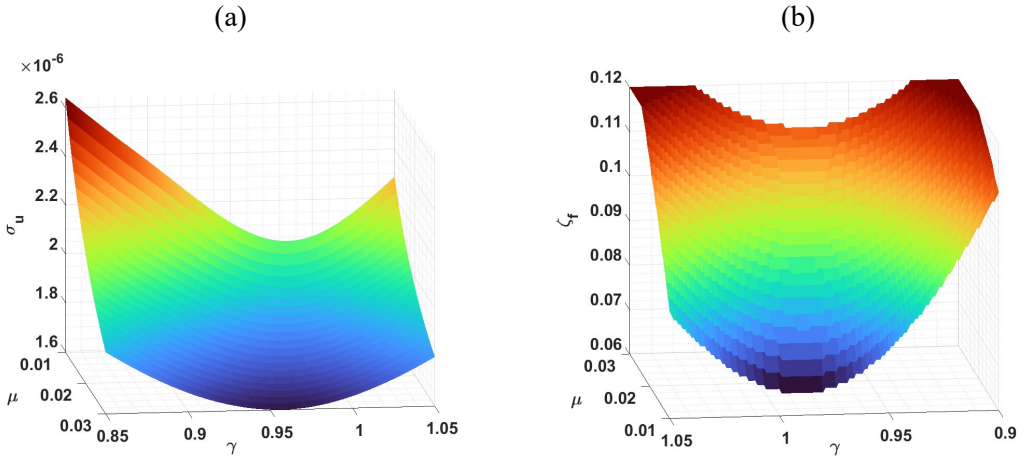

Figure 6.3. OWT under white noise load 3D response map: displacement at the tower top (a); and TLCD optimal damping ratio (b).

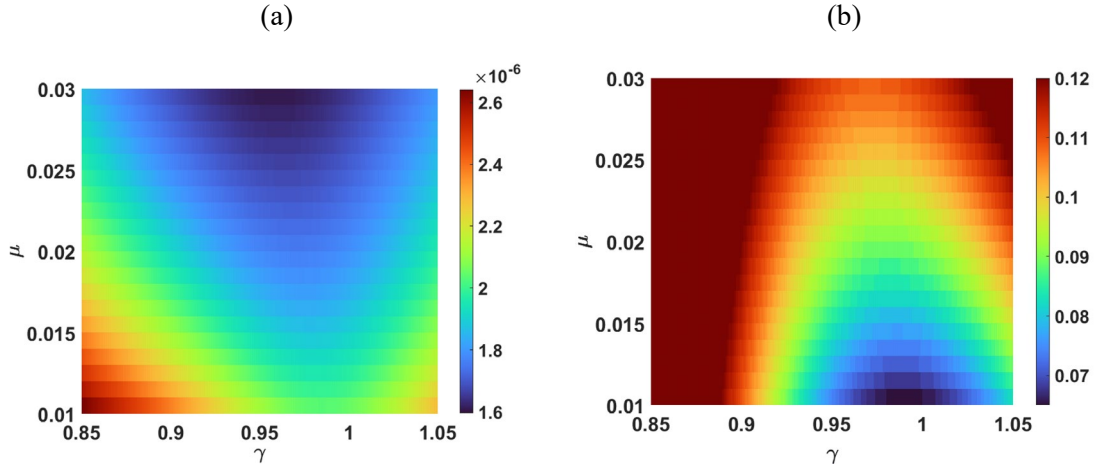

Figure 6.4. OWT under white noise load 2D response map: displacement at the tower top (a); and TLCD optimal damping ratio (b).

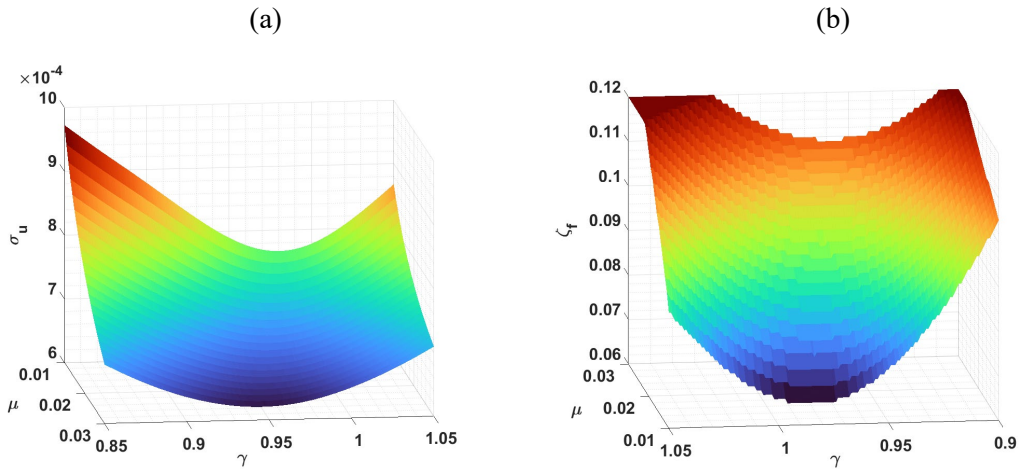

Figure 6.5. OWT under wind and wave load 3D response map: displacement at the tower top (a); and TLCD optimal damping ratio (b).

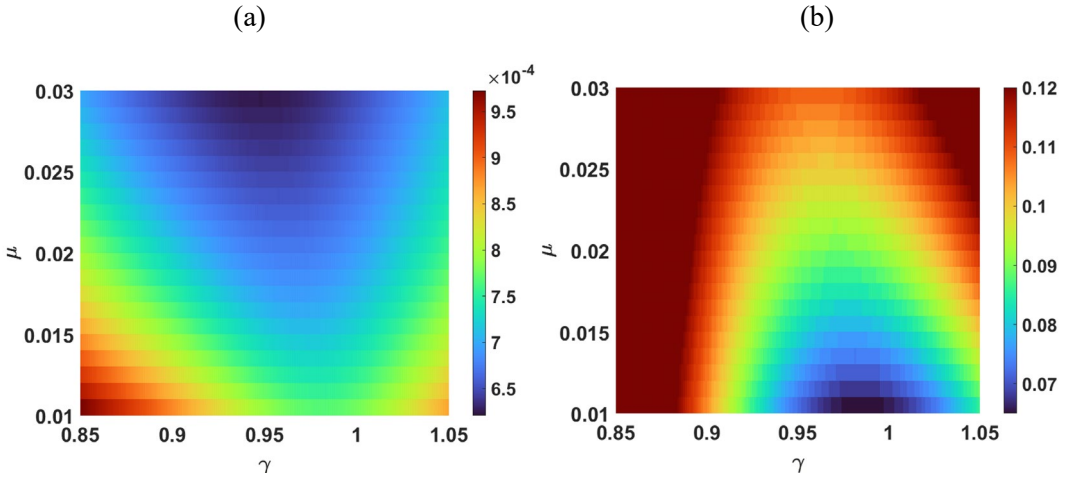

Figure 6.6. OWT under wind and wave load 2D response map: displacement at the tower top (a); and TLCD optimal damping ratio (b).

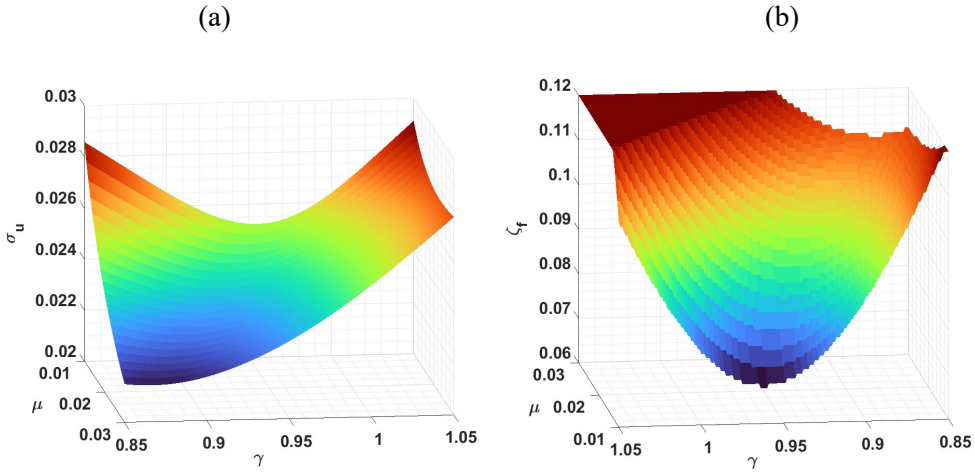

Figure 6.7. OWT under rotor thrust 3D response map: displacement at the tower top (a); and TLCD optimal damping ratio (b).

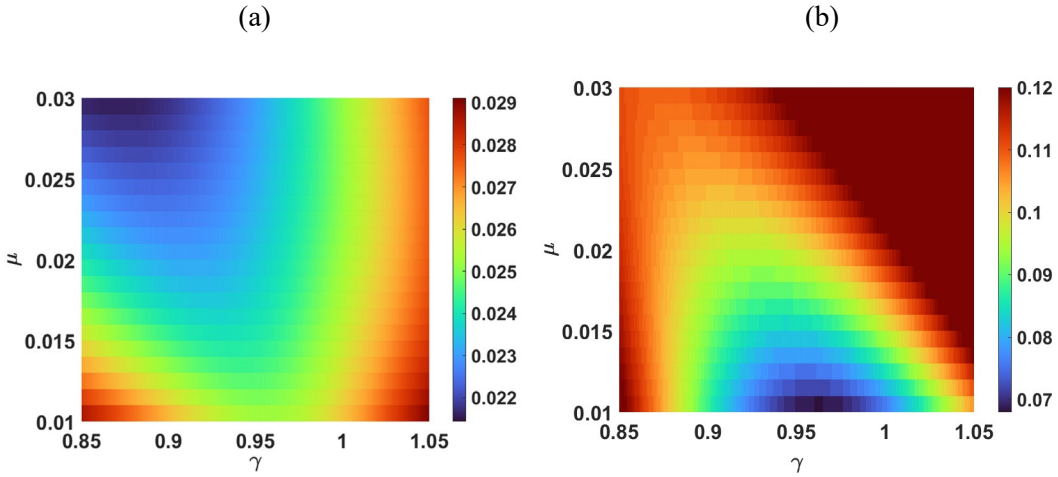

Figure 6.8 OWT under rotor thrust 2D response map: displacement at the tower top (a); and TLCD optimal damping ratio (b).

The TLCD optimal tuning ratio γ_f is sensible to the mass ratio μ_f and the load frequency range. Furthermore, the structure response σ_x mitigation is very sensitive to changes in the liquid column mass linked to the TLCD optimal frequency ratio and the optimal damping rate. This behavior highlights the need to optimize the passive damper and justifies the optimization methods application presented throughout the work.

After presenting the response map analysis method, the TLCD optimal parameters (related to the smallest response at the top of the turbine, σ_x) computed through the GA script are compared to the results obtained by the response map analysis (Table 6.2 and Table 6.3). The results presented by both methods are very close, with differences of less than 0.5%. An important factor to highlight for computational analysis is that the time required to define the TLCD optimal parameters using the genetic algorithm script is much shorter.

Table 6.2. TLCD tuning ratio computed through GA and response map analyses.

α_f (0,9)	White Noise			Kaimal and JONSWAP			Rotor Thrust		
μ_f (%)	$\gamma_{f_{GA}}$	$\gamma_{f_{map}}$	*dif.*	$\gamma_{f_{GA}}$	$\gamma_{f_{map}}$	*dif.*	$\gamma_{f_{GA}}$	$\gamma_{f_{map}}$	*dif.*
1.0	0.9846	0.9850	0.04%	0.9803	0.9800	0.03%	0.9546	0.9550	0.04%
1.5	0.9768	0.9780	0.12%	0.9714	0.9710	0.04%	0.9323	0.9320	0.03%
2.0	0.9704	0.9700	0.04%	0.9624	0.9620	0.04%	0.9090	0.9090	0.00%
2.5	0.9635	0.9630	0.05%	0.9538	0.9540	0.02%	0.8864	0.8860	0.05%
3.0	0.9566	0.9570	0.04%	0.9454	0.9450	0.04%	0.8666	0.8670	0.05%

Table 6.3. TLCD damping ratio obtained through GA and response map analyses.

α_f (0,9)	White Noise			Kaimal and JONSWAP			Rotor Thrust		
μ_f (%)	$\zeta_{f_{GA}}$	$\zeta_{f_{map}}$	*dif.*	$\zeta_{f_{GA}}$	$\zeta_{f_{map}}$	*dif.*	$\zeta_{f_{GA}}$	$\zeta_{f_{map}}$	*dif.*
1.0	0.0652	0.0650	0.31%	0.0649	0.0650	0.15%	0.0690	0.0690	0.00%
1.5	0.0793	0.0790	0.38%	0.0792	0.0790	0.25%	0.0850	0.0850	0.00%
2.0	0.0912	0.0910	0.22%	0.0908	0.0910	0.22%	0.0975	0.0970	0.52%
2.5	0.1016	0.1020	0.39%	0.1010	0.1010	0.00%	0.1054	0.1050	0.38%
3.0	0.1108	0.1110	0.18%	0.1100	0.1100	0.00%	0.1095	0.1090	0.46%

After comparing the optimum parameters computed by both methods, the TLCD optimal tuning ration and optimal damping ratio are determined via a genetic algorithm (Figure 6.9-Figure 6.11). The behavior of these parameters linked to the liquid column mass and aspect ratio are evaluated. As previously mentioned, different types of loads (white noise, wind, and wave) applied to the support structure and rotor are considered and the objective function is to minimize the OWT response.

(a) (b)

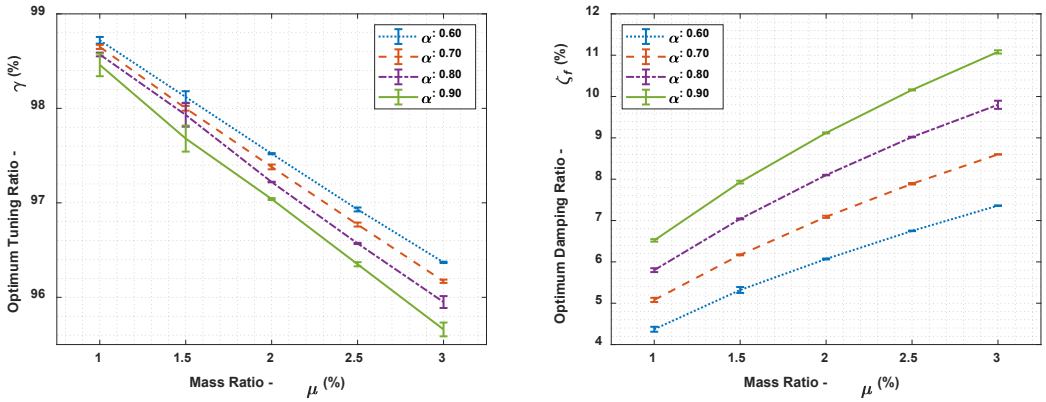

Figure 6.9. TLCD optimal parameters for OWT under white noise load: (a) tuning ratio γ_f; (b) damping ratio ζ_f.

A consistent pattern is observed in the parameter's curves, regardless of the considered load. The tuning ratio (γ_f) decreases as the liquid column mass ratio (μ_f) and aspect ratio (α_f) increase. Conversely, the TLCD damping ratio (ζ_f) exhibits the opposite behavior: it increases with both the mass ratio and the aspect ratio increase.

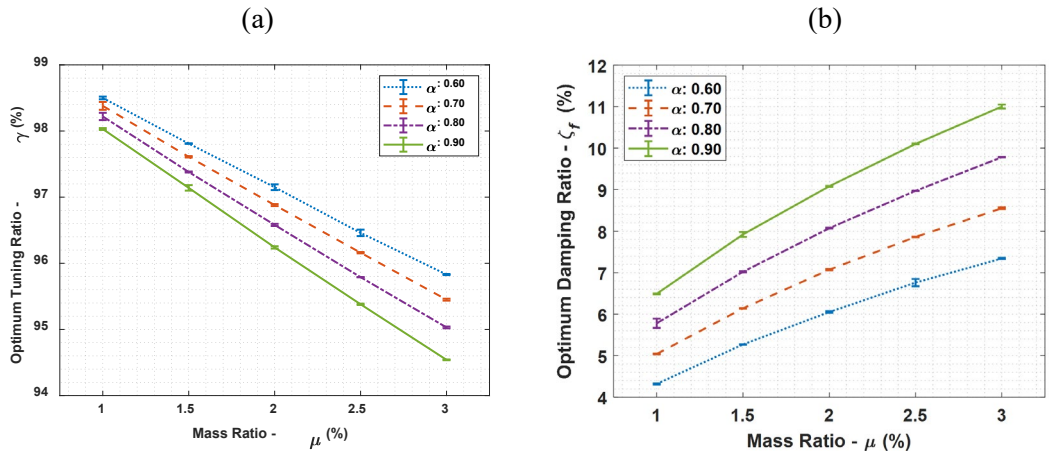

Figure 6.10. TLCD optimal parameters for OWT structure under wind and wave load: (a) tuning ratio γ_f; (b) damping ratio ζ_f.

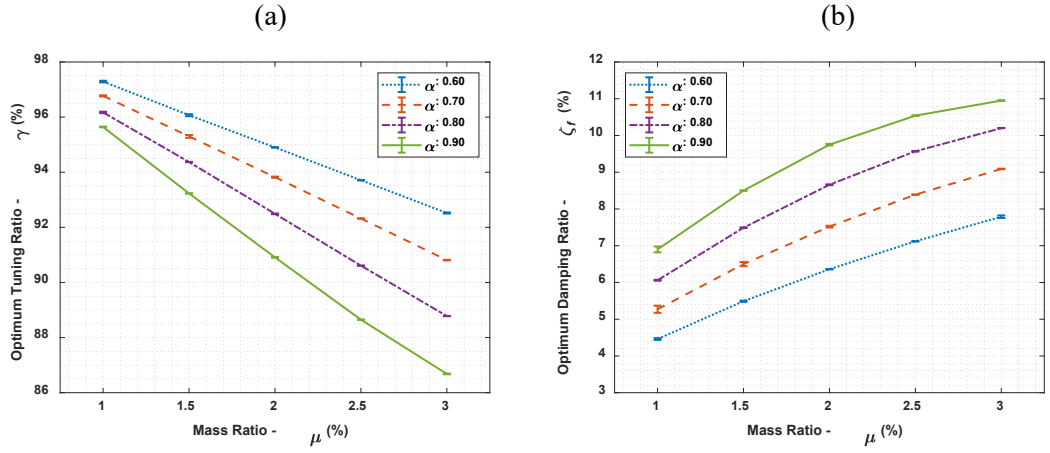

Figure 6.11. TLCD optimal parameters for OWT blades under wind load: (a) tuning ratio γ_f; (b) damping ratio ζ_f.

As observed in the response map, the TLCD optimal parameters determined for white noise load are close to the optimal parameters obtained for the wind and wave load along the structure. The variation in the TLCD's tuning ratio (γ_f) is more pronounced in the case of wind loads on the turbine blades. Additionally, higher values of the aspect ratio (α_f) lead to greater variation in the tuning ratio as the mass ratio (μ_f) increases.

Based on the TLCD optimal parameters obtained by the GA script, the device's performance in mitigating OWT random vibrations is evaluated. The OWT response decrease r_{σ_x} is calculated as the ratio between the OWT response with and without the use of the TLCD (Table 6.4-Table 6.6).

Table 6.4. OWT response mitigation for structure under white noise load.

α_f	0.6	0.7	0.8	0.9
μ_f (%)	r_{σ_x}	r_{σ_x}	r_{σ_x}	r_{σ_x}
1.0	42.16%	45.46%	48.27%	50.70%
1.5	46.48%	49.41%	52.42%	54.76%
2.0	49.49%	52.63%	55.27%	57.54%
2.5	51.77%	54.84%	57.42%	59.62%
3.0	53.60%	56.61%	59.13%	61.27%

Table 6.5. OWT response mitigation for structure under wind and wave load.

α_f	0.6	0.7	0.8	0.9
μ_f (%)	r_{σ_x}	r_{σ_x}	r_{σ_x}	r_{σ_x}
1.0	40.75%	43.97%	46.72%	49.09%
1.5	44.77%	47.92%	50.58%	52.87%
2.0	47.52%	50.60%	53.20%	55.42%
2.5	49.58%	52.60%	55.14%	57.31%
3.0	51.20%	54.18%	56.67%	58.79%

Table 6.6. OWT response mitigation for blades under wind load.

α_f	0.6	0.7	0.8	0.9
μ_f (%)	r_{σ_x}	r_{σ_x}	r_{σ_x}	r_{σ_x}
1.0	33.56%	36.46%	38.94%	41.12%
1.5	36.18%	39.14%	41.71%	44.03%
2.0	37.84%	40.92%	43.67%	46.22%
2.5	39.04%	42.30%	45.29%	48.15%
3.0	39.99%	43.49%	46.77%	49.95%

The TLCD with 0.90 aspect ratio, 3.0% mass ratio and the related tuning ratio (Table 6.2) and damping ratio (Table 6.3) presents the greatest mitigation. The OWT response mitigation considering the white noise load (Figure 6.12) was the greatest among those analyzed. It's observed a 61.27% reduction in the OWT displacements at the top of the tower. In the case of vibrations caused by wind and wave load (Figure 6.13) applied along the support structure the OWT response reduction was in a percentage close to white noise with values of 58.79%. Meanwhile, the decrease in OWT response under wind on the rotating blades (Figure 6.14) presented a lower value, 49.95%, but still significant.

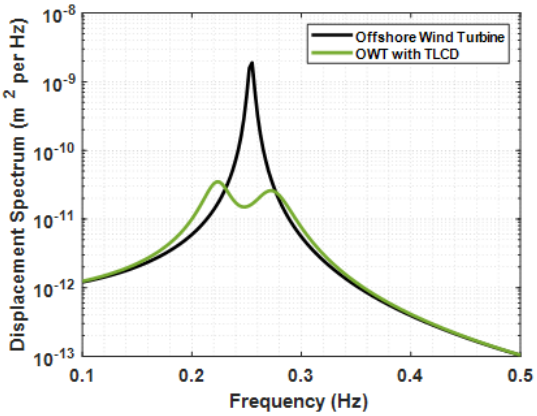

Figure 6.12. OWT response for structure under white noise load.

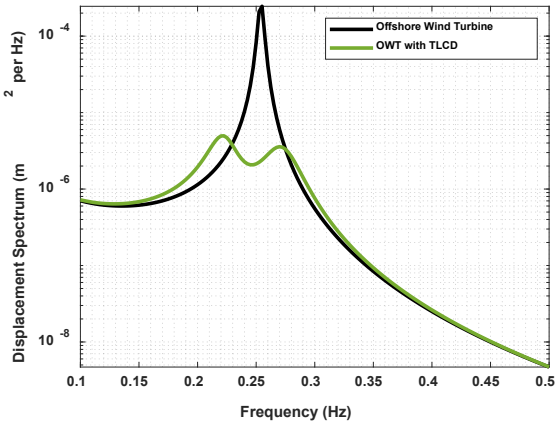

Figure 6.13. OWT response for structure under wind and wave load.

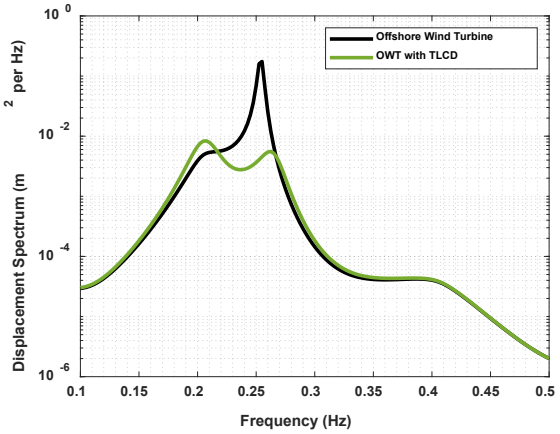

Figure 6.14. OWT response for blades under wind load.

The OWT random vibrations control by the optimal TLCD proved to be efficient. Analyzes were computed for OWT structural parameters and fixed basic wind and wave parameters.

In the (return) period of one year, the parameters related to the wind and wave random actions can assume different values. Also, the structure properties and parameters can be considered uncertain. The occurrence and values of these parameters are calculated by continuous distribution functions (presented in Appendix B). While the OWT vibration control analysis by TLCD considering the different sources of uncertainty is treated in probabilistic terms by Monte Carlo simulation

A Weibull probability distribution is assumed to represent the mean wind velocity annual occurrence (Figure 6.15). Scale parameter and shape parameter are equal to 20 and 2.02, respectively. Wave height and wave frequency peak are characterized by a log-normal distribution (Figure 6.16). The average values are computed from Equations (3.71) and (3.73). A covariance of 0.1 is assumed for these two parameters.

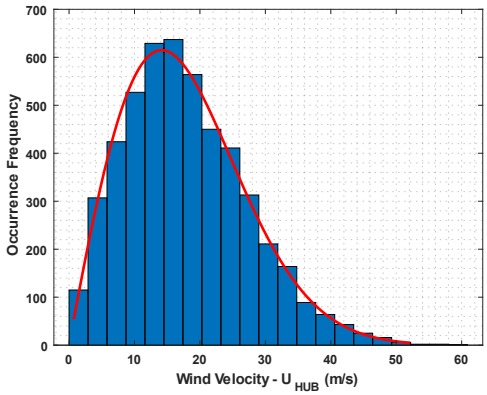

Figure 6.15. Mean wind velocity distribution at the hub height.

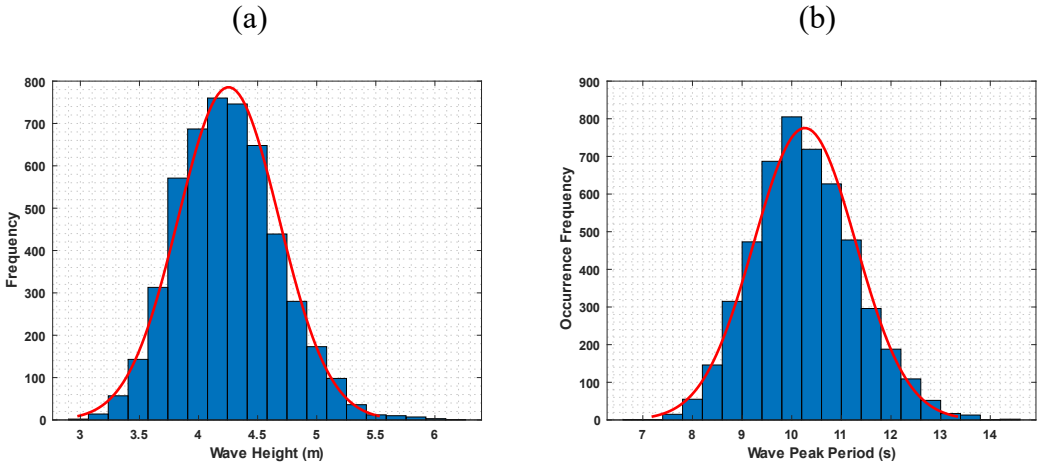

Figure 6.16. Wave height (a) and peak period (b) distribution.

The OWT uncertainties are also related to structural parameters such as the steel Young modulus and the structural damping ratio (Figure 6.17). A log-normal distribution is assumed for both parameters. A 210 GPa mean value with 0.02 of covariance is assumed for the Young Modulus and a mean value of 0.01 with 0.08 of covariance for the structural damping ratio.

(a) (b)

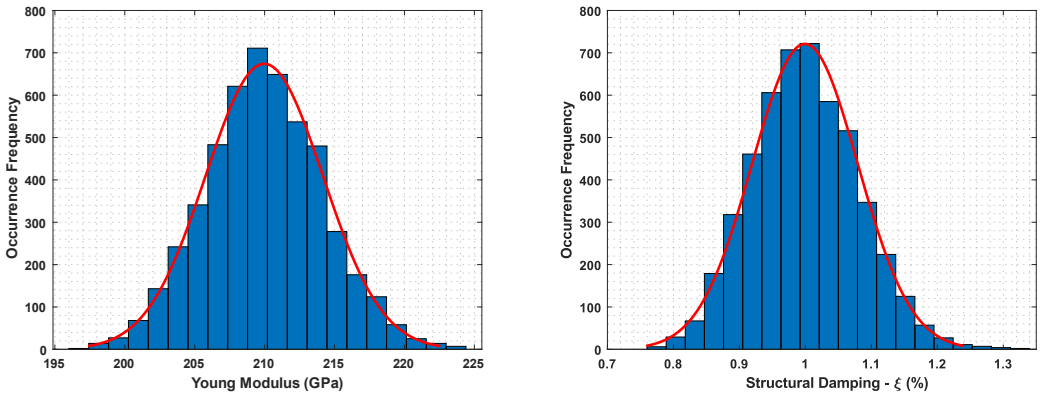

Figure 6.17. Offshore wind turbine material elasticity modulus (a) and damping ratio (b).

Figure 6.18 presents two distinct risk curves related to the OWT tower longitudinal displacement (fore-aft) due to wind and wave actions. A curve for the wind turbine without TLCD with flexible base (SSI due to coupled springs) and a curve for the OWT with optimized TLCD with flexible base. For the OWT and TLCD system, a 3.0% mass ratio, 0.90 aspect ratio, 0.867 tuning ratio, and 0.11 damping ratio are considered for the device. These are optimal TLCD parameters obtained from Figure 6.11 and represent the TLCD case with greater efficiency in reducing OWT displacements, as observed in Table 6.6.

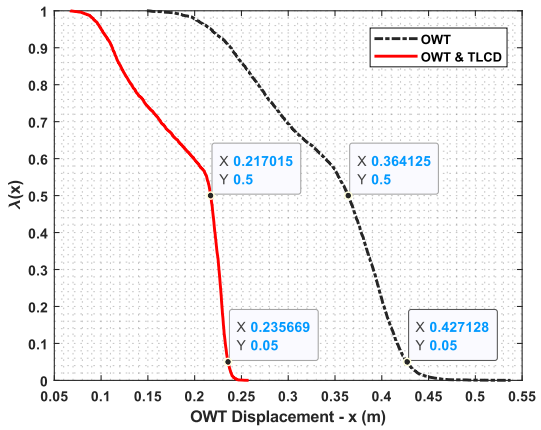

Figure 6.18. Risk curves related to the OWT longitudinal displacement (fore-aft) at the top due to wind and wave loads

The vibration control analysis in probabilistic terms by the PBWE approach, as proposed in Petrini (2009) and Ciampoli and Petrini (2011), presents a significant improvement in the OWT performance considering the TLCD to control the offshore environment random and uncertain loads associated with uncertain structural parameters. The risk curve exposes the OWT response mitigation for different wind and wave conditions using the optimized TLCD. The response decrease reaches 45% average.

6.2 SIMULTANEOUS OPTIMIZATION OF OWT CONTROLLED BY TLCD CONSIDERING STRUCTURAL AND DAMPER PERFORMANCE CONSTRAINTS

In addition to ensuring a gain in structural performance, the use of a tuned liquid column damper (TLCD) also offers the possibility of additional savings in material and manufacturing of offshore wind turbine (OWT) support structures (tower and foundation). Using Genetic Algorithms, this analysis optimizes the structure of a standard NREL 5MW offshore wind turbine coupled to the TLCD installed in the turbine, considering performance constraints for both mechanical systems.

The objective of optimizing the structure is to reduce its volume by modifying its diameter and thickness at the top and base of the support structure, i.e., tower and monopile. Optimizing the volume of the wind turbine tower aims to reduce the production costs of the support structure.

The structural performance of the optimized support structure in the face of natural and random wind and wave actions is ensured using the liquid column damper. The proper definition and use of the optimized damper parameters help search for the smallest tower volume, accompanied by compliance with the global and local structural requirements established for the wind turbine. Displacement at the top and buckling at the tower's base, respectively. Also, a restriction is imposed on the fluid maximum displacement in the reservoir to guarantee its operation in accordance with the theoretical formulation.

Table 6.7 presents the reference OWT (Jonkman et al., 2009) parameters and the design variables domain for the optimization. The minimum and maximum values assumed for the domain of the DVs of the OWT structure are equivalent to 80% and 110% (lower limit and upper limit) of the original values of the standard structure, respectively. The TLCD is assumed to have a mass ratio (μ_f) of 2.0% and an aspect

ratio (α_f) of 0.30. Both parameters are kept constant during the optimization process. The aspect ratio is low because the TLCD is considered installed inside the tower.

Table 6.7. Design variables of the standard OWT with lower and upper limits adopted for the DVs domain.

DVs	d_m (m)	t_m (cm)	$d_{t,b}$ (m)	$t_{t,b}$ (cm)	$d_{t,t}$ (m)	$t_{t,t}$ (cm)	γ_f (-)	ζ_f (-)	volume (m^3)
ref.	6,000	6,000	6,000	2,700	3,870	1,900	-	-	101,78
máx..	6,600	6,600	6,600	2,970	4,257	2,090	1,000	0,100	123,16
min.	4,800	4,800	4,800	2,160	3,096	1,520	0,900	0,010	65,14

Wind and wave loads are computed from Equations (3.29), (3.38), and (3.74). For wind, the OWT rated speed of 11.4 m/s at the hub height is adopted as the reference speed for the optimization process. From the wind velocity, the wave height and its peak frequency are calculated (Eq. (3.73 and (3.71, respectively). The load due to the self-weight of the structure and the rotor-nacelle assembly is also considered to assess the critical buckling stress at the base of the optimized tower (Equation (4.8). To ensure the safety of the OWT against the tower buckling at the base, stiffening rings are considered welded to the tower every 18m.

Based on the parameters used in Gentils et al. (2017), Colherinhas et al. (2020), and Mendes et al. (2023), the optimization process in this paper adopts a crossover probability of 0.80, an elitism probability of 0.02, and a mutation probability of 0.02. Given the complexity of the problem, a decimation probability of 0.15 with four generations steps is computed. These values aim to prevent the optimum design problem from being a local solution. A population of 300 individuals and 300 generations are predicted for one optimization process. A total of 90,000 cases were analyzed for each optimization process. It is a complex optimization process with many DVs and restrictions. The optimized OWT represents the optimal design case with the minimum structure volume after running the optimization process 15 times. Figure 6.19 shows the average value of the OWT volume during the optimization process and the range containing the standard deviation with a confidence of 95%. Considering all optimization cases, an average of 85.34 m³ and a standard deviation of 0.37 m³ were obtained for the OWT volume.

Figure 6.20 and Table 6.8 presents the optimum design variables for the best OWT solution with TLCD. It achieved nearly a 17 % volume reduction of the wind

turbine support structure with the TLCD. Using the method presented in Uys et al. (2006) this OWT design represents a cost reduction of approximately 21%.

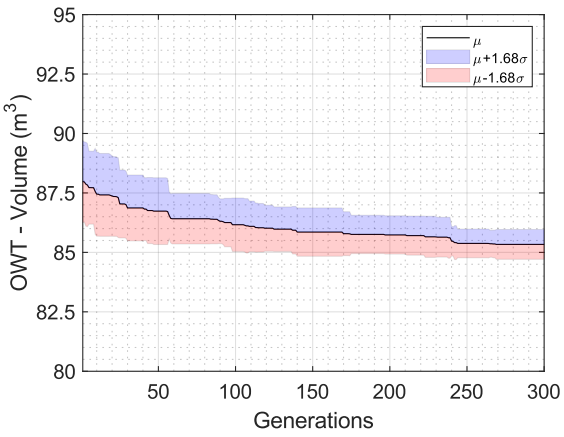

Figure 6.19. OWT structure volume variation through generations in simultaneous optimization.

(a) (b)

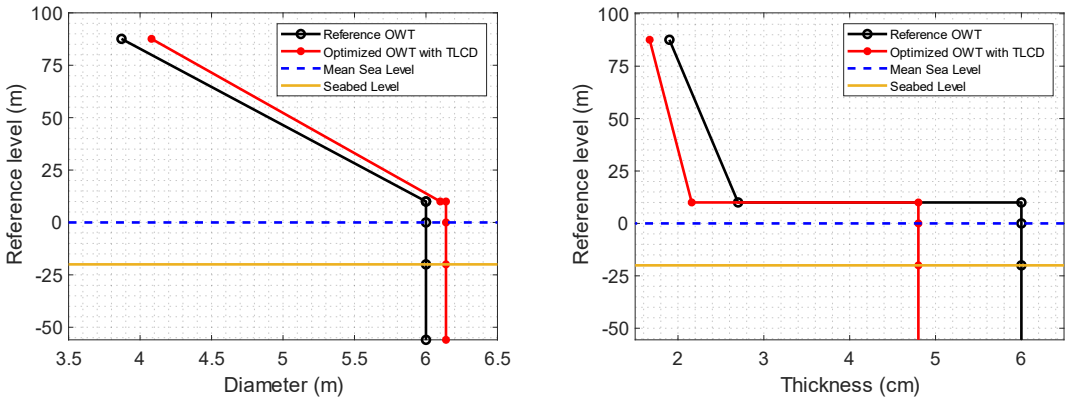

Figure 6.20. OWT support structure with TLCD optimal design values for the outer diameter (a) and thickness (b).

Table 6.8. Optimal design values for the best OWT solution with TLCD compared to the reference NREL OWT 5-MW.

DVs	d_m (m)	t_m (cm)	$d_{t,b}$ (m)	$t_{t,b}$ (cm)	$d_{t,t}$ (m)	$t_{t,t}$ (cm)	γ_f ( )	ζ_f ( )	volume (m^3)
Standard	6.00	6.00	6.00	2.70	3.87	1.90	-	-	101.48
Optimum	6.14	4.80	6.10	2.16	4.08	1.67	0.98	0.06	84.61
Dif. (%)	+2.03	-20.0	+1.67	-20.0	+5.42	-12.20	-	-	-16.62

Figure 6.21 shows the structural DVs trend in each generation. In the best optimal design case, the OWT monopile presents a small variation in its diameter d_m with a maximum reduction in its thickness t_m. This behavior is also seen in Gentils et al. (2017), where it is highlighted that the pile design (Jonkman and Musial, 2009) is much

less sophisticated than other parts of the wind turbine developed over the years. The tower had a small diameter increase of 1.67% at the base $d_{t,b}$ and 5.42 % at the top $d_{t,t}$. The tower thickness presented an expressive reduction of 20 % at the base $t_{t,b}$ and 12.2 % at the top $t_{t,t}$. As a result, an approximately 17 % volume reduction in the OWT structure (tower and monopile) volume.

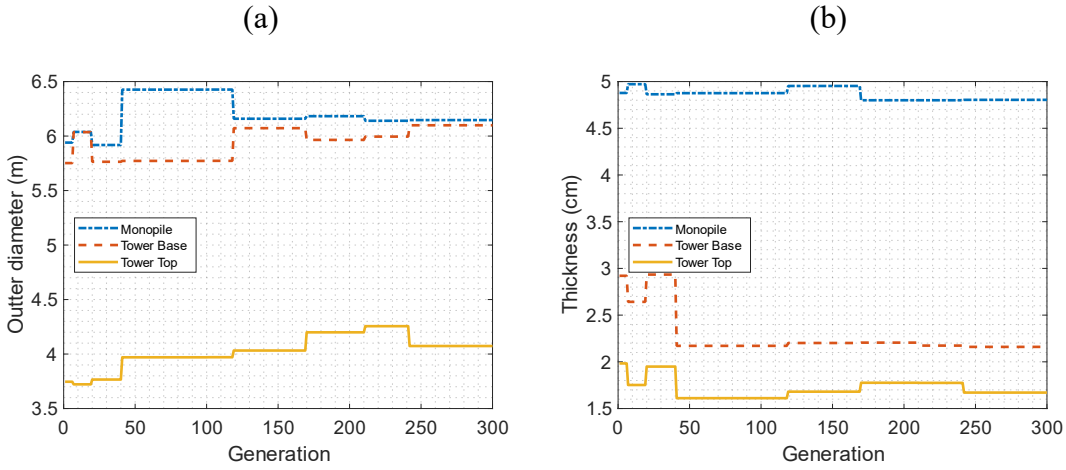

Figure 6.21. Optimum OWT outer diameter (a) and thickness (b) through different generations.

The volume obtained through the optimization process is possible through TLCD use, which guarantees the OWT structural performance. The optimal OWT tip displacement with TLCD (Figure 6.22.a) results in a displacement slightly lower than the value obtained for the reference OWT (≈ 38 cm). It is possible to state that the OWT optimized simultaneously with TLCD has no increase in the dynamic response. The OWT optimum design with the presence of stiffening rings guarantees a design buckling stress lower than the critical buckling stress calculated according to DNV (2013) with $\sigma_{t,b}/\sigma_{cr} \approx 0.55$. Thus, the optimal design presented for the OWT support structure indicates that there will be no buckling failure at the tower base (critical point) for the conditions analyzed (Figure 6.22.b).

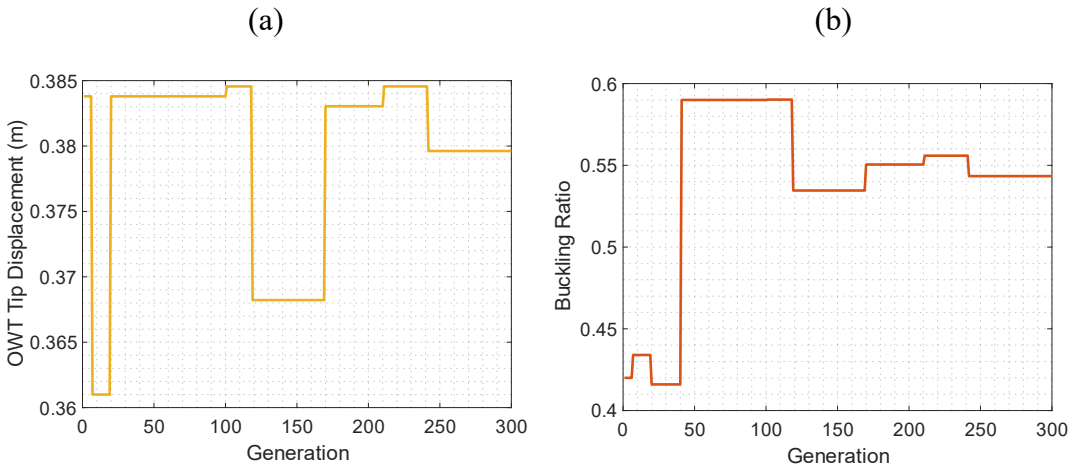

Figure 6.22. Optimum OWT constrains: (a) tip displacement and (b) buckling ratio ($\sigma_{t,b}/\sigma_{cr}$) through different generations.

OWTs are dynamically active and dynamically sensitive structures due to their design (slender support structure with a significant and rotating mass at the top). Their fundamental frequency is very close to the main excitation loads frequency imposed by the environment (wind and wave) and their mechanical functioning (1P and 3P loads due to vibration at the rotor level and due to blade shadowing effects, respectively). Thus, the structure fundamental frequency assumes great relevance for OWTs design, to avoid the structural response amplification during resonance (a phenomenon that occurs when the load frequency equals the system's natural frequency). The TLCD installed on the OWT is tuned precisely to act on the structure natural frequency.

The liquid column damper (like other tuned dampers) presents its greatest performance in resonance. Furthermore, it guarantees that there is no longitudinal response amplification for the tower with reduced mass compared to the original tower (constraint for the optimization process). However, the OWT natural frequency is relevant for the optimization due to the 1P and 3P loads. The natural frequency is not considered as a constraint parameter for the simultaneous optimal design but is assessed at the end of the process. For the optimized OWT the fundamental frequency is 0,273 Hz and lies between the NREL 5-MW Reference WT 1P and 3P loads

Finally, the maximum displacement of the liquid column (Equation 42) is also respected with $\sigma_y = 0.1878$. Thus, $y_{f,max} < h_f$ and the adequate liquid column displacement inside the reservoir is guaranteed in accordance with the theoretical formulation (Figure 6.23).

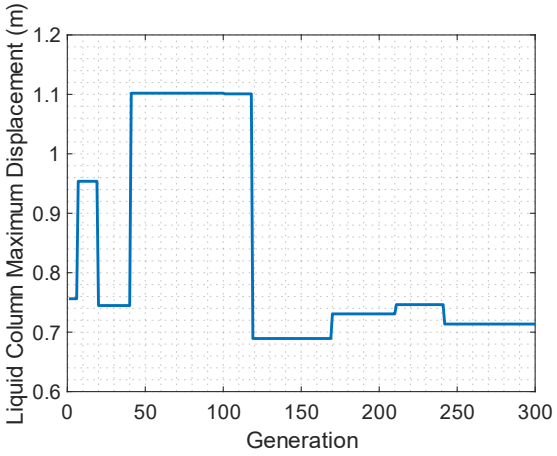

Figure 6.23. Optimum TLCD liquid column maximum displacement through different generations.

The OWT and TLCD optimally designed and the original OWT should present a similar dynamic performance. The performances are expressed in terms of risk curves, representing the occurrence in a certain reference period (typically 1 year) of different response levels (e.g., peak displacement at the tower top). To evaluate the risk curves, a Monte Carlo Analysis is conducted for 5,000 samples where the OWT is considered under environmental and structural uncertainties.

Environmental uncertainties are due to the high complexity of the offshore environment. Different values for the mean wind velocity (longitudinal), wave height, and peak wave frequency are adopted. For the mean wind velocity (Figure 6.24) to represent its annual occurrence at the site where the OWT is located, a Weibull probability distribution is assumed to have scale parameters equal to 20 and shape parameters equal to 2.02. While for the wave, the average value of the wave height and average value of the frequency peak are determined by Equations (3.71) and (3.73). A lognormal distribution is assumed for these two parameters with a covariance of 0.1. Figure 6.25 show these variables distribution.

OWT uncertainties also consider possible variations in the structure, such as changes in the steel elastic modulus and the structural damping ratio (Figure 6.26). To represent possible changes in the steel's elasticity, a log-normal distribution is assumed with a mean value of 210 GPa and covariance of 0.02. For the structural damping ratio, a log-normal distribution is also assumed with a mean value of 0.01 and covariance of 0.08.

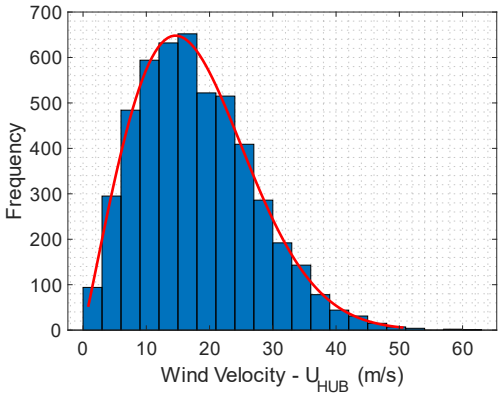

Figure 6.24. Mean wind velocity distribution at the hub height.

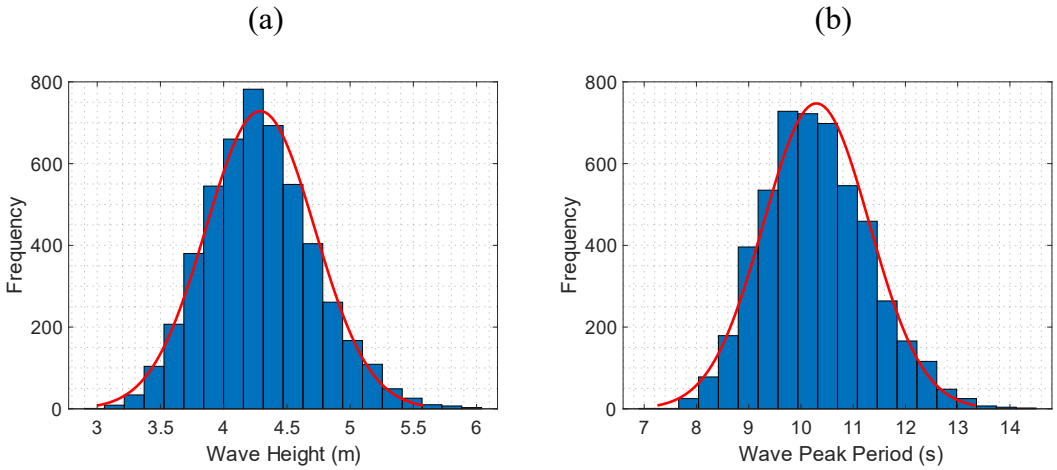

Figure 6.25. Wave height (a) and peak period distribution (b).

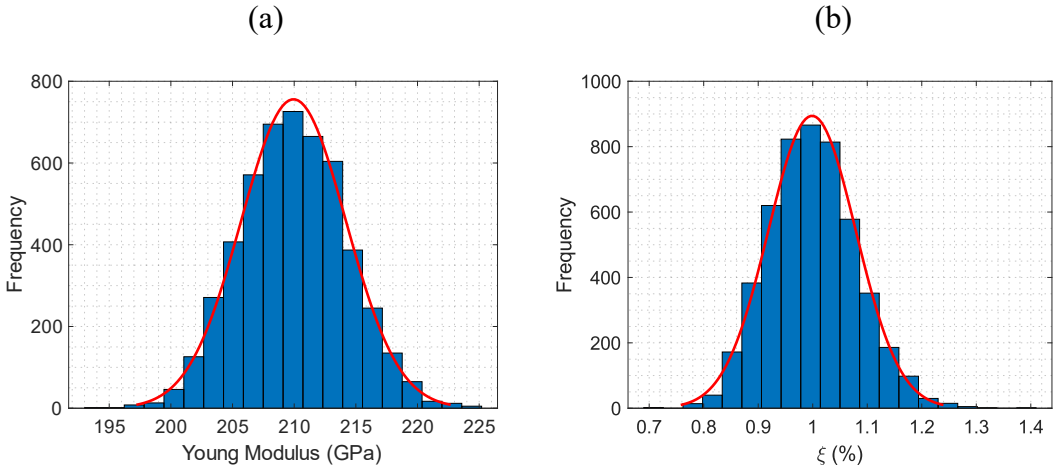

Figure 6.26. Offshore wind turbine material elasticity modulus (a) and damping ratio (b).

Using the distributions and values presented above to determine the uncertain wind, wave, and structural parameters, a Monte Carlo analysis was performed for the optimum OWT with TLCD (Table 6.8) and for the reference OWT (Jonkman and

Musial, 2009; Jonkman et al., 2010). The OWT tip displacement was considered as the EDP parameter

When analyzing the OWT response, it is possible to observe (Figure 6.27) that the structure optimized with TLCD presents a similar performance to the original structure. The use of TLCD allows the optimized structure with a reduced steel volume to present the same level of structural performance. This result demonstrates another damper contribution with the integrated analysis proposed for the optimization process.

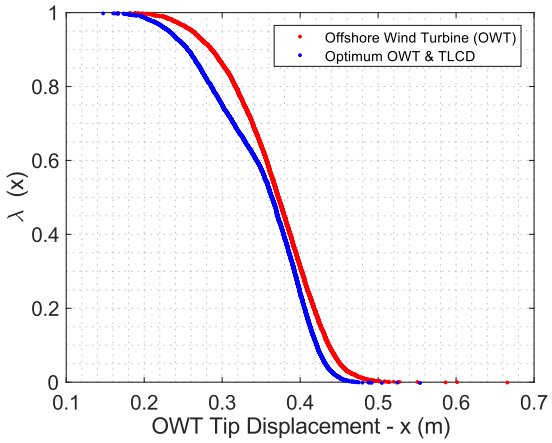

Figure 6.27.Original reference 5-MW OWT and optimized 5-MW OWT with TLCD performance analysis.

6.3 OWT RESPONSE WITH SEMIATIVE TLCD

The use of vibration control technologies can help or even enable the advancement of projects and construction of large OWTs. Control devices allow economic savings, greater durability, and safety increase in OWT projects under presence of random wind and wave loading. Semi-active devices, when compared to passive devices, present more robust performance in controlling vibrations for random loads.

In this section, the OWT performance with semi-active TLCD is evaluated. The on-off damping is regulated by a general controller. The hypothesis of an electro valve that controls the TLCD orifice blocking ratio changes the control device damping alternately is considered. Among the Groundhook control strategies presented, the groundhook control law is adopted based on the increments (Equation (2.15) and (2.16).

The application and interference of semi-active TLCD on the structure's response are evaluated in a 5-MW, a 10-MW, and a 15-MW OWT with monopile foundations (Figure 6.28). For each turbine, the semi-active device maximum and minimum blocking ratio is defined based on parametric study. Also, the OWT response with

TLCD is analyzed under different scenarios. Different wind speed and wave parameters (peak frequency and wave height related to mean wind speed). Cases of OWT in operation and parked are considered. Conditions determined according to the mean wind speed and the OWT cut-in and cut-out speed.

The OWT models adopted for analysis are the NREL 5-MW (Jonkman et al., 2010), 10-MW (Bortolotti et al., 2019) and IEA Wind 15-MW (Gaertner et al., 2020) turbines. The wind turbines main design parameters used for the support structure numerical model are gathered in Table 6.9. Parameters such as the rotor-nacelle assembly mass and the tower and the monopile design properties. The offshore wind turbine structure is modeled numerically using beam elements. The RNA is considered as a lumped mass at the structure (tower) top. For the three turbines, a 1% structural damping ratio is assumed (Padrón et al., 2022).

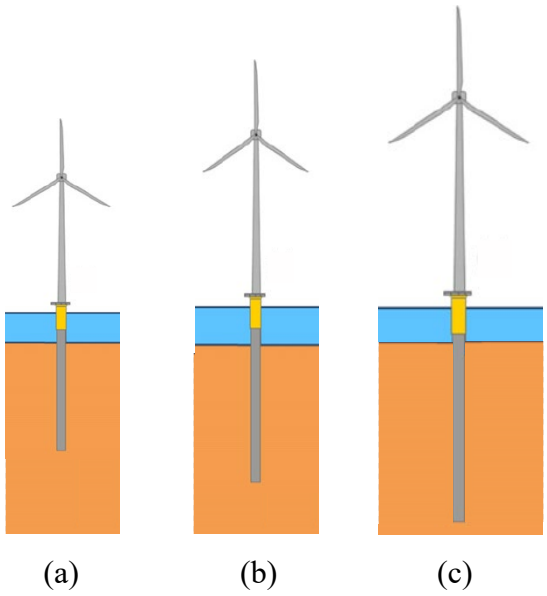

Figure 6.28. 5-MW (a), 10-MW (b), and 15-MW (c) OWT with monopile foundation.

Table 6.9. Reference OWTs and parameters considered for semiactive vibration control analysis.

Offshore Wind Turbine	**5-MW**	**10-MW**	**15-MW**
RNA mass (t)	350.0	720.7	1,017.0
Hub height (m)	90.0	119.0	150.0
Tower mass density (kg/m³)	8,500.0	8,500	7,850.0
Tower Young modulus (GPa)	210.0	200.0	200.0
Tower length (m)	77.6	105.6	129.6
Tower top diameter (m)	3.87	5.5	6.5
Tower top thickness (mm)	19.0	20.0	24.0
Tower base diameter (m)	6.0	8.3	10.0
Tower base thickness (mm)	27.0	38.0	41.1
Monopile length above soil (m)	30.0	40.0	45.0
Monopile diameter (m)	6.0	9.0	10.0
Mean sea level (m)	20.0	30.0	30.0

The mean sea level height assumed for each OWT is shown. This height is considered to determine the wave loading in time by the Morison equation (Equation (3.59)). For the wave load, the drag coefficient is adopted as 1.2 and the inertia coefficient defined by C_i $(= 1 + C_m)$ is assumed as 2.0. These values are considered constant over time. The sea density adopted for analysis is 1.025 kg/m³. The wave height H_s and the peak frequency f_p are related to the wind speed at a 10 m height. To calculate the average wind speed affecting the structure at different heights, the wind exponential profile with $\alpha = 0.14$ is adopted. For wind turbulence, a wind class with $I_{ref} = 0.14$ is considered.

The random characteristic of wind and wave overtime are represented from the Kaimal spectrum and the JONSWAP spectrum. The random wind load on the structure is determined from the drag force. The wave load is expressed using the Morison equation. Finally, the rotor thrust is approximately defined based on the thrust curve's characteristic of each turbine and related to the wind speed. These processes are described in page 55.

6.3.1 TLCD PRELIMINAR DESING

Different control devices and different vibration control strategies have been explored to reduce wind turbines structural problems related to dynamic amplification. There are design limitations to control device dimensions and placement inside the OWT. Most of the works in the field consider the TLCD installed in the nacelle (Duenas-Osorio and Basu, 2008; Colwell and Basu, 2009; Mensah and Duenas-Osorio, 2014). However, the OWT nacelle has a valuable and reduced space to combine the wind turbine mechanical components and the TLCD. As illustrated in Figure 6.29, the semi-active TLCD will be positioned inside the OWT tower.

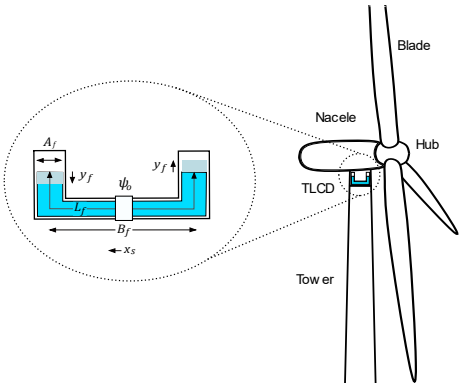

Figure 6.29 . Semi-active TLCD with electro valve positioned inside the OWT tower.

Seeking a TLCD design compatible with the internal diameter of each of the OWT towers, a TLCD aspect ratio for the 5-MW, 10-MW, and 15-MW OWT of 0.30, 0.30, and 0.27, respectively, were adopted. To compensate for the TLCD low aspect ratio (as shown in the parametric study, it reduces the damper efficiency) a 2% mass ratio is assumed for the device design. The TLCD tuning ratio of 0.98 is common to all devices installed in different OWTs.

A passive TLCD with the parameters described above and a blocking ratio of 50% when installed in the 5-MW, 10-MW, and 15-MW OWTs presents an average decrease (among 100 analyzed cases of random wind and wave actions for each OWT) in the OWT response (tower tip rms fore-aft displacement) of 25.2%, 27.9%, and 25.5%, respectively. The rated speed of each turbine is considered as the average wind speed at the hub height (11.4 m/s, 10.75 m/s, and 10.60 m/s for the 5-MW, 10-MW, and 15-MW OWTs, respectively) in the forementioned analyses. This condition is relevant for the OWT structure, as this speed produces the greatest rotor thrust and, consequently, a significant force at the structure top.

To evaluate the semi-active TLCD control on each of the three OWTs performance, a parametric study is employed to evaluate the alternate blocking ratio variation (Table 6.10-Table 6.12). For the maximum damping condition, the blocking ratio admits a range value between 55% and 90% and for the minimum damping condition the blocking ratio assumes values between 45% and 5%.

It is possible to verify that the minimum damping condition has a greater influence on the OWT response with the semi-active TLCD. The blocking ratio (row) range from 45% to 5% has more influence in the OWT response decrease, when compared to the variation of the blocking ratio from 55% to 80% (column). The values of 85% and 90% for the maximum damping condition are not presented because the liquid column maximum displacement exceeds the established theoretical limit (Equation (4.11)). Values not shown in the table (-) represent combinations of maximum and minimum blocking ratio in which the liquid column limit for the maximum displacement is not respected. The highest decrease in the OWTs displacement with semi-active TLCD represents approximately a 10% decrease in OWT response obtained with the passive TLCD.

Table 6.10. 5-MW OWT response mitigation obtained by the semi-active TLCD blocking ratio combination.

ψ_0	45%	40%	35%	30%	25%	20%	15%	10%	5%
55%	26,8%	27,9%	28,8%	29,7%	30,5%	31,2%	31,9%	32,6%	33,4%
60%	27,0%	28,1%	29,1%	30,0%	30,8%	31,5%	32,3%	33,0%	-
65%	27,2%	28,4%	29,4%	30,3%	31,1%	31,9%	32,7%	-	-
70%	27,5%	28,6%	29,7%	30,6%	31,5%	32,3%	-	-	-
75%	27,8%	28,9%	30,0%	31,0%	-	-	-	-	-
80%	28,1%	29,3%	-	-	-	-	-	-	-

Table 6.11. 10-MW OWT response mitigation obtained by the semi-active TLCD blocking ratio combination.

ψ_0	45%	40%	35%	30%	25%	20%	15%	10%	5%
55%	28,4%	29,2%	30,0%	30,6%	31,2%	31,7%	32,2%	32,6%	33,2%
60%	28,8%	29,6%	30,4%	31,1%	31,7%	32,3%	32,8%	33,3%	33,8%
65%	29,2%	30,1%	30,9%	31,6%	32,3%	32,9%	33,4%	34,0%	34,6%
70%	29,6%	30,6%	31,4%	32,2%	32,8%	33,5%	34,1%	34,6%	35,3%
75%	30,1%	31,1%	32,0%	32,7%	33,4%	34,1%	34,7%	-	-
80%	30,6%	31,6%	32,5%	33,3%	-	-	-	-	-

Table 6.12. 15-MW OWT response mitigation obtained by the semi-active TLCD blocking ratio combination.

ψ_0	45%	40%	35%	30%	25%	20%	15%	10%	5%
55%	24,7%	25,9%	26,9%	27,8%	28,7%	29,6%	30,4%	31,2%	32,1%
60%	25,0%	26,1%	27,2%	28,2%	29,1%	29,9%	30,8%	31,6%	32,6%
65%	25,2%	26,4%	27,5%	28,5%	29,4%	30,3%	31,2%	32,1%	-
70%	25,5%	26,7%	27,8%	28,9%	29,8%	30,7%	31,6%	-	-
75%	25,8%	27,0%	28,2%	29,3%	30,3%	-	-	-	-
80%	26,1%	27,4%	28,6%	-	-	-	-	-	-

6.3.2 SEMI-ACTIVE TLCD ANALYSIS FOR OPERATING OWT

Vibration control analysis with the semi-active TLCD, measured by the OWTs displacement decrease at the tower top, have been computed for maximum and minimum blocking ratio different combinations. The mean wind speed for each of the turbines was considered constant and equal to the OWT rated speed, specified in Jonkman et al. (2010), Bortolotti et al. (2019), and Gaertner et al. (2020).

In the following analysis, the OWTs response with passive and semi-active TLCDs are measured for different average wind speeds, and consequently for different wave heights and wave peak frequencies, are presented. Computed values are the mean

values. One hundred cases were processed for each wind speed analyzed, and the mean OWT response is presented.

The wind turbine operates while the mean wind has its speed between the cut-in and cut-out speed. For each OWT, the on-off blocking ratio combination assumed for the semi-active TLCD is the one that resulted in the most significant reductions in OWT response, as shown in Table 6.10-Table 6.12. The on-off blocking ratios for the semi-active TLCD connected to the 5-MW OWT, the 10-MW OWT, and the 15-MW OWT are 55%-5%, 70%-5%, and 60%-5%, respectively.

The TLCD in the 5-MW OWT, for the mean wind speed range analyzed (Figure 6.30), presented an average response reduction of 25.9% with passive control and 31.4% with semi-active control. An additional 7.4% average reduction was achieved with the semi-active TLCD compared to the passive TLCD. Near the OWT's rated speed, the mean response reduction was 24.7% with passive control and 31.0% with semi-active control, resulting in an 8.4% decrease between semi-active and passive control. Figure 6.31 illustrates a case of the 5-MW OWT at the rated turbine speed (11.4 m/s). In this analysis, a reduction of 23.57% was obtained with the passive TLCD and 34.91% with the semi-active TLCD. The response of the 5-MW OWT with the semi-active TLCD, using electro valve damping control, demonstrated a reduction of 14.84% compared to the passive TLCD, exceeding the average reduction presented.

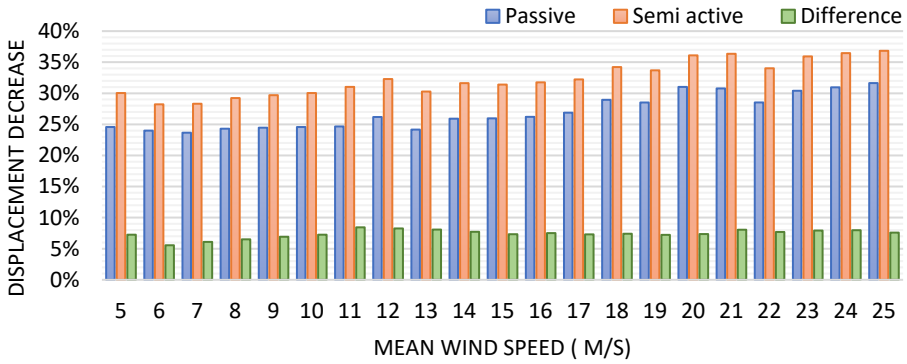

Figure 6.30. 5-MW OWT rms fore-aft top displacement decrease with passive and semiactive TLCD.

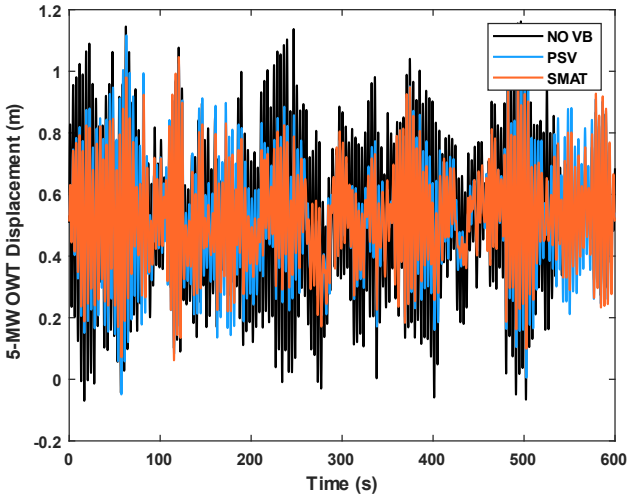

Figure 6.31. 5-MW OWT fore-aft displacement at the top for a mean wind speed of 11.40 m/s.

For the 10-MW OWT (Figure 6.32), the TLCD showed an average reduction in the OWT response of 26.6% with passive control and 32.6% with semi-active control, resulting in an 8.1% reduction between the two types of control. Near the rated speed, the average OWT response reduction was 29% with passive control and 36% with semi-active control, leading to an average 10% decrease with semi-active control compared to passive control. Figure 6.32 presents an analyzed case of the 10-MW OWT at the rated turbine speed (10.75 m/s). The average response reduction of the 10-MW OWT with passive and semi-active control was 32.11% and 39.30%, respectively. The response of the 10-MW OWT with semi-active TLCD showed a reduction of 10.59% compared to passive control.

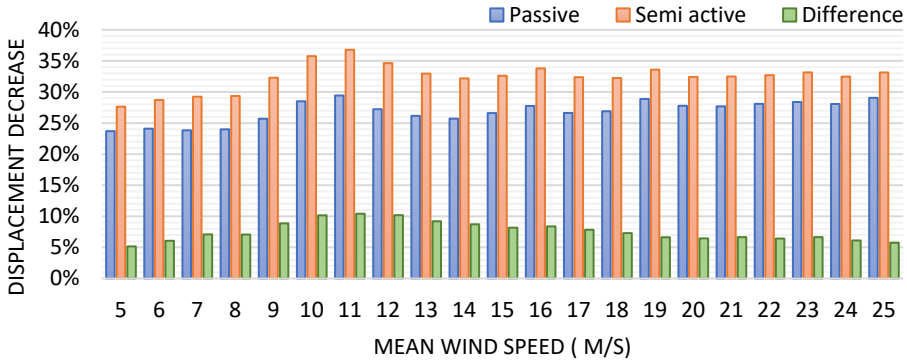

Figure 6.32. 10-MW OWT rms fore-aft top displacement decrease with passive and semiactive TLCD.

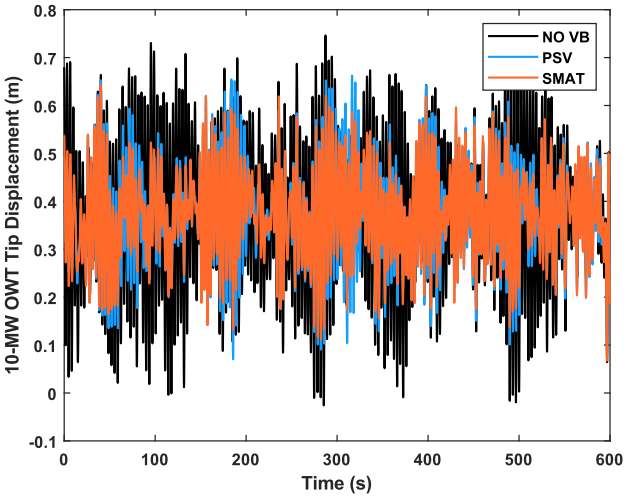

Figure 6.33. 10-MW OWT fore-aft displacement at the top for a mean wind speed of 10.75 m/s.

Finally, for the 15-MW OWT (Figure 6.34), an average reduction in OWT response of 24.8% with passive control and 31.7% with semi-active control was observed, resulting in an average reduction of 9.2% with semi-active control. Near the nominal speed, there was an average reduction in the OWT response of 24% with passive control and 33% with semi-active control, yielding an 11.5% reduction with semi-active control. Figure 6.35 presents an analyzed case of the 15-MW OWT at the turbine rated speed (10.59 m/s). In this analysis, a reduction of 27.9% was achieved with the passive TLCD and 32.38% with the semi-active TLCD, which is below the average presented. The response of the 15-MW OWT with semi-active TLCD showed a reduction of 6.22% compared to passive control.

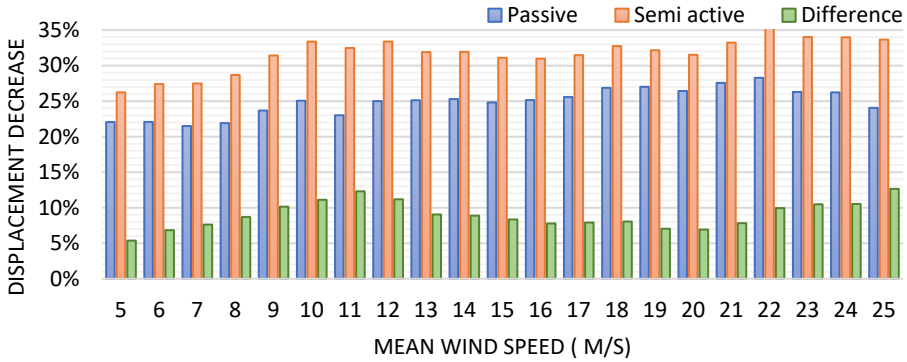

Figure 6.34. 15-MW OWT rms fore-aft top displacement decrease with passive and semiactive TLCD.

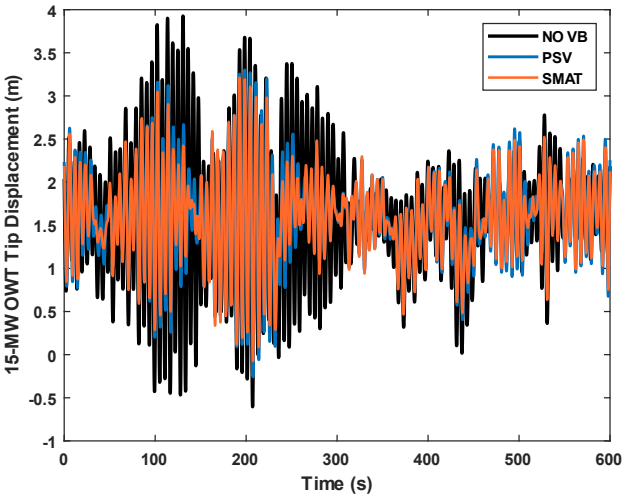

Figure 6.35. 15-MW OWT fore-aft displacement at the top for a mean wind speed of 10.59 m/s.

6.3.3 TLCD ANALYSIS FOR PARKED OWT

Figure 6.36-Figure 6.38 shows the average reduction in the OWTs fore-aft rms displacement at the tower top using passive and semi-active TLCD, considering the OWT parked. In this position, the OWT is analyzed without the dynamic thrust force on the rotor caused by wind turbulence on the rotating blades. For each OWT with semi-active TLCD, the same on-off blocking ratio combinations are adopted as those used in the previously analyzed cases.

In the 5-MW OWT (Figure 6.36), the TLCD resulted in an average response reduction of 29.7% with passive control and 30.4% with semi-active control, showing an average difference of 1%. For the 10-MW OWT (Figure 6.37), the TLCD achieved an average response reduction of 26.5% with passive control and 30.4% with semi-active control, indicating an average difference of 5.4%. Finally, in the case of the 15-MW OWT (Figure 6.38), there was an average response reduction of 29.4% with passive control and 31.6% with semi-active control, with an average difference of 3.2%. The performance of the passive TLCD closely matches that of the semi-active TLCD when the wind turbine is in parked position.

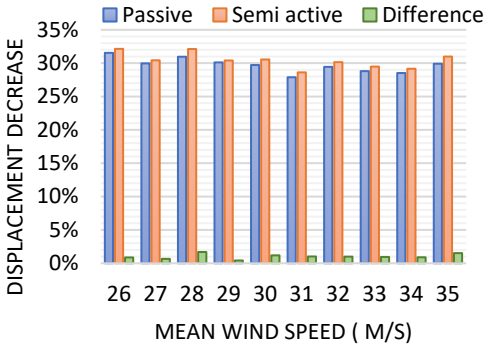

Figure 6.36**.** Parked 5-MW OWT rms fore-aft top displacement decrease with TLCD.

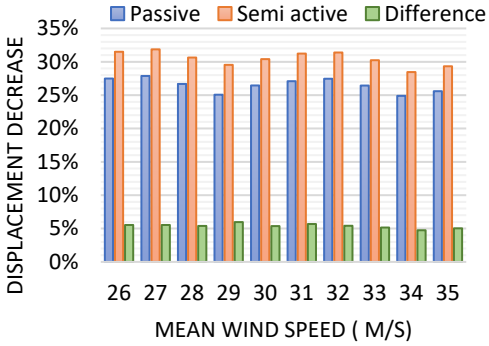

Figure 6.37. Parked 10-MW OWT rms fore-aft top displacement decrease with TLCD.

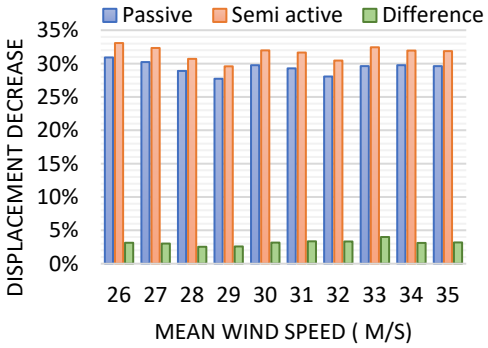

Figure 6.38. Parked 15-MW OWT rms fore-aft top displacement decrease TLCD.

7. CONCLUSION & SUGGESTIONS

In this work, the Tuned Liquid Column Damper use was proposed to control offshore wind turbines random vibrations. Different design possibilities and configurations (TLCD and OWT support structure) are addressed and analyzed from aspects of OWT and device performance.

System design and performance assessment are embedded in optimization and performance-based procedures, respectively. A Genetic Algorithm routine was adopted for the optimization process given the numerical model complexity. The performance assessment considers the parameters uncertainties involved in the system and in the offshore environment and employs the Performance-Based Wind Engineering (PBWE) approach in a simplified way.

For the OWT and TLCD optimal design approach and performance assessment, the thesis gathers fundamental aspects and theoretical formulations for random vibration control. The TLCD dynamic equation is presented, as well as the main parameters for its optimal design. Next, the formulation of the semi-active TLCD is highlighted considering different groundhook control laws to define the damping related to the alternately regulated electro valve. In fact, a groundhook formulation is proposed, where the increments in the system's response are observed. For the formulation of the OWT with a fixed monopile foundation, an extensive review of the main soil-structure interaction models for the monopile foundation is presented. For analysis in stochastic terms, the random and uncertain model for wind and wave actions on the turbine (structure and rotor) is also developed and exposed.

Initially, the passive TLCD optimal design for the NREL 5-MW OWT vibration control under random wind and wave loads was analyzed. Despite the computational cost (processing time), an analysis of the optimal TLCD parameters was carried out using the response map for comparison purposes. There was a solid agreement between the optimal TLCD parameters obtained by the map response analyses and the GA analyses, with less than 0.5% differences. From the optimization with GA, a parametric study focused on the TLCD was evaluated with the objective of minimizing the response of the OWT in terms of longitudinal displacement at the top of the tower. It could be observed that the greater the TLCD mass ratio μ_f and aspect ratio α_f, the greater the reduction in OWT displacements. Although, in practice the OWT configuration limits the device design and dimensions. Also, it was noted that the

increase in the TLCD damping ratio ζ_f is related to devices with larger dimensions (higher mass ratio) and with a horizontally aspect (higher aspect ratio). Linked to the progressive increase of these three parameters, the optimal TLCD presents a reduction in the tuning ratio γ_f with the distancing from the structure fundamental frequency. This TLCD parameters behavior pattern was seen as the different actions considered in the analysis. The optimal TLCD showed, in general, a reduction in the longitudinal displacements of the turbine of more than 35%, reaching a maximum value of 60%. OWT vibration control by the optimal TLCD proved to be efficient and robust. Considering different sources of uncertainty, such as basic wind and wave parameters and structural parameters, the average response decreases 45%.

Second, a simultaneous optimal design is proposed and evaluated also for the NREL 5-MW Reference OWT and TLCD under wind and wave random loads. The proposed procedure, through the GA optimization script, jointly seeks an optimal solution for the support structure and TLCD that minimizes the structural steel volume and, consequently, the OWT cost. The structure (tower and monopile) diameter and thickness are defined as the structural design variables, while the tuning and damping ratios are the damper design variables. The optimization process accounts with restrictions established for the model, such as the tower top displacement, the critical buckling stress at the tower base, and the liquid column maximum displacement inside the reservoir.

The simultaneous optimal design allowed a 17% decrease in the OWT support structure volume. This represents more than 20% reduction in materials and production costs according to the method presented in Uys et al. (2006). The OWT foundation and tower design had its thickness significantly reduced by 20%, while the structural and damper design met the established displacement and tension restrictions. The OWT fundamental frequency lies between the NREL 5-MW Reference WT 1P and 3P loads. Furthermore, using the optimal TLCD allows greater freedom for the structure's design. The TLCD is highly efficient in mitigating structure displacements in the resonance range, which is an OWT relevant design factor. Also, the TLCD allows the optimized OWT to present the same level of structural performance as the original reference OWT configuration. The proposed simultaneous optimization is generic and adaptable to the intended analysis. It can be extended to optimize other OWT structures and support types. The optimization objective function can be adapted, and other design variables and restrictions can be considered. The adopted procedure performs efficiently and is possible to solve real problems in the design of offshore structures.

Finally, to increase vibration reduction in OWTs, the use of semi-active TLCD with on-off damping regulated by an electro valve is evaluated. 5-MW, 10-MW and 15-MW OWTs with different dimensions, parameters, and properties were adopted for the analysis. Random wind and wave loads, respectively, were computed in time from the Kaimal spectrum and the JONSWAP spectrum transforms. Different average wind speeds and, consequently, different wave heights and peak frequencies were considered. To compare the OWT and semi-active TLCD performance, passive devices were also considered in the study.

In OWTs with semi-active TLCD, a 30% decrease in the response was observed and, in the best scenario, cases with reductions close to 35%. The semi-active TLCD with the inclusion of the electro valve to regulate the damping showed reductions in the response of the OWTs that were greater than the reductions obtained by the passive TLCD. Especially for the OWT in operation, for the average wind speed between the turbine cut-in and cut-out speeds.

Based on the applications and results presented, this work contributes to the different possibilities analysis and investigation for applying TLCD to wind turbines. Defines and evaluates the TLCD parameters optimal behavior. It also proposes the support structure and device simultaneous optimization in accordance with system constraints. Investigates the semi-active TLCD damping mechanism implementation. The studies in the thesis attest the device robustness with OWT performance improvement and indicate the possibility of optimizing the OWT support structure with TLCD while maintaining structural performance.

It is important to highlight that future studies involving the scope, concepts, and applications developed and presented throughout the thesis may advance in points such as:

- Consider interaction parameters related to the uncertainties of aeroelastic, aerodynamic, hydrodynamic and soil-structure phenomena for the OWT with TLCD performance analysis.

- Proceed with the OWT with TLCD reliability and risk analysis considering a low level of performance (excessive deformations or vibrations) and a high level of performance (fatigue failure, local or global instability).

- Search and apply a robust method for performance-based optimum design.

BIBLIOGRAPHY

Abed, Y., Bouzid, D. A., Bhattacharya, S., & Aissa, M. H. (2016). Static impedance functions for monopiles supporting offshore wind turbines in nonhomogeneous soils-emphasis on soil/monopile interface characteristic. Earthquake and Structures, 10(5), 1143–1179. https://doi.org/10.12989/eas.2016.10.5.1143

Aissa, M. H., Amar Bouzid, D., & Bhattacharya, S. (2017). Monopile head stiffness for serviceability limit state calculations in assessing the natural frequency of offshore wind turbines. Https://Doi.Org/10.1080/19386362.2016.1270794, 12(3), 267–283. https://doi.org/10.1080/19386362.2016.1270794

Alkmim, M. H., Fabro, A. T., & de Morais, M. V. G. (2018). Optimization of a tuned liquid column damper subject to an arbitrary stochastic wind. Journal of the Brazilian Society of Mechanical Sciences and Engineering, 40(11). https://doi.org/10.1007/s40430-018-1471-3

Altay, O. Vibration Mitigation Systems in Structural Engineering. CRC Press, 2021

Altay, O., & Klinkel, S. (2018). A semi-active tuned liquid column damper for lateral vibration control of high-rise structures: Theory and experimental verification. Structural Control and Health Monitoring, 25(12). https://doi.org/10.1002/stc.2270

Amar Bouzid, D. (2018). Numerical Investigation of Large-Diameter Monopiles in Sands: Critical Review and Evaluation of Both API and Newly Proposed p-y Curves. International Journal of Geomechanics, 18(11). https://doi.org/10.1061/(ASCE)GM.1943-5622.0001204

Amar Bouzid, D., Bhattacharya, S., & Dash, S. R. (2013). Winkler Springs (p-y curves) for pile design from stress-strain of soils: FE assessment of scaling coefficients using the Mobilized Strength Design concept. Geomechanics and Engineering, 5(5). https://doi.org/10.12989/gae.2013.5.5.379

Andersen, K. H. (2015). Cyclic soil parameters for offshore foundation design. Frontiers in Offshore Geotechnics III - Proceedings of the 3rd International Symposium on Frontiers in Offshore Geotechnics, ISFOG 2015. https://www.proquest.com/conference-papers-proceedings/cyclic-soil-parameters-offshore-foundation-design/docview/2115979786/se-2

Anson, M., Ko, J. M., Lam, E. S. S., Wang, J. Y., Ni, Y. Q., & Spencer, B. F. (2002). Semi-active TLCDs using magneto-rheological fluids for vibration mitigation of tall buildings. In Advances in Building Technology (Vol. 1).

Arany, L., Bhattacharya, S., Macdonald, J. H. G., & Hogan, S. J. (2016). Closed form solution of Eigen frequency of monopile supported offshore wind turbines in deeper waters incorporating stiffness of substructure and SSI. Soil Dynamics and Earthquake Engineering, 83, 18–32. https://doi.org/10.1016/J.SOILDYN.2015.12.011

Ashasi-Sorkhabi, A., Malekghasemi, H., Ghaemmaghami, A., & Mercan, O. (2017). Experimental investigations of tuned liquid damper-structure interactions in resonance considering multiple parameters. Journal of Sound and Vibration, 388, 141–153. https://doi.org/10.1016/j.jsv.2016.10.036

Augusti, G., & Ciampoli, M. (2008). Performance-Based Design in risk assessment and reduction. Probabilistic Engineering Mechanics, 23(4), 496–508. https://doi.org/10.1016/j.probengmech.2008.01.007

Balendra, T., Wang, C. M., & Cheong, H. F. (1995). Effectiveness of tuned liquid column dampers for vibration control of towers. In Engineering Structures (Vol. 17, Issue 9).

Barbato, M., Ciampoli, M., & Petrini, F. (2010). Effects of modeling parameter uncertainty on the structural response of offshore wind turbines. Proceedings of the 12th International Conference on Engineering, Science, Construction, and Operations in Challenging Environments - Earth and Space 2010, 2027–2038. https://doi.org/10.1061/41096(366)185

Bhattacharya, S. (2019). Design of foundations for offshore wind turbines. John Wiley & Sons Ltd.

Bhattacharya, S., Lombardi, D., Amani, S., Aleem, M., Prakhya, G., Adhikari, S., Aliyu, A., Alexander, N., Wang, Y., Cui, L., Jalbi, S., Pakrashi, V., Li, W., Mendoza, J., & Vimalan, N. (2021). Physical Modelling of Offshore Wind Turbine Foundations for TRL (Technology Readiness Level) Studies. Journal of Marine Science and Engineering 2021, Vol. 9, Page 589, 9(6), 589. https://doi.org/10.3390/JMSE9060589

Bhattacharyya, S., Ghosh, A. (Dey), & Basu, B. (2017). Nonlinear modeling and validation of air spring effects in a sealed tuned liquid column damper for structural control. Journal of Sound and Vibration, 410, 269–286. https://doi.org/10.1016/j.jsv.2017.07.046

Bisoi, S., & Haldar, S. (2014). Dynamic analysis of offshore wind turbine in clay considering soil–monopile–tower interaction. Soil Dynamics and Earthquake Engineering, 63, 19–35. https://doi.org/10.1016/j.soildyn.2014.03.006

Bisoi, S., & Haldar, S. (2015). Design of monopile supported offshore wind turbine in clay considering dynamic soil-structure-interaction. Soil Dynamics and Earthquake Engineering, 73, 103–117. https://doi.org/10.1016/j.soildyn.2015.02.017

Borri, C.; Pastò, S.. Lezioni di ingegneria del vento. Firenze University Press, 2006.

Bortolotti, P., Canet Tarres, H., Dykes, K., Merz, K., Sethuraman, L., Verelst, D., & Zahle, F. (2019). IEA Wind TCP Task 37 Systems Engineering in Wind Energy-WP2.1 Reference Wind Turbines Technical Report. www.nrel.gov/publications.

Brasil sobe para 6ª posição no ranking de capacidade de energia eólica da matéria. Exame, 2022. Disponível em: < https://exame.com/esg/brasil-sobe-para-6a-posicao-no-ranking-de-capacidade-de-energia-eolica/>. Acesso em: 07 de fevereiro de 2023.

Brebbia, C., Walker, S.. Dynamic Analysis of Offshore Structures. Newnes, 1979.

British Standards Institution. (2006a). Wind turbines. British Standards Institution.

British Standards Institution. (2009). BS EN 61400-3: Wind turbines. Part 3: design requirements for offshore wind turbines. BSI.

Buckley, T., Watson, P., Cahill, P., Jaksic, V., Pakrashi, V. (2018). Mitigating the structural vibration of wind turbines using tuned liquid column dampers considering soil-structure interaction. Renewable Energy, Elsevier, 120, 322-341.

Burton, T., Jenkins, N., Bossanyi, E., Sharpe, D., & Graham, M. (2021). Wind Energy Handbook 3e. Wiley. https://doi.org/10.1002/9781119451143

Byrne, B., Houlsby, G., Martin, C., & Fish, P. (2002). Suction Caisson Foundations for Offshore Wind Turbines. Http://Dx.Doi.Org/10.1260/030952402762056063, 26(3), 145–155.

Byrne, B. W., Burd, H. J., Zdravković, L., McAdam, R. A., Taborda, D. M. G., Houlsby, G. T., Jardine, R. J., Martin, C. M., Potts, D. M., & Gavin, K. G. (2019). PISA: new design methods for offshore wind turbine monopiles. Revue Française de Géotechnique, 158, 3. https://doi.org/10.1051/geotech/2019009

Byrne, B. W., McAdam, R. A., Burd, H. J., Houlsby, G. T., Martin, C. M., Beuckelaers, W. J. A. P., Zdravkovic, L., Taborda, D. M. G., Potts, D. M., Jardine, R. J., Ushev, E., Liu, T., Abadias, D., Gavin, K., Igoe, D., Doherty, P., Skov-Gretlund, J., Pacheco-Andrade, M., Muir-Wood, A., … Plummer, M. A. L. (2017). PISA: New design methods for offshore wind turbine monopiles. 8th International Conference for Offshore Site Investigation and Geotechnics, 142–161. https://www.issmge.org/events/osig-2017

Carswell, W., Arwade, S. R., DeGroot, D. J., & Lackner, M. A. (2015). Soil-structure reliability of offshore wind turbine monopile foundations. Wind Energy, 18(3), 483–498. https://doi.org/10.1002/we.1710

Casciati, F., Magonette, G., & Marazzi, F. (2006). Technology of Semiactive Devices and Applications in Vibration Mitigation. Wiley.

Chakrabarti, S. K. (2005). HANDBOOK OF OFFSHORE ENGINEERING Volume I 2005 ELSEVIER.

Chakraborty, S., Debbarma, R., & Marano, G. C. (2012). Performance of tuned liquid column dampers considering maximum liquid motion in seismic vibration control of structures. Journal of Sound and Vibration, 331(7), 1519–1531. https://doi.org/10.1016/j.jsv.2011.11.029

Chaves Júnior, C. V., Araújo, R. C. de A., de Souza, C. M. C., Ferreira, A. C. A., & Ribeiro, P. M. V. (2020). A collocation method for bending, torsional, and axial vibrations of offshore wind turbines on monopile foundations. Ocean Engineering, 217(October 2019). https://doi.org/10.1016/j.oceaneng.2020.107735

Ciampoli, M., & Petrini, F. (2010). Performance-Based Design of Offshore Wind Turbines. Earth and Space 2010: Engineering, Science, Construction, and Operations in Challenging Environments, 2063–2078. https://doi.org/10.1061/41096(366)189

Ciampoli, M., Petrini, F., & Augusti, G. (2011). Performance-Based Wind Engineering: Towards a general procedure. Structural Safety, 33(6), 367–378. https://doi.org/10.1016/j.strusafe.2011.07.001

Clough, R. W., & Penzien, J. (2003). DYNAMICS OF STRUCTURES.

Colherinhas, G. B., de Morais, M. V. G., & Petrini, F. (2024). Global vibration control of offshore wind turbines with a flexible monopile foundation using a pendulum-tuned mass damper: Risk mitigation and performance incrementation. Ocean Engineering, 297. https://doi.org/10.1016/j.oceaneng.2024.117168

Colherinhas, G., Petrini, F., de Morais, M. V. G., & Bontempi, F. (2021). Optimal design of passive-adaptive pendulum tuned mass damper for the global vibration control of offshore wind turbines. Wind Energy, 24(6), 573–595. https://doi.org/10.1002/we.2590

Colherinhas, G., Petrini, F., Morais, M. V. G., & Bontempi, F. (2021). Optimal design of passive-adaptive pendulum tuned mass damper for the global vibration control of offshore wind turbines. Wind Energy, 24(6), 573–595. https://doi.org/10.1002/we.2590

Colwell, S., & Basu, B. (2009). Tuned liquid column dampers in offshore wind turbines for structural control. Engineering Structures, 31(2), 358–368. https://doi.org/10.1016/j.engstruct.2008.09.001

Custódio, P.. Capacidade instalada da energia eólica no Brasil pode abastecer 28,8 milhões de residências por mês. Brasil 61, Brasília, 05 de novembro de 2022. Disponível em: <https://brasil61.com/n/capacidade-instalada-da-energia-eolica-no-brasil-pode-abastecer-28-8-milhoes-de-residencias-por-mes>.

Dai, K., Huang, H., Lu, Y., Meng, J., Mao, Z., & Camara, A. (2021). Effects of soil–structure interaction on the design of tuned mass damper to control the seismic response of wind turbine towers with gravity base. Wind Energy, 24(4), 323–344. https://doi.org/10.1002/we.2576

Damgaard, M., Ibsen, L. B., Andersen, L. V., & Andersen, J. K. F. (2013). Cross-wind modal properties of offshore wind turbines identified by full scale testing. Journal of Wind Engineering and Industrial Aerodynamics, 116, 94–108. https://doi.org/10.1016/j.jweia.2013.03.003

Ding, H., Chen, Y. N., Wang, J. T., & Altay, O. (2022). Numerical analysis of passive toroidal tuned liquid column dampers for the vibration control of monopile wind turbines using FVM and FEM. Ocean Engineering, 247. https://doi.org/10.1016/j.oceaneng.2022.110637

DNV, & Risø. (2002). Guidelines for design of wind turbines. Det Norske Veritas.

DNVGL-RP-202, RECOMMENDED PRACTICE Buckling strength of shells. (2017). http://www.dnvgl.com,

DNVGL-ST-0126. (2018a). Support structures for wind turbines. http://www.dnvgl.com,

DNV-OS-J101. (2014). Design of Offshore Wind Turbine Structures.

DNV-RP-C205. (2007). Environmental conditions and environmental loads. In DET NORSKE VERITAS Recommended Practices (Issue April).

Dueñas-Osorio, L., & Basu, B. (2008). Unavailability of wind turbines due to wind-induced accelerations. Engineering Structures, 30(4), 885–893. https://doi.org/10.1016/j.engstruct.2007.05.015

Esteban, M. D., López-Gutiérrez, J. S., Negro, V., Matutano, C., García-Flores, F. M., & Millán, M. Á. (2015). Offshore Wind Foundation Design: Some Key Issues. Journal of Energy Resources Technology, Transactions of the ASME, 137(5). https://doi.org/10.1115/1.4030316

Ferreira, Y. A., Vernizzi, G. J., Futai, M. M., & Franzini, G. R. (2024). Modeling strategies for wind turbines considering soil–structure interaction. Ocean Engineering, 309. https://doi.org/10.1016/j.oceaneng.2024.118310

Fitzgerald, B., & Basu, B. (2020). Vibration control of wind turbines: recent advances and emerging trends. In Int. J. Sustainable Materials and Structural Systems (Vol. 4).

Gaertner, E., Rinker, J., Sethuraman, L., Zahle, F., Anderson, B., Barter, G., Abbas, N., Meng, F., Bortolotti, P., Skrzypinski, W., Scott, G., Feil, R., Bredmose, H., Dykes, K., Shields, M., Allen, C., & Viselli, A. (2020). Definition of the IEA Wind 15-Megawatt Offshore Reference Wind Turbine Technical Report. www.nrel.gov/publications.

Gao, H., Kwok, K. C. S., & Samali, B. (1997). Optimization of tuned liquid column dampers. In Engineering Structures (Vol. 19, Issue 6).

Gazetas, G. (1984). Seismic response of end-bearing single piles. International Journal of Soil Dynamics and Earthquake Engineering, 3(2), 82–93. https://doi.org/10.1016/0261-7277(84)90003-2

Gazetas, G. (1991). Formulas and Charts for Impedances of Surface and Embedded Foundations. Journal of Geotechnical Engineering, 117(9), 1363–1381. https://doi.org/10.1061/(ASCE)0733-9410(1991)117:9(1363)

Ghosh, A., & Basu, B. (2004). Seismic vibration control of short period structures using the liquid column damper. Engineering Structures, 26(13), 1905–1913. https://doi.org/10.1016/j.engstruct.2004.07.001

Ghosh, A., & Basu, B. (2005). Effect of soil interaction on the performance of liquid column dampers for seismic applications. Earthquake Engineering and Structural Dynamics, 34(11), 1375–1389. https://doi.org/10.1002/eqe.485

Girão de Morais, M. V., Mendes, M. V., & Pedroso, L. J. (2024). Foundation and Support Structures of Wind Turbines and Optimization. In Reference Module in Earth Systems and Environmental Sciences. Elsevier. https://doi.org/10.1016/b978-0-323-93940-9.00243-7

Goldberg, D.. Genetic Algorithms in Search, Optimization and Machine Learning. Addison-Wesley Longman Publishing Co., Inc., Boston, MA, USA, 1989.

Gur, S., Roy, K., & Mishra, S. K. (2015). Tuned liquid column ball damper for seismic vibration control. Structural Control and Health Monitoring, 22(11), 1325–1342. https://doi.org/10.1002/stc.1740

Hamilton, C. M., & Abadie, C. N. (2023). Seismic excitation of offshore wind turbines and transition piece response. Earthquake Engineering & Structural Dynamics, 52(7), 2091–2114. https://doi.org/10.1002/EQE.3872

Hassanzadeh, M. (2012). Cracks in onshore wind power foundations Causes and consequences.

Hemmati, A., Oterkus, E., & Barltrop, N. (2019). Fragility reduction of offshore wind turbines using tuned liquid column dampers. Soil Dynamics and Earthquake Engineering, 125. https://doi.org/10.1016/j.soildyn.2019.105705

Hochrainer, M. J., & Fotiu, P. A. (2018). Design of coupled tuned liquid column gas dampers for multi-mode reduction in vibrating structures. Acta Mechanica, 229(2), 911–928. https://doi.org/10.1007/s00707-017-2007-0

Hochrainer, M. J., & Ziegler, F. (2006). Control of tall building vibrations by sealed tuned liquid column dampers. Structural Control and Health Monitoring, 13(6), 980–1002. https://doi.org/10.1002/stc.90

Hokmabady, H., Mohammadyzadeh, S., & Mojtahedi, A. (2019). Suppressing structural vibration of a jacket-type platform employing a novel Magneto-Rheological Tuned Liquid Column Gas Damper (MR-TLCGD). Ocean Engineering, 180, 60–70. https://doi.org/10.1016/j.oceaneng.2019.03.055

Horgan, C. (2013). Using energy payback time to optimise onshore and offshore wind turbine foundations. Renewable Energy, 53, 287–298. https://doi.org/10.1016/j.renene.2012.10.044

Inman, D.. Engineering Vibration. Pearson, 2014.

Ishihara, T., & Wang, L. (2019). A study of modal damping for offshore wind turbines considering soil properties and foundation types. Wind Energy, 22(12), 1760–1778. https://doi.org/10.1002/we.2401

Jahani, K., Langlois, R. G., & Afagh, F. F. (2022a). Structural dynamics of offshore Wind Turbines: A review. In Ocean Engineering (Vol. 251). Elsevier Ltd. https://doi.org/10.1016/j.oceaneng.2022.111136

Jahani, K., Langlois, R. G., & Afagh, F. F. (2022b). Structural dynamics of offshore Wind Turbines: A review. Ocean Engineering, 251, 111136. https://doi.org/10.1016/j.oceaneng.2022.111136

Jiang, Z. (2021). Installation of offshore wind turbines: A technical review. Renewable and Sustainable Energy Reviews, 139, 110576. https://doi.org/10.1016/j.rser.2020.110576

Jonkman, J., Butterfield, S., Musial, W., & Scott, G. (2009). Definition of a 5-MW Reference Wind Turbine for Offshore System Development. http://www.osti.gov/bridge

Jonkman, J., & Musial, W. (2010). Offshore Code Comparison Collaboration (OC3) for IEA Task 23 Offshore Wind Technology and Deployment. http://www.osti.gov/bridge

Jostad, H. P., Grimstad, G., Andersen, K. H., Saue, M., Shin, Y., & You, D. (2014). A FE procedure for foundation design of offshore structures - Applied to study a potential OWT monopile foundation in the Korean Western Sea. Geotechnical Engineering, 45(4).

Kallehave, D., Byrne, B. W., LeBlanc Thilsted, C., & Mikkelsen, K. K. (2015). Optimization of monopiles for offshore wind turbines. Philosophical Transactions of the Royal Society A: Mathematical, Physical and Engineering Sciences, 373(2035). https://doi.org/10.1098/RSTA.2014.0100

Kallehave, D., Thilsted, C. L. B., & Liingaard, M. A. (2012). Modification of the API p-y formulation of initial stiffness of sand. Offshore Site Investigation and Geotechnics 2012: Integrated Technologies - Present and Future, OSIG 2012.

Kaynia, A. M. (2021). Analysis of Pile Foundations Subject to Static and Dynamic Loading. In Analysis of Pile Foundations Subject to Static and Dynamic Loading. https://doi.org/10.1201/9780429354281

Kikuchi, R. (2010). Risk formulation for the sonic effects of offshore wind farms on fish in the EU region. Marine Pollution Bulletin, 60(2), 172–177. https://doi.org/10.1016/J.MARPOLBUL.2009.09.023

Konar, T., & Ghosh, A. (2023). A review on various configurations of the passive tuned liquid damper. In JVC/Journal of Vibration and Control (Vol. 29, Issues 9–10, pp. 1945–1980). SAGE Publications Inc. https://doi.org/10.1177/10775463221074077

Koo et al. (2004) In Search of Suitable Control Methods for Semi-Active Tuned Vibration Absorbers. (n.d.).

La, V. D. (2012). Semi-active on-off damping control of a dynamic vibration absorber using Coriolis force. Journal of Sound and Vibration, 331(15), 3429–3436. https://doi.org/10.1016/j.jsv.2012.03.026

La, V. D., & Adam, C. (2018). General on-off damping controller for semi-active tuned liquid column damper. JVC/Journal of Vibration and Control, 24(23), 5487–5501. https://doi.org/10.1177/1077546316648080

Lantz, E., Roberts, O., Nunemaker, J., Demeo, E., Dykes, K., & Scott, G. (2019). Increasing Wind Turbine Tower Heights: Opportunities and Challenges. www.nrel.gov/publications.

Lee, S. K., Min, K. W., & Lee, H. R. (2011). Parameter identification of new bidirectional tuned liquid column and sloshing dampers. Journal of Sound and Vibration, 330(7), 1312–1327. https://doi.org/10.1016/j.jsv.2010.10.016

Lee, Y. S., Choi, B. L., Lee, J. H., Kim, S. Y., & Han, S. (2014). Reliability-based design optimization of monopile transition piece for offshore wind turbine system. Renewable Energy, 71, 729–741. https://doi.org/10.1016/J.RENENE.2014.06.017

Letcher (Ed.), T. M. (2023). Wind Energy Engineering. Elsevier. https://doi.org/10.1016/C2021-0-00258-3

Lin, Y. H., Chen, H. K., & Wu, K. Y. (2023). Prediction of aerodynamic performance of NREL offshore 5-MW baseline wind turbine considering power loss at varying wind speeds. Wind Energy, 26(5), 493–515. https://doi.org/10.1002/we.2812

Luque, G.; Alba, E.. Parallel Genetic Algorithms: Theory and Real-World Applications. Springer Publishing Company, Inc., 2013.

Machado, M. R., & Dutkiewicz, M. (2024). Wind turbine vibration management: An integrated analysis of existing solutions, products, and Open-source developments. In Energy Reports (Vol. 11, pp. 3756–3791). Elsevier Ltd. https://doi.org/10.1016/j.egyr.2024.03.014

Manwell, J.; McGowan, J.; Rogers, A.. Wind Energy Explained: Theory, Design and Application. John Wiley & Sons, Ltd, Chichester, 2009.

Matlock, H. (1970). Correlations for design of laterally loaded piles in soft clay. Proceedings of the Annual Offshore Technology Conference, 1970-April. https://doi.org/10.4043/1204-ms

Medina, C., Álamo, G. M., & Padrón, L. A. (2023). Contribution of the rotational kinematic interaction to the seismic response of monopile-supported offshore wind turbines. Ocean Engineering, 280. https://doi.org/10.1016/j.oceaneng.2023.114778

Mendes, M. V., Colherinhas, G. B., Girão de Morais, M. V., & Pedroso, L. J. (2023). Optimum TLCD for Mitigation of Offshore Wind Turbine Dynamic Response Considering Soil–Structure Interaction. International Journal of Structural Stability and Dynamics, 23(19). https://doi.org/10.1142/S0219455423501870

Mensah, A. F., & Dueñas-Osorio, L. (2014). Improved reliability of wind turbine towers with tuned liquid column dampers (TLCDs). Structural Safety, 47, 78–86. https://doi.org/10.1016/j.strusafe.2013.08.004

Mililitsky, J. (2019). Fundações de Torres - Aerogeradores, Linhas de Transmissão e Telecomunicações. Oficina de Textos.

Mousavi, S. A., Bargi, K., & Zahrai, S. M. (2013). Optimum parameters of tuned liquid columngas damper for mitigation of seismic-induced vibrations of offshore jacket platforms. Structural Control and Health Monitoring, 20(3), 422–444. https://doi.org/10.1002/stc.505

Musial, W., Spitsen, P., Duffy, P., Beiter, P., Marquis, M., Hammond, R., & Shields, M. (2022). Offshore Wind Market Report: 2022 Edition.

Nardelli, A., & Futai, M. M. (2022). Assessment of Brazilian onshore wind turbines foundations. Revista IBRACON de Estruturas e Materiais, 15(5). https://doi.org/10.1590/s1983-41952022000500008

Ni, Y. Q., Ying, Z. G., Wang, J. Y., Ko, J. M., & Spencer, B. F. (2004). Stochastic optimal control of wind-excited tall buildings using semi-active MR-TLCDs. Probabilistic Engineering Mechanics, 19(3), 269–277. https://doi.org/10.1016/j.probengmech.2004.02.010

O'Neill, M.; Murchinson, J.. An Evaluation of p-y Relationships in Sands. Report PRAC 82-41-1. Houston, University of Houston, 1983.

Orlando, A., Pagnini, L., & Repetto, M. P. (2021). Structural response and fatigue assessment of a small vertical axis wind turbine under stationary and non-stationary excitation. Renewable Energy, 170, 251–266. https://doi.org/10.1016/j.renene.2021.01.123

Padrón, L. A., Carbonari, S., Dezi, F., Morici, M., Bordón, J. D. R., & Leoni, G. (2022). Seismic response of large offshore wind turbines on monopile foundations including dynamic soil–structure interaction. Ocean Engineering, 257. https://doi.org/10.1016/j.oceaneng.2022.111653

Park, B. J., Lee, Y. J., Park, M. J., & Ju, Y. K. (2018). Vibration control of a structure by a tuned liquid column damper with embossments. Engineering Structures, 168, 290–299. https://doi.org/10.1016/j.engstruct.2018.04.074

Passon, P. (2015). Offshore wind turbine foundation design: selected topics from the perspective of a foundation designer [PhD Thesis]. Danmarks Tekniske Universitet. DTU Vindenergi.

Pender, M. J. (1993). Aseismic pile foundation design analysis. Bulletin of the New Zealand Society for Earthquake Engineering, 26(1), 49–160. https://doi.org/10.5459/bnzsee.26.1.49-160

Petrini, F. (2009). A probabilistic approach to Performance-Based Wind Engineering (PBWE). PhD Thesis, Università degli Studi di Roma “La Sapienza, Roma, Italy.

Petrini, F., Manenti, S., Gkoumas, K., & Bontempi, F. (2010). Structural Design and Analysis of Offshore Wind Turbines from a System Point of View (Vol. 34, Issue 1).

Pham, H. V, Dias, D., Miranda, T., Cristelo, N., & Araújo, N. (2018). 3D Numerical Modeling of Foundation Solutions for Wind Turbines. International Journal of Geomechanics, 18(12), 4018164. https://doi.org/10.1061/(ASCE)GM.1943-5622.0001318

Potter, J. N., Neild, S. A., & Wagg, D. J. (2010). Generalisation and optimisation of semi-active, on-off switching controllers for single degree-of-freedom systems. Journal of Sound and Vibration, 329(13), 2450–2462. https://doi.org/10.1016/j.jsv.2009.12.011

Poulos, H. G., & Davis, E. H. (1980). Pile foundation analysis and design. Rainbow-Bridge Book Co. https://drive.google.com/file/d/0BxlQHeKi4f-6a0dBR3MzRmxUVDY0OW1tRzRMOTdoQQ/view?resourcekey=0-zkeVKpHjbzKPinNwevAhhA

Randolph, M. F. (1981). The response of flexible piles to lateral loading. Géotechnique, 31(2), 247–259. https://doi.org/10.1680/geot.1981.31.2.247

Reese, L. C., Cox, W. R., & Koop, F. D. (1974). Analysis of laterally loaded piles in sand. Proceedings of the Annual Offshore Technology Conference, 1974-May. https://doi.org/10.4043/2080-ms

Reese, L. C., Cox, W. R., & Koop, F. D. (1975). Field Testing and Analysis of Laterally Loaded Piles om Stiff Clay. Proceedings of the Offshore Technology Conference, Houston, Texas. Paper Number: OTC-2312-MS, 1975-May. https://doi.org/10.4043/2312-MS

Rollins, K.; Gerber, T.; Lane, J.; Ashford, S.. Lateral Resistance of a Full-Scale Pile Group in Liquefied Sand. Journal of the Geotechnical and Geoenvironmental Engineering Division, ASCE. Vol. 131, pp 115-125, 2005.

Rozas, L., Boroschek, R. L., Tamburrino, A., & Rojas, M. (2016). A bidirectional tuned liquid column damper for reducing the seismic response of buildings. Structural Control and Health Monitoring, 23(4), 621–640. https://doi.org/10.1002/stc.1784

Saaed, T. E., Nikolakopoulos, G., Jonasson, J. E., & Hedlund, H. (2015). A state-of-the-art review of structural control systems. In JVC/Journal of Vibration and Control

(Vol. 21, Issue 5, pp. 919–937). SAGE Publications Inc. https://doi.org/10.1177/1077546313478294

Sarkar, S., & Chakraborty, A. (2018). Optimal design of semiactive MR-TLCD for along-wind vibration control of horizontal axis wind turbine tower. Structural Control and Health Monitoring, 25(2). https://doi.org/10.1002/stc.2083

Shadlou, M., & Bhattacharya, S. (2016). Dynamic stiffness of monopiles supporting offshore wind turbine generators. Soil Dynamics and Earthquake Engineering, 88, 15–32. https://doi.org/10.1016/J.SOILDYN.2016.04.002

Shen, Y. J., Wang, L., Yang, S. P., & Gao, G. S. (2013). Nonlinear dynamical analysis and parameters optimization of four semi-active on-off dynamic vibration absorbers. JVC/Journal of Vibration and Control, 19(1), 143–160. https://doi.org/10.1177/1077546311433610

Shum, K. M., & Xu, Y. L. (2004). Multiple tuned liquid column dampers for reducing coupled lateral and torsional vibration of structures. Engineering Structures, 26(6), 745–758. https://doi.org/10.1016/j.engstruct.2004.01.006

Shum, K. M., Xu, Y. L., & Guo, W. H. (2008). Wind-induced vibration control of long span cable-stayed bridges using multiple pressurized tuned liquid column dampers. Journal of Wind Engineering and Industrial Aerodynamics, 96(2), 166–192. https://doi.org/10.1016/j.jweia.2007.03.008

Sonmez, E., Nagarajaiah, S., Sun, C., & Basu, B. (2016). A study on semi-active Tuned Liquid Column Dampers (sTLCDs) for structural response reduction under random excitations. Journal of Sound and Vibration, 362, 1–15. https://doi.org/10.1016/j.jsv.2015.09.020

Sørensen, S. P. H. (2012). Soil-structure interaction for non slender, large diameter offshore monopiles (pp. 1–203).

Sørensen, S. P. H., & Ibsen, L. B. (2013). Assessment of foundation design for offshore monopiles unprotected against scour. Ocean Engineering, 63, 17–25. https://doi.org/10.1016/j.oceaneng.2013.01.016

Sørensen, S. P. H., Ibsen, L. B., & Augustesen, A. H. (2010). Effects of diameter on initial stiffness of p-y curves for large-diameter piles in sand. Numerical Methods in Geotechnical Engineering - Proceedings of the 7th European Conference on Numerical Methods in Geotechnical Engineering. https://doi.org/10.1201/b10551-166

Souza, R. Controle passivo-ativo das oscilações de estruturas esbeltas por meio de dispositivos fluido-dinâmicos. PhD Thesis, Universidade Federal do Rio de Janeiro, Rio de Janeiro, Brasil, 2003.

Sun, C., Jahangiri, V., & Sun, H. (2019). Performance of a 3D pendulum tuned mass damper in offshore wind turbines under multiple hazards and system variations. Smart Structures and Systems, 24(1), 53–65. https://doi.org/10.12989/sss.2019.24.1.053

Taflanidis, A. A., Angelides, D. C., & Manos, G. C. (2005). Optimal design and performance of liquid column mass dampers for rotational vibration control of structures under white noise excitation. Engineering Structures, 27(4), 524–534. https://doi.org/10.1016/j.engstruct.2004.11.011

Trojnar, K. (2019). Multi scale studies of the new hybrid foundations for offshore wind turbines. Ocean Engineering, 192, 106506. https://doi.org/10.1016/J.OCEANENG.2019.106506

Varghese, R., Pakrashi, V., & Bhattacharya, S. (2022). A Compendium of Formulae for Natural Frequencies of Offshore Wind Turbine Structures. Energies 2022, Vol. 15, Page 2967, 15(8), 2967. https://doi.org/10.3390/EN15082967

Wang, J. Y., Ni, Y. Q., Ko, J. M., & Spencer, B. F. (2005). Magneto-rheological tuned liquid column dampers (MR-TLCDs) for vibration mitigation of tall buildings: Modelling and analysis of open-loop control. Computers and Structures, 83(25–26), 2023–2034. https://doi.org/10.1016/j.compstruc.2005.03.011

Wang, P., Zhao, M., Du, X., Liu, J., & Xu, C. (2018). Wind, wave and earthquake responses of offshore wind turbine on monopile foundation in clay. Soil Dynamics and Earthquake Engineering, 113, 47–57. https://doi.org/10.1016/j.soildyn.2018.04.028

Wang, X., Zeng, X., Li, J., Yang, X., & Wang, H. (2018). A review on recent advancements of substructures for offshore wind turbines. Energy Conversion and Management, 158, 103–119. https://doi.org/10.1016/J.ENCONMAN.2017.12.061

Welch, R.; Reese, L.. Laterally loaded behavior of drilled shafts. Research Report 35-65-89. Center for Highway Research. University of Texas, Austin, 1972.

Wiemann, J., Lesny, K., & Richwien, W. (2004). Evaluation of Pile Diameter Effects on Soil-Pile Stiffness. 7th German Wind Energy Conference (DEWEK)., 0, 183–201. www.uni-essen.de/grundbau/1Dipl.-Ing

Winkler, E.. Die lehre von der elasticitaet und festigkeit mit besonderer rucksicht auf ihre anwen- dung in der technik fur polytechnische shulen, bauakademien,

ingenieure, maschinenbauer, architek- ten, etc. Verlag von H. Domenicus, Prag, 1867.

Wu, J. C., Shih, M. H., Lin, Y. Y., & Shen, Y. C. (2005). Design guidelines for tuned liquid column damper for structures responding to wind. Engineering Structures, 27(13), 1893–1905. https://doi.org/10.1016/j.engstruct.2005.05.009

Wu, X., Hu, Y., Li, Y., Yang, J., Duan, L., Wang, T., Adcock, T., Jiang, Z., Gao, Z., Lin, Z., Borthwick, A., & Liao, S. (2019). Foundations of offshore wind turbines: A review. Renewable and Sustainable Energy Reviews, 104, 379–393. https://doi.org/10.1016/J.RSER.2019.01.012

Xie, F., & Aly, A.-M. (2020). Structural control and vibration issues in wind turbines: A review. Engineering Structures, 210, 110087. https://doi.org/10.1016/j.engstruct.2019.110087

Yalla (2001) Liquid Dampers for Mitigation of Structural Response. Theoretical Development and Experimental Validation. PhD Thesis, University of Notre Dame, Notre Dame, United States of America, 2001.

Yalla, S. K., Kareem, A., & Kantor, J. C. (2000). Semiactive variable-damping liquid column dampers. Smart Structures and Materials 2000: Smart Systems for Bridges, Structures, and Highways, 3988, 75–83. https://doi.org/10.1117/12.383128

Yalla, S. K., Kareem, A., & Kantor, J. C. (2001). Semi-active tuned liquid column dampers for vibration control of structures. In Engineering Structures (Vol. 23). www.elsevier.com/locate/engstruct

Yang, G., Spencer, B. F., Carlson, J. D., & Sain, M. K. (2002). Large-scale MR fluid dampers: modeling and dynamic performance considerations. In Engineering Structures (Vol. 24). www.elsevier.com/locate/engstruct

Zhang, Z., De Risi, R., & Sextos, A. (2023). Multi-hazard fragility assessment of monopile offshore wind turbines under earthquake, wind and wave loads. Earthquake Engineering and Structural Dynamics, 52(9), 2658–2681. https://doi.org/10.1002/eqe.3888

Zuo, H., Bi, K., Hao, H., Xin, Y., Li, J., & Li, C. (2020). Fragility analyses of offshore wind turbines subjected to aerodynamic and sea wave loadings. Renewable Energy, 160, 1269–1282. https://doi.org/10.1016/j.renene.2020.07.066

APPENDIX A. ELASTIC BUCKLING STRENGTH OF AN UNSTIFFENED CIRCULAR CYLINDRICAL SHELL

As presented in the recommended practice at the DNV-GL (2018) for shells buckling stress, the axial and bending stresses sum cannot surpass the critical buckling stress:

$$\sigma_a + \sigma_b \leq \sigma_{cr} \tag{A.1}$$

The axial stress σ_a at the given shell segment is given by

$$\sigma_a = \frac{G}{2\pi r t} \tag{A.2}$$

where, G is the OWT self-weight and r, and t the radius and thickness at the shell segment.

The bending stress σ_b for a given design moment M on the shell segment is computed as:

$$\sigma_b = \frac{M}{2\pi r^2 t} \tag{A.3}$$

Finally, the critical buckling stress σ_{cr}

$$\sigma_{cr} = \frac{f_y}{\sqrt{1+\lambda^4}} \tag{A.4}$$

depends on the material yield stress f_y and λ, obtained from

$$\lambda^2 = \frac{f_y}{\sigma_a + \sigma_b}\left(\frac{\sigma_a}{\sigma_{Ea}} + \frac{\sigma_b}{\sigma_{Eb}}\right) \tag{A.5}$$

with

$$\sigma_{Ea} = (1.5 - 50\beta)C_a \frac{\pi E}{12(1-\nu^2)}\left(\frac{t}{L_r}\right)^2 \tag{A.6}$$

$$\sigma_{Eb} = (1.5 - 50\beta)C_b \frac{\pi E}{12(1-\nu^2)}\left(\frac{t}{L_r}\right)^2 \tag{A.7}$$

where, E is the Young modulus, ν the Poisson ratio (0,3), β the reduction factor (for safety equal to 2,0). The reduced buckling coefficients (C_a and C_b) may be expressed as (DNV-GL, 2018):

$$C_a = \sqrt{1 + (\psi_a \xi)^2} \tag{A.8}$$

$$C_b = \sqrt{1 + (\psi_b \xi)^2} \tag{A.9}$$

for

$$\psi_a = 0.5 \left(1 + \frac{r}{150t}\right)^{-0.5} \tag{A.10}$$

$$\psi_b = 0.5 \left(1 + \frac{r}{300t}\right)^{-0.5} \tag{A.11}$$

and

$$\xi = \frac{l}{rt}\sqrt{(1 - \nu^2)} \tag{A.12}$$

l is the distance between ring frames.

APPENDIX B. SOME CONTINUOUS PROBABILITY DISTRIBUTIONS

The table below presents the continuous distribution functions mentioned in Chapter 5 of the thesis and is used in performance analysis to generate an array of random numbers related to the uncertain parameters. An array with continuous random variable x, mean μ, and standard deviation σ. For the Weibull Distribution we have the scale parameter α and the shape parameter β.

Table B.1. Continuous distribution functions employed for performance analysis.

Distribution	**Function**	**Graph**
Normal	$f(x,\mu,\sigma) = \frac{1}{\sqrt{2\pi}\sigma}\exp[-\frac{1}{2\sigma^2}(x-\mu)^2], -\infty \le x \le \infty$	Figure B.1
Lognormal	$f(x,\mu,\sigma) = \frac{1}{\sqrt{2\pi}\sigma x}\exp[-\frac{1}{2\sigma^2}(\ln x-\mu)^2], x \ge 0$	Figure B.2
Weibull	$f(x,\alpha,\beta) = \alpha\beta x^{\beta} - \exp(-\alpha x^{\beta}), x > 0$ $\mu = \alpha^{-1/\beta}\,\Gamma\left(1+\frac{1}{\beta}\right)$ $\sigma^2 = \alpha^{-2/\beta}\left\{\Gamma\left(1+\frac{2}{\beta}\right) - \left[\Gamma\left(1+\frac{1}{\beta}\right)\right]^2\right\}$	Figure B.3

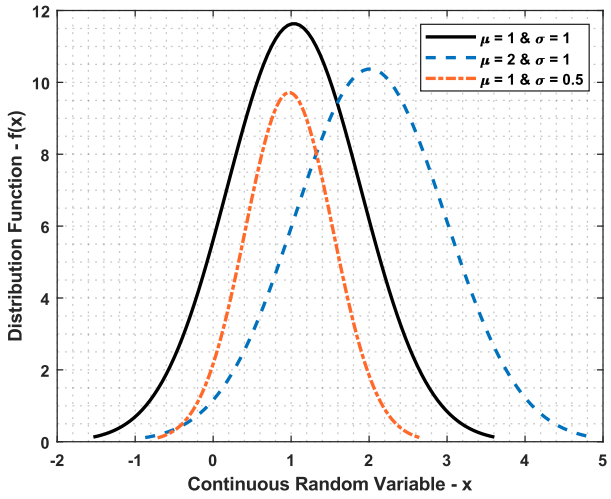

Figure B.1. Normal distribution.

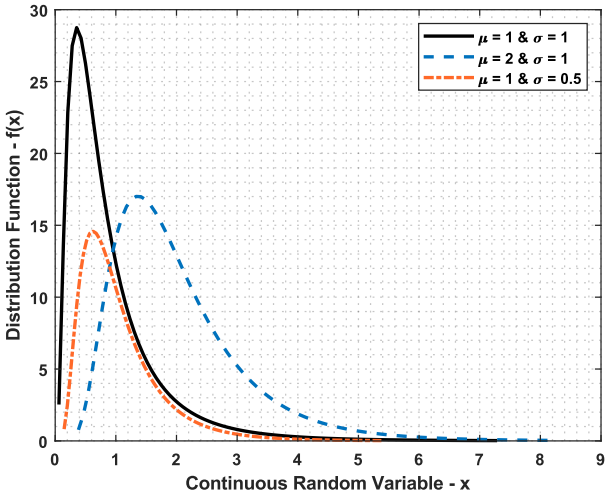

Figure B.2. Lognormal distribution.

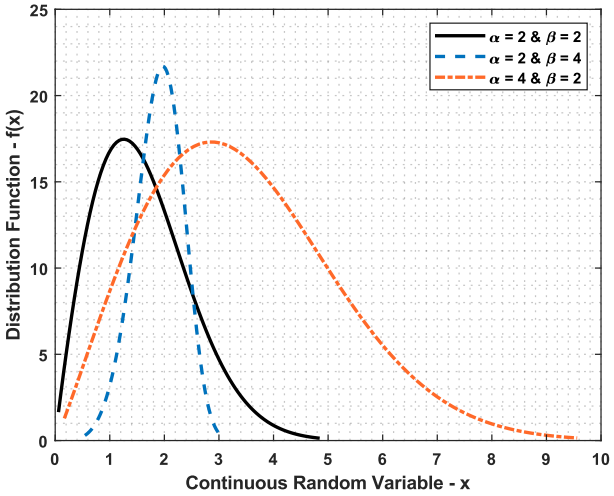

Figure B.3. Weibull distribution.

APPENDIX C. ANALYSIS OF MESH CONVERGENCE AND GEOMETRIC STIFFNESS INFLUENCE OF THE NREL 5-MW REFERENCE WIND TURBINE

In this work, for the random vibrations control analysis of the offshore wind turbine with TLCD, the support structure (monopile and tower) of the OWT is numerically simulated through one-dimensional beam elements. Considering only the bending deformations and the linear-elastic behavior of the element, the stiffness matrix k_f and the consistent mass matrix m_s of the beam element based on the Euler-Bernoulli Theory are given, respectively, by (Clough & Penzien, 2003; Chopra, 2017; Logan, 2017):

$$\boldsymbol{k_f} = \frac{EI}{L^3}\begin{bmatrix} 12 & 6L & -12 & 6L \\ 6L & 4L^2 & -6L & 2L^2 \\ -12 & -6L & 12 & -6L \\ 6L & 2L^2 & -6L & 4L^2 \end{bmatrix} \tag{C.1}$$

$$\boldsymbol{m_s} = \frac{\rho AL}{420}\begin{bmatrix} 156 & 22L & 54 & -13L \\ 22L & 4L^2 & 13L & -3L^2 \\ 54 & 13L & 156 & -22L \\ -13L & -3L^2 & -22L & 4L^2 \end{bmatrix} \tag{C.2}$$

The OWT structural system supports heavy elements and assemblies, such as the rotor, nacelle, transmission shaft, generator, etc. The effect of the self-weight of these different OWT systems in addition to the bending deformations of the structure can induce the supporting structure to buckle.

The tendency toward buckling of the structure induced by axially load components is represented by the geometric stiffness $\boldsymbol{k_G}$. The structure configuration and the loading magnitude determines the beam element geometric-stiffness matrix (Clough & Penzien, 2003):

$$\boldsymbol{k_G} = \frac{N}{30L}\begin{bmatrix} 36 & 3L & -36 & 3L \\ 3L & 4L^2 & -3L & -L^2 \\ -36 & -3L & 36 & -3L \\ 3L & -L^2 & -3L & 4L^2 \end{bmatrix} \tag{C.3}$$

To evaluate the influence of geometric stiffness on the structure stiffness and, consequently, on the OWT structural system, this appendix carries out a frequency assessment through modal analysis.

The 5-MW NREL reference wind turbine is adopted for the study (Table 6.1). The tower has a hollow circular cross-section with linear decrease in its outer diameter and thickness (cross-section decreases from base to top). The OWT monopile has a constant cross-section through its length. The OWT tower and monopile have different geometry, cross-section, and lengths. Initially, in the numerical study of the OWT structure, the discrete model has the number of elements increased alternately. First, the increase in the number of tower elements is computed, and then the number of monopile elements is increased. Table C.1 and Table C.2 present the results for the first 5 natural frequencies of the OWT following this procedure with and without consideration of the geometric stiffness for the structure. Figure C.1 and Figure C.2 present the behavior for the first two frequencies.

Table C.1. Natural frequencies of the OWT without considering geometric stiffness.

Elements (Monopile)	Elements (Tower)	Elements (OWT)	1st Freq (Hz)	2nd Freq (Hz)	3rd Freq (Hz)	4th Freq (Hz)	5th Freq (Hz)
1	2	3	0.2781	1.6158	3.7192	7.9023	18.7881
2	2	4	0.2781	1.6158	3.7188	7.8877	18.4453
2	3	5	0.2817	1.5851	3.5745	7.8827	14.8670
3	3	6	0.2817	1.5851	3.5745	7.8816	14.8584
3	4	7	0.2831	1.5760	3.5327	7.8431	14.9749
4	4	8	0.2831	1.5760	3.5327	7.8429	14.9734
4	5	9	0.2839	1.5725	3.5177	7.8339	14.9637
5	5	10	0.2839	1.5725	3.5177	7.8339	14.9637
5	6	11	0.2844	1.5712	3.5119	7.8352	14.9677
6	6	12	0.2844	1.5712	3.5119	7.8352	14.9676

Table C.2. Natural frequencies of the OWT considering geometric stiffness.

Elements (Monopile)	Elements (Tower)	Elements (OWT)	1st Freq (Hz)	2nd Freq (Hz)	3rd Freq (Hz)	4th Freq (Hz)	5th Freq (Hz)
1	2	3	0.2740	1.6116	3.7164	7.8987	18.7844
2	2	4	0.2740	1.6117	3.7162	7.8844	18.4419
2	3	5	0.2784	1.5812	3.5726	7.8797	14.8639
3	3	6	0.2784	1.5813	3.5726	7.8787	14.8554
3	4	7	0.2804	1.5723	3.5314	7.8406	14.9721
4	4	8	0.2804	1.5723	3.5314	7.8405	14.9706
4	5	9	0.2816	1.5692	3.5168	7.8319	14.9612
5	5	10	0.2816	1.5692	3.5168	7.8318	14.9608
5	6	11	0.2824	1.5680	3.5112	7.8336	14.9656
6	6	12	0.2824	1.5680	3.5112	7.8336	14.9655

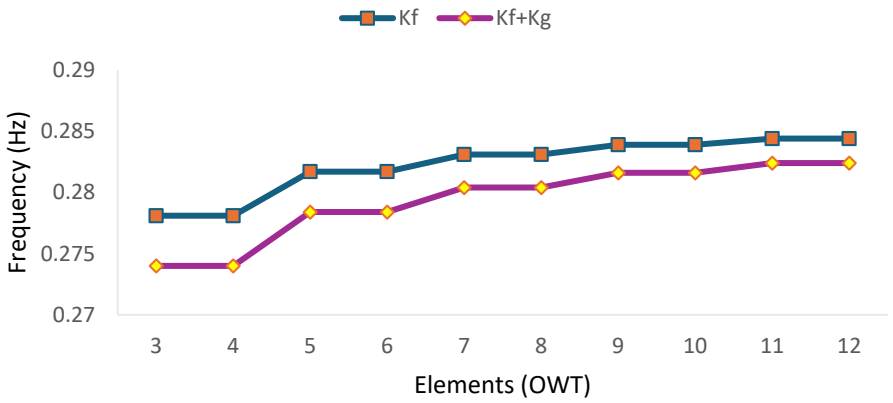

Figure C.1. OWT 1st Frequency according to number of elements of the discrete model.

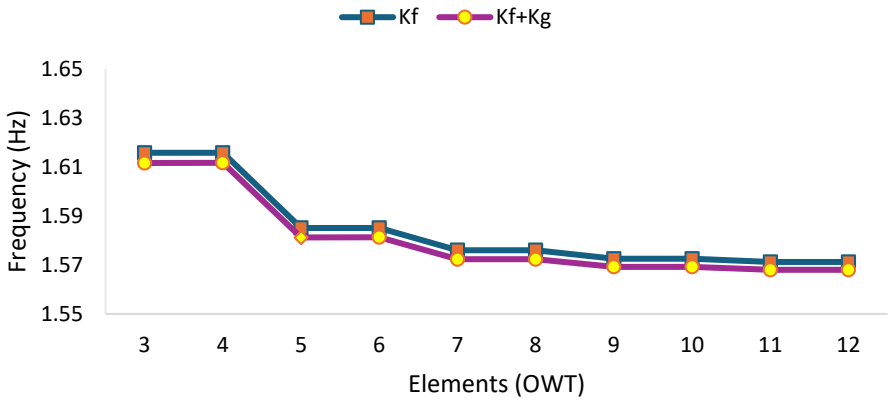

Figure C.2. OWT 2nd Frequency according to number of elements of the discrete model.

Increasing the number of monopile elements (hollow cylinder with constant cross-section along its height) in the discrete model has little effect on the OWT frequencies, while increasing the number of tower elements causes changes in the OWT frequencies. Furthermore, for the linear elastic beam element, considering geometric stiffness causes a small reduction in the OWT frequency.

After observing that the changes in the OWT frequencies are mainly related to the variation in the number of elements used in the discrete model of the tower, the study continues to verify the influence of geometric rigidity and mesh convergence only with the increase in the number of elements used in the discrete model of the tower. Table C.3 and Table C.4 present the results for the first 5 natural frequencies of the OWT with and without consideration of the geometric stiffness for the structure. Figure C.3 and Figure C.4 present the behavior for the first two frequencies of the OWT.

Table C.3. Natural frequencies of the OWT without considering geometric stiffness for tower refined mesh.

Elements (Monopile)	Elements (Tower)	Elements (OWT)	1st Freq (Hz)	2nd Freq (Hz)	3rd Freq (Hz)	4th Freq (Hz)	5th Freq (Hz)
6	7	13	0.2847	1.5706	3.5099	7.8398	14.9790
6	8	14	0.2849	1.5705	3.5095	7.8453	14.9921
6	9	15	0.2850	1.5706	3.5099	7.8508	15.0049
6	10	16	0.2851	1.5708	3.5107	7.8560	15.0167
6	11	17	0.2852	1.5710	3.5116	7.8607	15.0273
6	12	18	0.2853	1.5712	3.5125	7.8649	15.0368
6	13	19	0.2854	1.5714	3.5135	7.8688	15.0453
6	14	20	0.2854	1.5716	3.5144	7.8723	15.0530
6	15	21	0.2855	1.5718	3.5153	7.8754	15.0598
6	16	22	0.2855	1.5720	3.5161	7.8783	15.0660
6	17	23	0.2856	1.5722	3.5169	7.8809	15.0716
6	18	24	0.2856	1.5723	3.5176	7.8832	15.0767
6	19	25	0.2856	1.5725	3.5183	7.8854	15.0813
6	20	26	0.2856	1.5726	3.5189	7.8874	15.0856

Table C.4. Natural frequencies of the OWT without considering geometric stiffness for tower refined mesh.

Elements (Monopile)	Elements (Tower)	Elements (OWT)	1st Freq (Hz)	2nd Freq (Hz)	3rd Freq (Hz)	4th Freq (Hz)	5th Freq (Hz)
6	7	13	0.2830	1.5677	3.5093	7.8385	14.9772
6	8	14	0.2834	1.5678	3.5090	7.8443	14.9906
6	9	15	0.2837	1.5681	3.5095	7.8499	15.0036
6	10	16	0.2839	1.5684	3.5103	7.8552	15.0155
6	11	17	0.2841	1.5687	3.5112	7.8600	15.0263
6	12	18	0.2843	1.5691	3.5122	7.8644	15.0359
6	13	19	0.2844	1.5694	3.5132	7.8683	15.0446
6	14	20	0.2845	1.5697	3.5141	7.8718	15.0523
6	15	21	0.2846	1.5700	3.5150	7.8750	15.0592
6	16	22	0.2847	1.5703	3.5158	7.8779	15.0654
6	17	23	0.2848	1.5705	3.5166	7.8805	15.0711
6	18	24	0.2849	1.5708	3.5173	7.8829	15.0762
6	19	25	0.2849	1.5710	3.5180	7.8851	15.0809
6	20	26	0.2850	1.5712	3.5187	7.8871	15.0852

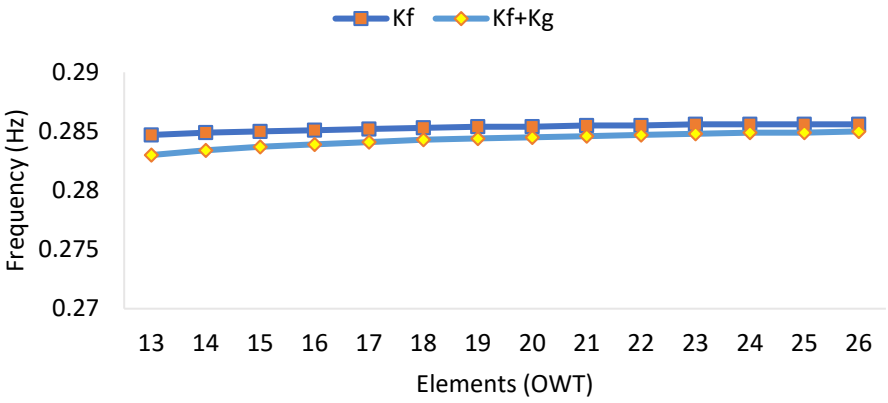

Figure C.3. OWT 1st Frequency according to number of elements of the discrete model with a tower refined mesh.

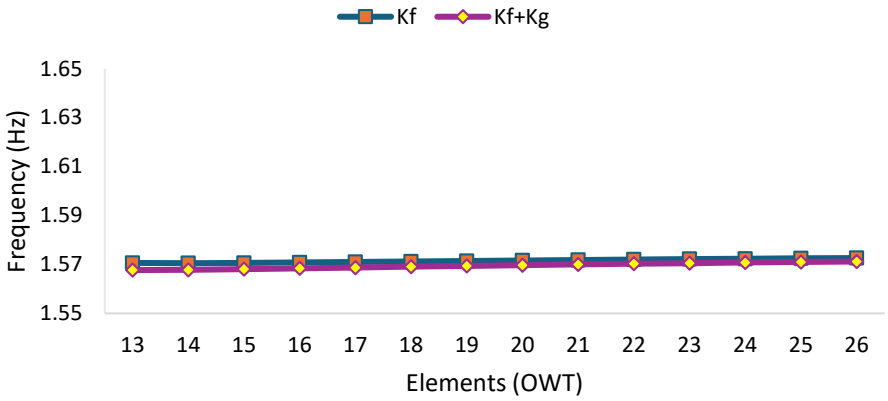

Figure C.4. OWT 2nd Frequency according to number of elements of the discrete model with a tower refined mesh.

Monotonic asymptotic convergence of the OWT frequencies is observed with differences lower than 0.3% with the increase in the number of beam elements used in the discrete model of the tower. It is also noted in this study that geometric stiffness produces changes lower than 0.6% and is therefore disregarded throughout the thesis.

Reliable solutions must have numerical errors close to zero. To verify the convergence for the given study and to compute the estimative of the numerical model frequency the Richardson error estimator may be employed (Marchi & Silva, 2005; Souza et al., 2021). For the given procedure the estimative of the numerical solution $\phi_\infty(PU)$ is given by

$$\varphi_\infty(PU) = \varphi_1 + \left(\frac{\varphi_1 - \varphi_2}{r^{PU} - 1}\right) \tag{C.4}$$

where r is the grid refinement ratio

$$r = \frac{\Delta L_2}{\Delta L_1} = \frac{\Delta L_3}{\Delta L_2} \tag{C.5}$$

and PU the apparent order of uncertainty, computed through:

$$PU = \frac{log\left(\frac{\varphi_2 - \varphi_3}{\varphi_1 - \varphi_2}\right)}{\log(r)} \tag{C.6}$$

where, φ define different meshes, coarse (φ_3), medium (φ_2), and fine (φ_1), with lengths ΔL_3, ΔL_2, and ΔL_1, respectively.

For the given NREL 5-MW reference WT with monopile, **Erro! Fonte de referência não encontrada.** and Table C.6 presents the estimative of the numerical solution φ_∞ for the OWT first and second natural frequency with and without consideration of geometric stiffness, respectively.

Table C.5. Estimation of the numerical solution for Natural frequencies of the OWT without considering geometric stiffness.

Elements (Monopile)	Elements (Tower)	Elements (OWT)	1st Freq (Hz)	2nd Freq (Hz)	PU	1st Freq φ_∞ (Hz)	2nd Freq φ_∞ (Hz)
3	8	11	0.2849	1.5705	-	0.2864	1.5738
6	16	22	0.2855	1.5720	-	0.2862	1.5762
12	32	44	0.2858	1.5738	1.2429	0.2861	1.5766
24	64	88	0.2859	1.5750	1.1351	0.2861	1.5766
48	128	176	0.2860	1.5757	0.8335	-	-

Table C.6. Estimation of the numerical solution for Natural frequencies of the OWT considering geometric stiffness.

Elements (Monopile)	Elements (Tower)	Elements (OWT)	1st Freq (Hz)	2nd Freq (Hz)	PU	1st Freq φ_∞ (Hz)	2nd Freq φ_∞ (Hz)
3	8	11	0.2834	1.5678	-	0.2862	1.5728
6	16	22	0.2847	1.5703	-	0.2861	1.5756
12	32	44	0.2854	1.5729	1.0566	0.2861	1.5763
24	64	88	0.2857	1.5745	1.0305	0.2861	1.5764
48	128	176	0.2859	1.5755	0.9670	-	-

Using the result of the estimation of the numerical solution φ_∞ for the OWT presented above and comparing it with the values previously obtained for the natural vibration frequencies of the structure for different mesh refinements, we can estimate the error of the analyzed cases. Figure C.5 and Table C.7 present the error of the first

and second vibration frequencies of the structure without the influence of geometric stiffness, while Figure C.6 and Table C.8 present the error considering the geometric stiffness for the structure. It can be observed that from 20 elements onwards the error graph presents monotonic asymptotic behavior.

In this thesis, the discrete model adopted for the NREL 5-MW Reference WT with monopile contains 22 elements, 16 elements for the tower and 6 elements for the monopile. The estimated error for the first two natural frequencies of the OWT is less than 0.3% and the difference for the system with geometric stiffness is minimal for the linear-elastic case, thus, the stiffness matrix is not adopted for the evaluated cases.

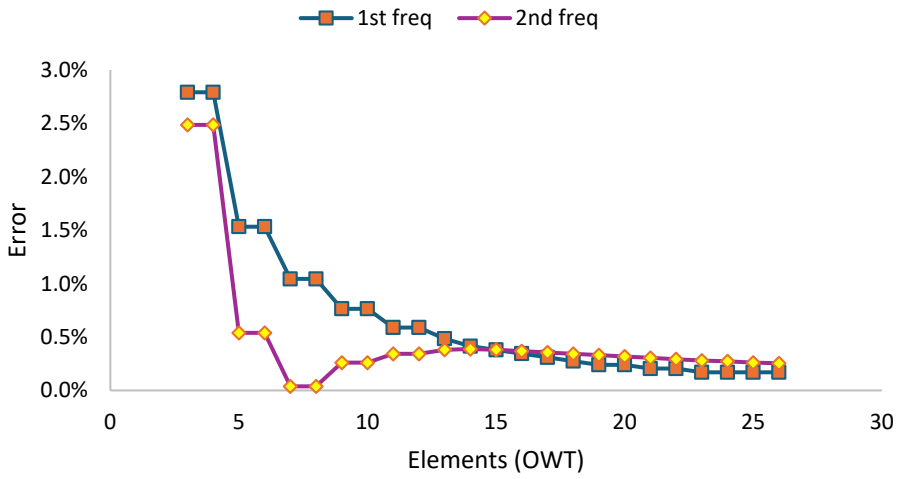

Figure C.5. Error of the numerical solution for the structure first and second vibration frequencies without the influence of geometric stiffness.

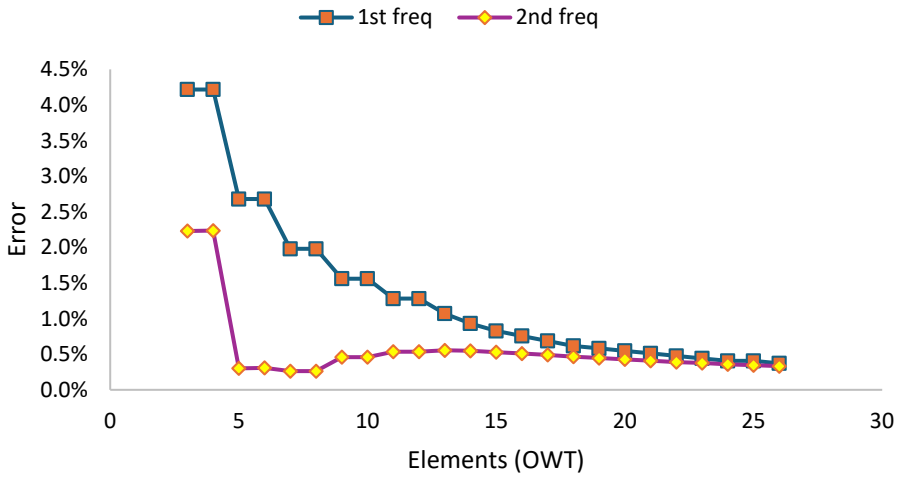

Figure C.6. Error of the numerical solution for the structure first and second vibration frequencies with the influence of geometric stiffness.

Table C.7. Error of the numerical solution for the structure first and second vibration frequencies without the influence of geometric stiffness.

Elements Monopile	Elements Tower	Elements OWT	1st Freq (Hz)	1st Freq Error	1st Freq Error %	2nd Freq (Hz)	2nd Freq Error	2nd Freq Error %
1	2	3	0.2781	-0.0080	2.7914%	1.6158	0.0392	2.4860%
2	2	4	0.2781	-0.0080	2.7914%	1.6158	0.0392	2.4860%
2	3	5	0.2817	-0.0044	1.5330%	1.5851	0.0085	0.5388%
3	3	6	0.2817	-0.0044	1.5330%	1.5851	0.0085	0.5388%
3	4	7	0.2831	-0.0030	1.0436%	1.576	-0.0006	0.0384%
4	4	8	0.2831	-0.0030	1.0436%	1.576	-0.0006	0.0384%
4	5	9	0.2839	-0.0022	0.7640%	1.5725	-0.0041	0.2604%
5	5	10	0.2839	-0.0022	0.7640%	1.5725	-0.0041	0.2604%
5	6	11	0.2844	-0.0017	0.5892%	1.5712	-0.0054	0.3429%
6	6	12	0.2844	-0.0017	0.5892%	1.5712	-0.0054	0.3429%
6	7	13	0.2847	-0.0014	0.4844%	1.5706	-0.0060	0.3809%
6	8	14	0.2849	-0.0012	0.4144%	1.5705	-0.0061	0.3873%
6	9	15	0.2850	-0.0011	0.3795%	1.5706	-0.0060	0.3809%
6	10	16	0.2851	-0.0010	0.3445%	1.5708	-0.0058	0.3682%
6	11	17	0.2852	-0.0009	0.3096%	1.571	-0.0056	0.3555%
6	12	18	0.2853	-0.0008	0.2746%	1.5712	-0.0054	0.3429%
6	13	19	0.2854	-0.0007	0.2397%	1.5714	-0.0052	0.3302%
6	14	20	0.2854	-0.0007	0.2397%	1.5716	-0.0050	0.3175%
6	15	21	0.2855	-0.0006	0.2047%	1.5718	-0.0048	0.3048%
6	**16**	**22**	**0.2855**	**-0.0006**	**0.2047%**	**1.572**	**-0.0046**	**0.2921%**
6	17	23	0.2856	-0.0005	0.1698%	1.5722	-0.0044	0.2794%
6	18	24	0.2856	-0.0005	0.1698%	1.5723	-0.0043	0.2731%
6	19	25	0.2856	-0.0005	0.1698%	1.5725	-0.0041	0.2604%
6	20	26	0.2856	-0.0005	0.1698%	1.5726	-0.0040	0.2541%

Table C.8. Error of the numerical solution for the structure first and second vibration frequencies with the influence of geometric stiffness.

Elements Monopile	Elements Tower	Elements OWT	1st Freq (Hz)	1st Freq Error	1st Freq Error %	2nd Freq (Hz)	2nd Freq Error	2nd Freq Error %
1	2	3	0.2740	-0.0121	4.2171%	1.6116	0.0352	2.2302%
2	2	4	0.2740	-0.0121	4.2171%	1.6117	0.0353	2.2365%
2	3	5	0.2784	-0.0077	2.6790%	1.5812	0.0048	0.3018%
3	3	6	0.2784	-0.0077	2.6790%	1.5813	0.0049	0.3081%
3	4	7	0.2804	-0.0057	1.9798%	1.5723	-0.0041	0.2628%
4	4	8	0.2804	-0.0057	1.9798%	1.5723	-0.0041	0.2628%
4	5	9	0.2816	-0.0045	1.5603%	1.5692	-0.0072	0.4594%
5	5	10	0.2816	-0.0045	1.5603%	1.5692	-0.0072	0.4594%
5	6	11	0.2824	-0.0037	1.2807%	1.5680	-0.0084	0.5355%
6	6	12	0.2824	-0.0037	1.2807%	1.5680	-0.0084	0.5355%
6	7	13	0.2830	-0.0031	1.0709%	1.5677	-0.0087	0.5546%
6	8	14	0.2834	-0.0027	0.9311%	1.5678	-0.0086	0.5482%
6	9	15	0.2837	-0.0024	0.8262%	1.5681	-0.0083	0.5292%
6	10	16	0.2839	-0.0022	0.7563%	1.5684	-0.0080	0.5102%
6	11	17	0.2841	-0.0020	0.6864%	1.5687	-0.0077	0.4911%
6	12	18	0.2843	-0.0018	0.6165%	1.5691	-0.0073	0.4658%
6	13	19	0.2844	-0.0017	0.5815%	1.5694	-0.0070	0.4467%
6	14	20	0.2845	-0.0016	0.5466%	1.5697	-0.0067	0.4277%
6	15	21	0.2846	-0.0015	0.5116%	1.5700	-0.0064	0.4087%
6	**16**	**22**	**0.2847**	**-0.0014**	**0.4767%**	**1.5703**	**-0.0061**	**0.3896%**
6	17	23	0.2848	-0.0013	0.4417%	1.5705	-0.0059	0.3770%
6	18	24	0.2849	-0.0012	0.4068%	1.5708	-0.0056	0.3579%
6	19	25	0.2849	-0.0012	0.4068%	1.5710	-0.0054	0.3452%
6	20	26	0.2850	-0.0011	0.3718%	1.5712	-0.0052	0.3326%

APPENDIX D. LIST OF PUBLICATIONS

The publications listed below directly result from the research and work developed during the doctoral period and are related to the scope of the thesis.

Mendes, M.; Morais, M.; Ávila, S.. Semi-active tuned liquid column damper applied for offshore wind turbines random vibration control using groundhook control strategies. Ocean Engineering, 2024. (Submitted)

Mendes, M.; Petrini, F.; Morais, M.. Simultaneous optimization of OWT controlled by TLCD considering structural and damper performance constraints. Structures, 2024. (Submitted)

Morais, M.; Mendes, M.; Pedroso, L.. Foundation and Support Structures of Wind Turbines and Optimization. Reference Module in Earth Systems and Environmental Sciences, Elsevier, 2024. ISBN 9780124095489. (In press)
https://doi.org/10.1016/B978-0-323-93940-9.00243

Mendes, M.; Colherinhas, G.; Morais, M.; Pedroso, L.. Optimum TLCD for mitigation of OWT dynamic response considering SSI. International Journal of Structural Stability and Dynamics, Vol. 23, No. 19, 2350187, 2023.
https://doi.org/10.1142/S0219455423501870

Mendes, M.; Ghedini, L.; Batista, R.; Pedroso, L.. A study of TLCD parameters for structural vibration mitigation. Latin American Journal of Solids and Structures, Vol. 20, No. 1, 2023. https://doi.org/10.1590/1679-78257412

Mendes, M.; Ribeiro, P.; Pedroso, L.. Effects of soil-structure interaction in seismic analysis of buildings with multiple pressurized tuned liquid column dampers. Latin American Journal of Solids and Structures, Vol. 16, No. 8, 2019.
https://doi.org/10.1590/1679-78255707